CAROLINE SATYE MARTINS NAKAMA

DEVELOPMENT OF MATHEMATICAL TOOLS FOR MODELING BIOLOGICAL SYSTEMS BASED ON METABOLIC FLUXES AND PARAMETER ESTIMATION OF ILL-CONDITIONED PROBLEMS

São Paulo

2020

CAROLINE SATYE MARTINS NAKAMA

DEVELOPMENT OF MATHEMATICAL TOOLS FOR MODELING BIOLOGICAL SYSTEMS BASED ON METABOLIC FLUXES AND PARAMETER ESTIMATION OF ILL-CONDITIONED PROBLEMS

Versão corrigida

Tese apresentada à Escola Politécnica da Universidade de São Paulo para obtenção do título de Doutora em Ciências.

Área de concentração: Engenharia Química

Orientador: Prof. Dr. Galo Antonio Carrillo Le Roux

Coorientador: Prof. Dr. José Gregório Cabrera Gomez

São Paulo

2020

Este exemplar foi revisado e corrigido em relação à versão original, sob responsabilidade única do autor e com a anuência de seu orientador.

São Paulo, 4 de agosto de 2020

Assinatura do autor: _____

Assinatura do orientador: _____

Catalogação-na-publicação

Nakama, Caroline Satye Martins
Development of Mathematical Tools for Modeling Biological Systems Based on Metabolic Fluxes and Parameter Estimation of Ill-Conditioned Problems / C. S. M. Nakama -- versão corr. -- São Paulo, 2020.
133 p.

Tese (Doutorado) - Escola Politécnica da Universidade de São Paulo. Departamento de Engenharia Química.

1.Engenharia metabólica 2.Modelagem estequiométrica 3.Estimação de parâmetros 4.Regularização I.Universidade de São Paulo. Escola Politécnica. Departamento de Engenharia Química II.t.

Acknowledgements

Palavras que não expressam fatos e teorias são mais difíceis de serem escritas, apesar de não menos importantes. Então começo dizendo que muitas pessoas não citadas nominalmente aqui contribuíram, direta ou indiretamente, para a conclusão dessa etapa da minha vida e eu sempre serei grata a todas(os) vocês.

Cada professora e professor que tive durante a vida adicionou, de alguma forma, um bloco na minha formação acadêmica. Sempre fui muito grata a todas(os). Em especial, agradeço a meu orientador Prof. Galo Le Roux pela orientação, paciência, disponibilidade, humildade, amizade e todos os ensinamentos, sejam eles técnicos ou sobre a vida. Meus agradecimentos também são direcionados ao Prof. Gregório Gomez pela orientação e ensino sobre bioquímica e microbiologia. *I would also like to thank Prof. Victor Zavala for accepting to receive me as a visitor twice, patiently advising me, and always making me feel part of your research group; I will never be able to measure how much I learned from you or to express how grateful I am.*

Como já diziam os Beatles, "*I get by with a little help from my friends*". Agradeço a todas minhas amigas e todos meus amigos pelas tão necessárias distrações, apoio e por sempre acreditarem em mim. Particularmente, gostaria também de expressar minha gratidão a minhas(meus) colegas da pós graduação; tudo foi menos difícil com a ajuda e paciência de vocês. Rafael e José Otávio, obrigada pela direta contribuição lendo essa tese. *I also feel I have to give special thanks to my colleagues and friends from Madison; you are part of the reason my time there was so enriching both personal and professionally. Santiago, thank you for your help and letting me use your code.*

Eu gostaria de agradecer às agências de fomento Conselho Nacional de Desenvolvimento Científico e Tecnológico (CNPq) e Coordenação de Aperfeiçoamento de Pessoal de Nível Superior (CAPES) pelo apoio financeiro nacional e para a realização do doutorado sanduíche respectivamente.

Meu eterno agradecimento à minha família, especialmente meu pai José, por ter me oferecido oportunidades e criado possibilidades para que eu tivesse a liberdade de seguir o caminho que quisesse. Por fim, agradeço ao André Dondon pelo apoio incondicional; essa maratona teria sido extremamente mais desafiadora, quiçá impossível, sem você.

“Quando os caminhos se confundem, é necessário voltar ao começo”

(Leandro "Emicida" Roque de Oliveira)

Resumo

Modelagem matemática é um dos pilares da engenharia metabólica, guiando modificações genéticas através do estudo de fluxos metabólicos. Modelos estequiométricos são uma ferramenta importante para analisar redes metabólicas, especialmente para organismos não modelo ou durante a fase de análise inicial, pois são modelos lineares que requerem essencialmente a matriz estequiométrica e informações sobre a reversibilidade das reações como dados de entrada. Eles podem ser usados para explorar diferentes hipóteses e cenários, além de elucidar algumas propriedades do metabolismo. Com isso, algumas técnicas de modelagem estequiométrica foram implementadas em um software único e independente e usadas para estudar o metabolismo central da bactéria *Burkholderia sacchari* para produção de poli-hidroxialcanoato. O estudo mostrou que a modelagem estequiométrica é uma ferramenta valiosa para explorar como o metabolismo funciona e orientar o planejamento de experimentos futuros. No entanto, o metabolismo celular é, na realidade, função de dinâmicas não lineares e, portanto, modelos não lineares são mais adequados para representar uma abrangente variedade de estados fisiológicos, resultando em melhores previsões. Modelos mecanísticos são uma classe de modelos não lineares; porém, no contexto da engenharia metabólica, todos os modelos propostos para estimar os parâmetros cinéticos envolvidos são propensos a problemas de identificabilidade. Considerando esse obstáculo, um estudo sobre métodos de regularização para problemas de estimativa de parâmetros mal condicionados foi realizado. Os métodos de regularização baseados na decomposição em autovalores e autovetores da matriz Hessiana (reduzida) se mostraram ótimos para estimativa linear de parâmetros levando em consideração a redução da variância e podem auxiliar a lidar com problemas não lineares com vizinhança quase plana ao redor da solução. Além disso, a regularização baseada em autovetores em ambos os casos pôde ser usada para reconhecer grupos de parâmetros correlacionados, o que auxilia na compreensão dos inerentes problemas de identificação.

Palavras-chave: Engenharia metabólica, modelagem estequiométrica, estimação de parâmetros, regularização

Abstract

Mathematical modeling is one of the basis of metabolic engineering, guiding genetic modifications through the study of metabolic fluxes. Stoichiometric models are an important tool to analyze metabolic networks, especially for non-model organisms or during initial analysis, since they linear models and essentially require the stoichiometry matrix and information on reversibility of the reactions as input. They can be used to explore different assumptions and scenarios, and elucidate some properties of the metabolism. Therefore some stoichiometric modeling techniques were implemented in a single stand-alone software and used to study the core metabolism of the bacteria *Burkholderia sacchari* for polyhydroxyalkanoate production, showing that they are a valuable tool for exploring how metabolisms work and guiding future experiment design. However, cellular metabolism is actually subjected to nonlinear dynamics and, therefore, nonlinear models are better suited to represent more diverse physiological states, which can result in better predictions. Mechanistic models are a class of such models; however, in the metabolic engineering context, all frameworks that have been proposed to estimate the kinetic parameters involved are prone to identifiability issues. Based on this obstacle, an investigation on regularization methods for ill-conditioned parameter estimation problems was conducted. Regularization methods based on the eigenvalue decomposition of the (reduced) Hessian matrix were shown to be optimal for linear parameter estimation, in the sense of reducing parameter variance, and helpful in dealing with nonlinear problems with nearly flat neighborhood around the solution. Moreover, the eigenvector-based regularization in both cases was able to recognize groups of correlated parameters, which allows for better understanding the underlying identifiability issues.

Keywords: Metabolic engineering, stoichiometric modeling, parameter estimation, regularization

List of Figures

List of Tables

List of abbreviations and acronyms

3HB	3-hydroxybutyrate
3HHx	3-hydroxyhexanoate
AcCoA	Acetyl coenzyme A
ADP	Adenosine diphosphate
AIC	Akaike information criteria
ATP	Adenosine triphosphate
BIC	Bayesian information criteria
BPG13	1,3-Bisphosphoglycerate
Br	Bromine (atom)
Br_2	Bromine
ButCoA	Butanoyl-CoA
ButenCoA	Butenoyl-CoA
Cat	Catalyst
CButCoA	Keto-butyryl-CoA
CHexCoA	Keto-hexanoyl-CoA
Cit	Citrate
CO_2	Carbon dioxide
DHP	Dihydroxyacetone
DMFA	Dynamic metabolic flux analysis
E	Enzyme
E4P	Erythrose-4-phosphate
ED	Entner–Doudoroff (pathway)

EFM	Elementary flux modes
EFM-NS	Elementary flux modes with null space approach
EFV	Elementary flux vectors
EN	Elastic net
EN-OC	Elastic net with orthogonality constraints
EP	Enzyme-product complex
ES	Enzyme-substrate complex
ExP	Extreme pathways
F16P	Fructose 1,6-bisphosphate
F6P	Fructose-6-phosphate
$FADH_2$	Flavin adenine dinucleotide
FBA	Flux balance analysis
FIM	Fisher information matrix
Fum	Fumarate
FVA	Flux variable analysis
G3P	Glycerinaldehyde-3-phosphate
G6P	Glucose-6-phosphate
GLX	Glyoxylate
H	Hydrogen (atom)
H_2	Hydrogen
HBr	Hydrogen bromide
HButCoA	Hydroxybutyryl-CoA
HexCoA	Hexanoyl-CoA

HexenCoA	Hexenoyl-CoA
HHexCoA	Hydroxyhexanoyl-CoA
I	Inactive enzyme
IsoCit	Isocitrate
KDPG2	2-Keto-3-deoxy-6-phosphogluconate
KG2	α-ketoglutarate
KKT	Karush-Kuhn-Tucker
LP	Linear programming
M	Modifier
Mal	Malate
MFA	Metabolic flux analysis
MLE	Maximum likelihood estimation
NADH	Nicotinamide adenine dinucleotide
NADPH	Nicotinamide adenine dinucleotide phosphate
NLP	Nonlinear Programming
NNZ	Number of nonzero entries
O_2	Oxygen
OAA	Oxaloacetate
ODE	Ordinary differential equations
P	Product
P3HB	Poly-3-hydroxybutyrate
P3HB-co-3HHx	Poly(3-hydroxybutyrate-co-3-hydroxyhexanoate)
PCA	Principal component analysis

PCR	Principal component regression
PEP	Phosphoenolpyruvate
PG2	2-phosphoglycerate
PG3	3-phosphoglycerate
PG6	6-phosphogluconate
PHA	Polyhydroxyalkanoate
PIR	Pyruvate
PP	Pentose phosphate (pathway)
QP	Quadratic programming
Rb5P	Ribose-5-phosphate
Rbl5P	Ribulose-5-phosphate
S	Substrate
S7P	Sedoheptulose-7-phosphate
SQP	Sequential quadratic programming
SSE	Sum of squared errors
Suc	Succinate
SucCoA	Succinyl-CoA
UML	Unified modeling language
X5P	Xylulose-5-phosphate

List of Symbols

Part I - Stoichiometric models for metabolic networks

N	Stoichiometry matrix
m	Total number of internal metabolites
r	Total number of reactions
K	Null space of the the stoichiometry matrix
X_m	Concentration vector for internal metabolites
r_m	Vector of formation rates of internal metabolites
μ	Biomass specific growth rate
v	Flux vector
N_e	Stoichiometry matrix with experimentally measured reaction rates
v_e	Vector with experimentally measured reaction rates
N_u	Stoichiometry matrix with unknown reaction rates
v_u	Vector with unknown reaction rates
r_{exp}	Number of reactions with experimentally measured flux rate
$T^{(j)}$	j^{th} tableau for elementary flux mode/vector calculation
N_{rev}	Stoichiometry matrix with reversible reactions
N_{irr}	Stoichiometry matrix with irreversible reactions
I	Identity matrix
$t_{i,j+1}^{(j)}$	j^{th} tableau entry of row i and column $j+1$
$S(i)$	Set with column indices of zero elements in row i right hand side in $T^{(j)}$
v_{ext}	Vector with external flux rates
ε	Vector of random errors

Σ Covariance matrix of external flux rates

A Matrix with balancing equations for the external fluxes

W Weight matrix

n_{bal} Number of balancing equations

r_{ext} Number of external reactions

$\hat{v}$ Vector with estimated flux rates

f Vector representing a EFM

G Linear equality constraints

n_{eq} Number of equality constraints

b Vector with the right had side of the equality constraints

λ Auxiliary scalar variable

H Inequality constraints

n_{ineq} Number of inequality constraints

c Vector with bound values for inequality constraints

s Slack variables

α A scalar

n_{EFV} Number of elementary flux vectors

y A vector of dimension n

Part II - Regularization of parameter estimation problems

f Objective function

w Vector of unknown variables

n Total number of unknown variables

Q Square symmetric matrix / Hessian matrix

c	A known vector
A	Coefficients for linear constraints (for state variables)
b	Right-hand side of linear constraints
p	Total number of equality constraints / state variables
$\mathcal{L}$	Lagrange function
λ	Vector with Lagrange multipliers
d	Step / Search direction
Z	Null space matrix
α	A scalar that determines the step length in line search algorithms
m_k	Quadratic function approximation of the k^{th} iteration
c_1	Parameter for the first Wolfe condition
c_2	Parameter for the second Wolfe condition
h	Vector function of equality constraints
μ	Barrier parameter
z	Vector with Lagrange multipliers for variable bounds
W	Diagonal matrix with variables w in the main diagonal
$\mathcal{Z}$	Diagonal matrix with Lagrange multipliers z in the main diagonal
e	Vector of ones
H_k	Hessian of the Lagrange function at the k^{th} iteration
I	Identity matrix
Σ_k	Term added to H_k in a interior point algorithm
φ	Objective function with the barrier term
τ	Parameter that limits how close to the bound variables w gets

ρ	Constraint violation
γ_ρ	Parameter for the expression to assess constraint violation improvement
γ_ρ	Parameter for the expression to assess objective value improvement
x	Vector of state variables
θ	Vector of parameters
m	Total number of parameters
D^w	Unknown variables for reduced Hessian calculation
η	Vector of output observations / experiments
L	Total number of observations / experiments
ϵ_ℓ	Noise of the ℓ^{th} observation / experiment
σ^2	Variance
X	Matrix with state variables for all observations / experiments
ε	Vector of independent and identically distributed noise
K	Kernel / Hessian matrix
$\mathbb{V}$	Covariance matrix
V	Matrix of eigenvectors
Λ	Diagonal matrix with eigenvalues in the main diagonal
λ_j	Eigenvalue associated with the j^{th} eigenvector
v_j	Eigenvector associated with the j^{th} eigenvalue
R	Coefficients of linear constraints
r	Right-hand side of linear constraints
q	Number of small eigenvalues
γ	Reduced set of parameters

κ_1 Tuning parameter for the ℓ_1 norm

κ_2 Tuning parameter for the ℓ_2 norm

k_j Kinetic constant of the j^{th} reaction

F Volume flow rate

s Number of output observations for each experiment

ϕ Mapping function between problem variables and output observations

L_H Likelihood function

δ_H Multiple of the identity matrix that modifies the Hessian of the Lagrange function

δ_h Multiple of the identity used when ∇h is linearly dependent

β Threshold for splitting Λ into small and large eigenvalues

t Time

T Temperature

C Coefficients of linear ϕ for the state variables

D Coefficients of linear ϕ for the parameters

B Coefficients for linear constraints for the parameters

ð Columns of matrix D

β_ε Threshold for considering an eigenvalue zero

β_μ Limiting value of the barrier parameter for using eigenvalue-based regularization

$\mathcal{M}$ Set of measured species

$\mathcal{S}$ Complete set of species

$\mathcal{T}$ Set of measurement time points

Contents

1 Introduction

Due to environmental constraints and uncertainties regarding the availability of natural resources, the usage of renewable resources has been of great interest for the industry for the past decades. Alternative routes, such as biochemical, have been widely studied. However, there are still barriers that prevent its vast utilization. The main reason is the need to increase their economic rentability, since there are very few cases in which they can compete with traditional chemical processes. One possible way to overcome this problem is by improving the product yield of microorganisms.

Extensive research is still necessary to increase the efficiency of biochemical routes. Multi-level biological information and technological capacity for genetic manipulation can contribute to this end. In this scenario, several research areas have arisen. System biology and metabolic engineering are examples of such areas. The former treats organisms as a collection of functional modules just as chemical processes are represented by unit operations (ROLLIÉ et al., 2012). Whereas the latter is defined as the enhancement of biochemical products or cellular properties through modifications or addition of metabolic reactions using the recombinant DNA technique guided by the quantitative knowledge of metabolic fluxes (STEPHANOPOULOS, 1999). Applying these areas of knowledge requires computational tools to analyze and interpret how microorganisms work in order to predict the effects of modifications in their metabolism and how they will behave (NIELSEN et al., 2014).

Advances in this field have only been possible due to multidisciplinary groups that were formed worldwide, as it requires solid knowledge of concepts from distinct areas. Chemical engineers are particularly interested in this field, as it requires similar concepts and mathematical tools, such as chemical reactions, optimization and parameter estimation. Molecular biologists have a vast knowledge of biochemistry and genetics, but they tend to have difficulties when dealing with material balance and large amount of data. Hence, researchers from both areas developed techniques, such as metabolic fluxes analysis and flux balance analysis, that require a deep understanding on cellular metabolism and are based on tools already used in process engineering.

Mathematical modeling and simulation of biological systems are the basis of metabolic engineering, playing a fundamental role in characterizing and improving the metabolism of important industrial microorganisms. Understanding how the metabolic fluxes can be distributed inside a microorganism, for example, is a key factor for genetic modification and

adjusting bioprocess conditions in order to increase production efficiency. There are several different types of mathematical models that can be used to represent the metabolism of a microorganism. These models can be categorized into groups according to the level of detail required.

Wiechert (2002) reviewed different metabolic modeling approaches and subdivided them into structural models, stoichiometric models, carbon flux models, mechanistic (kinetic) models and models with gene regulation. According to the author, structural models are merely the graphic representation of a metabolic network with two kinds of nodes: metabolites and fluxes. Stoichiometric models use only the stoichiometry matrix of metabolites and enzymatic reactions. Metabolic flux analysis (MFA) and elementary flux modes (EFM) are common examples of application of such models. Carbon flux models are a special form of MFA using atom transitions to estimate internal flux distribution by experimentally measuring ^{13}C patterns in key metabolites (GUO et al., 2015). Mechanistic models are also based on the stoichiometry matrix, but they use mathematical expressions to describe reaction rates. Models with gene regulation require the most information about the microorganism, as they consider gene expression, which determines enzymatic activity in the metabolic network (WIECHERT, 2002).

Techniques used for modifying genetic material have improved greatly in the past few years (CONG et al., 2013), but system technology has not developed in the same pace when limited data is available. There are several tools available to address problems related to system biology and metabolic engineering; however, due to its complexity and limitation in data availability, it is still not possible to predict the consequences of manipulation of cellular metabolism with high accuracy in any microbial platform; successful cases are still expensive and demand great experimental effort. Despite the remarkable advances in the experimental area, there is room for improvement in the modeling and the data collection fields (NIELSEN et al., 2014).

1.1 Motivation and objectives

Considering the important role that mathematical modeling and simulation play in metabolic engineering, the main motivation of this project lies on developing mathematical tools for studying biological platforms, especially non-model microorganisms. Non-model organisms are those that, for historical or practical reason, have not been selected by

the research community to be extensively studied and, therefore, very few information at molecular and biological level is available. However, non-model organisms may have distinct properties that are worth exploring (RUSSELL et al., 2017). For instance, *Burkholderia sacchari* is a non-model bacteria isolated from sugarcane crops in Brazil that has the potential for producing high-value molecules from renewable carbon sources with five or six carbon atoms (GUAMÁN et al., 2018).

In this context, besides being used to analyze and elucidate properties and behavior of microorganisms, mathematical modeling and simulation are also useful for guiding experimental efforts to collect more information. Stoichiometric modeling is a good starting point; due to its simplicity and consolidated mathematical theory, it can be used to explore different assumptions and scenarios, being able to analyze the flexibility of metabolic networks and identify possibilities of environmental and genetic modification in a macro level. Therefore, some stoichiometric modeling techniques are implemented in this project and their choice is based on the need of better understanding and mastering how models can be used to identify optimal product yield, detect pathways and their importance, and guide experimental design. Although these features might appear simple to a user with mathematical modeling background, they may have some singularities and also help users with experimental leaning background interpret the results.

Even though stoichiometric models have many applications and are useful for metabolic engineering, they are not able to capture nonlinear dynamics to which metabolisms are subjected, which compromises their prediction capabilities. Mechanistic models are appealing in this sense as they can describe more complex behaviors and, thus, provide better predictions. Several approaches to build kinetic models have been proposed, being the ensemble modeling technique probably the most popular, as it requires minimal data (TRAN et al., 2008). However, every framework for kinetic modeling of metabolic fluxes have the limitation of data availability that directly affects parameter identification (STRUTZ et al., 2019).

Motivated by this limitation, regularization of ill-conditioned estimation problems is investigated in this project. Instead of studying frameworks for kinetic modeling, the focus is directed towards understanding how regularization methods work and their application in handling problems with identifiability issues. In addition, extracting and interpreting information that can be obtained with regularization methods based on eigenvalue decomposition is addressed.

1.2 Thesis overview

This doctoral thesis is divided in two parts, the first corresponding to the study of stoichiometric models for metabolic networks, and the second part addresses regularization methods for ill-conditioned parameter estimation problems. In Part I, Chapter 2 introduces the study of stoichiometric models and presents a brief literature review. In Chapter 3, the consolidated modeling techniques and algorithms that are implemented in this project are presented. Chapter 4 describes some key aspects of the development of the software that comprises the stoichiometric models, and a case study analyzing the core metabolism of a non-model microorganism of interest using this software is described in Chapter 5. Chapter 6 concludes the topic.

Part II comprises the investigation of regularization methods, with an introduction and a brief literature review on handling ill-conditioned parameter estimation problems and regularization approaches in Chapter 7. Chapter 8 presents an overview on quadratic and nonlinear optimization, which is a mathematical basis for parameter estimation. Chapter 9 examines linear parameter estimation and discuss constrained-based regularization approaches that minimizes parameter variance. Nonlinear parameter estimation is the topic in Chapter 10, focusing on the implementation of an eigenvalue decomposition based regularization method for line search interior point algorithms that can be used for dealing with ill-conditioned parameter estimation problems. Finally, Chapter 11 concludes this thesis with recommendations for possible future work.

Part I

Stoichiometric models for metabolic networks

2 Introduction

Complex models of microorganisms that can successfully simulate genome-scale representation of metabolisms have been developed and continuously enhanced for model organisms, such as *Escherichia coli* and *Saccharomyces cerevisiae*. However, when working with non-model organisms, those that have not been extensively studied, there is usually not sufficient information to apply these highly detailed models based on the complete genome. Despite that obstacle, non-model organisms are worth investigating, as they can reveal unique properties and have potential economical interest for industrial processes (GUAMÁN et al., 2018; ARMENGAUD et al., 2014). Taking it into consideration, the first part of this thesis describes the implementation of stoichiometric modeling techniques for small and medium metabolic networks that can help elucidate the physiological state of microorganisms and identify means to improve their metabolism to hopefully make their application in biotechnological processes viable.

The selected models implemented in this project are metabolic flux analysis (MFA), elementary flux modes (EFM) and elementary flux vectors (EFV). Metabolic flux analysis is a modeling approach that can only be effective in very few cases, since there are usually many degrees of freedom in the MFA formulation. Nevertheless, it can still be an interesting calculation for preliminary analysis of small networks representing parts of the metabolism or adopting theoretical assumptions (BONARIUS et al., 1996). Elementary flux modes and elementary flux vectors are modeling approaches that can explore all possible minimal pathways of metabolic networks in steady state; with the latter being able to incorporate existing flux information, such as bounds or measurements. The computation of complete sets of EFM and EFV is prohibitively expensive for genome-scale networks and, even for relatively large networks, there can be thousands of EFM or EFV, which can make an objective analysis challenging (QUEK; NIELSEN, 2014). However, for dealing with small or medium metabolic networks, they are an important tool for characterizing the complete set of possible pathways of a network, including the identification of all pathways that lead to the optimal yield, and identifying targets for genetic modification (ZANGHELLINI et al., 2013).

In this part, the theory and description of implementation of the selected stoichiometric models are presented. In addition, a case study focused on the core metabolism of *Burkholderia sacchari* producing polyhydroxyalkanoate (PHA) using this computational tool is discussed. PHA is a group of polyesters that are of interest as bio-derived and biodegrad-

able plastics (DIETRICH et al., 2017). This microorganism is a bacteria that is currently being investigated by our collaborators, so these results are important for a better understanding of its metabolism and for guiding experiments to be performed that can help elucidate the physiological state being analyzed. The case study is also used as an example of the applicability of this software in helping the study of core metabolisms.

2.1 Literature review

2.1.1 Stoichiometric Analysis

Depending on the question being asked, either a simpler or a more complex model can be used to find the answer or at least gain deeper insight. Stoichiometric models are relatively simple and can provide valuable information about the metabolism of a microorganism. They generally require relatively simple information, such as the stoichiometry of the metabolic network and reversibility of each reaction. From the stoichiometry matrix of a metabolic network, it is possible to identify biomass or product theoretical yield, detect pathways and their importance, and analyze the network flexibility. One can also characterize and quantify flux distribution in central metabolisms using experimental data of external metabolites (KLAMT et al., 2014). Stoichiometric analyses are mostly performed under the steady state assumption so, in this case, the system becomes linear, which is an advantage, as methods from linear algebra and convex analysis can be readily applied.

2.1.1.1 Metabolic flux analysis

Metabolic flux analysis is the determination of the metabolic fluxes *in vivo* and plays a fundamental role in metabolic engineering (STEPHANOPOULOS, 1999). When this research area first arose, MFA was conducted by splitting the stoichiometry matrix into a matrix with internal reactions and another with external reactions, whose flux values were experimentally obtained (ANTONIEWICZ, 2015). This approach leads to a linear system where the vector to be calculated normally corresponds to the internal metabolic fluxes. When the stoichiometry matrix has full rank and the number of metabolite balances is equal to the number of these fluxes, the system is said to be determined and has a unique solution; if there are more metabolites, the system is overdetermined and a more rigorous solution is obtained; and

if there are not enough flux measurements and there are fewer metabolite balances, the system is underdetermined and infinite solutions are possible (KLAMT et al., 2014).

When working with a steady state linear stoichiometric model for a metabolic network, almost every case falls into the underdetermined category. However, if a small and simple network can be used to represent a part of interest of the metabolism, MFA can be successfully used. Sridhar and Eiteman (2001) used MFA to analyze the effect of pH and redox potential on the batch fermentation of *C. thermosuccinogenes*. They considered a simplified metabolic network of the fermentation process and were able to build an overdetermined system, which was solved using the least-square method. Metabolic flux analysis of a strain of *E. coli* with amplified malic enzyme activity was also conducted on a simplified metabolic network for anaerobic culture (HONG; LEE, 2001).

A possible way of dealing with underdetermined system is to make a further assumption and treat the model as a linear programming problem; this approach is called flux balance analysis (FBA) (ORTH et al., 2010). Normally, maximizing biomass synthesis is defined as the objective function and measured fluxes are set as restrictions to the model; this way, a mathematical flux distribution is always obtained. FBA has been successfully employed with different purposes, such as the elucidation of cellular regulatory networks (COVERT et al., 2004), the analysis of the metabolic capabilities of a microorganism (FORSTER et al., 2003), and the prediction of the influence of gene knockouts in a cell metabolism (YOSHIKAWA et al., 2017).

2.1.1.2 Metabolic pathway analysis

Metabolic pathway analysis studies the right null space of stoichiometry matrices of metabolic networks, which contains all flux vectors, or pathways, that keep the system in a steady state. The two most consolidated concepts are elementary flux modes (EFM) and extreme pathways (ExP); they are very similar, as both derive from the stoichiometry matrix of internal metabolites and use methods developed in convex analysis, due to the positive constraints imposed by irreversible fluxes. The set of vectors that characterize them needs to have three properties, being the first two common for both approaches: this set is unique up to multiplication by positive scalars for each metabolic network, and each flux vector has the minimal number of reactions necessary to function, if one reaction is removed, the complete pathway ceases to exist. For EFM, the third property states that the set comprises

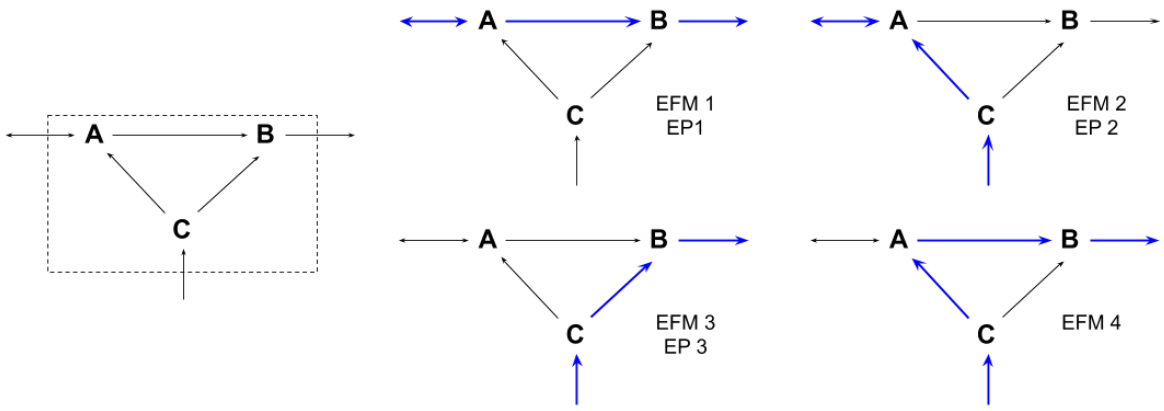

Figure 1 – A simple metabolic network with internal metabolites A, B and C, and the representation of its elementary flux modes and extreme pathways.

all flux vectors that are consistent with the second property; while ExP are independent convex vectors, i.e., each extreme pathway cannot be expressed as a non-negative linear combination of other extreme pathways (PAPIN et al., 2004). Figure 1 shows an example of a simple metabolic network with 3 internal metabolites and 6 reactions; note that this network has 3 ExP and 4 EFM, the fourth EFM can be described as a combination of the first and second EFM. By comparing the third property of both EFM and ExP, it is possible to conclude that extreme pathways are actually a subset of EFM. Since there normally are fewer vectors, calculating ExP tends to be less computationally demanding. Nonetheless, by not providing all possible pathways, it can be difficult to check, for example, the network robustness, since later analysis of extreme pathway combinations can be often very complex (KLAMT; STELLING, 2003).

2.1.1.2.1 Elementary flux modes

The term *elementary flux modes* was first defined by Schuster and Hilgetag (1994), referring to vectors that satisfy all three properties presented earlier. When all reactions in the metabolic network are irreversible, EFM equals ExP. However, in the presence of reversible reactions, the corresponding fluxes do not have sign restriction and the cone is flat, i.e., it contains a vector b_i and its opposite, $-b_i$, also belongs to the cone. Thus, the vectors that span it are not independent, as not all of them lie on an edge of the cone. Figure 2 shows a graphic representation of the EFM for a simple metabolic network with three fluxes; note that the three EFM lie in the plane corresponding to the null space of the stoichiometry matrix and

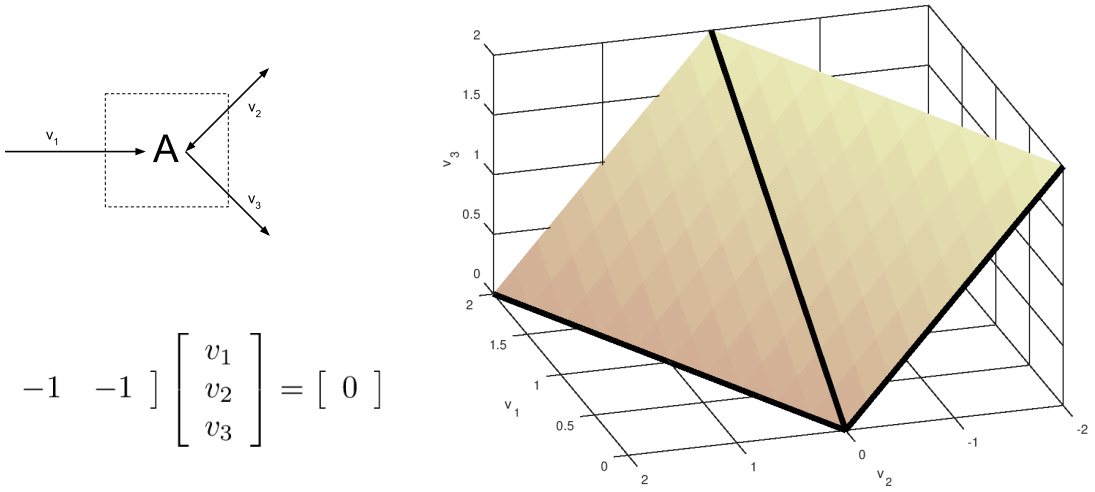

$$\begin{bmatrix} 1 & -1 & -1 \end{bmatrix} \begin{bmatrix} v_1 \\ v_2 \\ v_3 \end{bmatrix} = \begin{bmatrix} 0 \end{bmatrix}$$

Figure 2 – Graphic representation of the EFM (thick lines) of a simple metabolic network with one internal metabolite and three fluxes.

that, due to the presence of a reversible reaction, they are not independent. Nevertheless, this set of generating vectors representing the elementary flux modes can still be considered unique by defining them as the simplest flux vectors satisfying sign restriction that keep the system in steady state. Here, the word *simple* is related to the number of coefficients that are zero, each flux vector in the set cannot be described by non-negative combinations of other vectors that have more zeros. (SCHUSTER et al., 2002; SCHUSTER; HILGETAG, 1994).

Schuster and Hilgetag (1994) proposed the first algorithm for calculating EFM of metabolic networks. It is based on the double description method from convex analysis (MOTZKIN et al., 1953) used for calculating extreme rays of polyhedral cones. This method starts with a cone that initially has some constraints of the network and iteratively adds the remaining ones by using Gaussian elimination on pairs of already calculated extreme rays to create new flux vectors that are then tested to check if they are indeed elementary modes (TERZER; STELLING, 2008). It is very computationally demanding, resulting in an algorithm originally capable of obtaining EFM only for small networks as the number of iterations and memory requirement greatly increase with the size of the network.

Over the years, several improvements have been proposed that enabled the calculation of EFM for larger metabolic networks. The null space approach was the first important modification proposed; it uses a special basis of the null space as the initial cone. This way, more constraints are satisfied at the beginning, leaving less restrictions to be fulfilled iteratively, which considerably reduces computational time (WAGNER, 2004). In addition,

other improvements concerning memory management and algorithm implementation have been incorporated to speed up calculation of EFM (GAGNEUR; KLAMT, 2004; KLAMT et al., 2005; TERZER; STELLING, 2006; TERZER; STELLING, 2008; VAN KLINKEN; VAN DIJK, 2016). Other algorithms have also been proposed, such as one that uses thermodynamic information to limit the number of EFM (GERSTL et al., 2015; PERES et al., 2017) and another that formulates linear programming (LP) optimization problems (GUIL et al., 2020; QUEK; NIELSEN, 2014). With all these enhancements, it is now possible to obtain all EFM for relatively large networks, and identify a subset of EFM for genome-scale metabolic networks.

Despite of their limitation, elementary flux modes are an extremely relevant analysis and have several important applications in systems biology, biotechnology and metabolic engineering. They can be used to identify pathways, i.e., routes that transform substrates into products; assess the network's structural robustness (redundancy); identify the pathways with optimal product yield; check the importance of reactions, usually by the number of EFM they participate in and their flux values; identify correlations among reactions, such as an enzyme subset, when all reactions must operate together; and compute minimal cut sets, which are a minimal set of reactions that must be removed to guarantee that a desired function will fail (GAGNEUR; KLAMT, 2004).

Considering all these applications, EFM are an important tool to aid determining genetic engineering targets. EFM are considered an unbiased method, since it can describe the complete space of possible pathways. This characteristic can be seen as an advantage when compared to biased methods, like flux balance analysis (FBA). Biased methods require a biological optimization objective, usually the maximization of growth, which works well with wild types, but it is not the case when dealing with mutants, as they need time to adapt and often work with suboptimal flux distributions (RUCKERBAUER et al., 2015). Carlson and Srienc (2004) were the first to propose using EFM for identifying gene deletions to minimize the functionality of the cell metabolism, allowing to direct the fluxes to the production of the desired metabolite, for example. Trinh and Srienc (2009) designed an *E. coli* mutant strain to convert glycerol into ethanol efficiently by employing this approach. EFM analysis has also been used to design a *Pseudomonas putida* mutant to increase the production of polyhydroxyalkanoate (PHA) on glucose (POBLETE-CASTRO et al., 2013). Other authors have also successfully used this technique for targeting genetic modification (UNREAN et al., 2010; TRINH et al., 2011).

As already mentioned, a metabolic network can have a large number of EFM, e.g. medium networks may even contain millions of EFM, which confirms the robustness and adaptability of cellular metabolisms. However, not all of them are thermodynamically feasible or physiologically reachable (FERREIRA et al., 2011). Besides, any flux distribution in steady state can be expressed as a non negative linear combination of its EFM and, for a given distribution, only some elementary modes are active. Identifying only the EFM that explain a flux distribution can be an important asset to help focusing the pathway analysis on physiologically active processes, especially for large networks (VON STOSCH et al., 2016; ODDSDÓTTIR et al., 2016).

Several methods have been proposed for determining the weights of each EFM of a metabolic network that reconstruct a flux distribution. The first one, named α-*spectrum*, uses a LP formulation to calculate the lowest and highest value for each coefficient α_i, which represents the weight of each EFM (WIBACK et al., 2003). Some authors proposed approaches that select one solution by using external flux measurements and adopting a hypothesis, such as minimum norm (POOLMAN et al., 2004), minimum number of active EFM (SCHWARTZ; KANEHISA, 2005), maximum number of active EFM (NOOKAEW et al., 2007), assuming EFM are random events and maximizing Shanon's entropy (ZHAO; KURATA, 2009), and assuming EFM are latent variables, like in principal component analysis (PCA), and maximizing the variance in flux data (VON STOSCH et al., 2016). These are all mathematical assumptions and there is no way to be sure if they have biological meaning. Some authors also group the EFM according to their overall stoichiometry, since external flux data alone is usually not capable of differentiating redundant paths. This approach narrows the number of possible pathways, but the problem is usually still underdetermined and more information or assumptions are needed (WLASCHIN et al., 2006; VON STOSCH et al., 2016).

2.1.1.3 Elementary flux vectors

Elementary flux vectors (EFV), first proposed by Urbanczik (2007), are very similar to EFM, but they are capable of incorporating flux information, such as measurements and bounds. In geometrical terms, differently from EFM that only enumerate edges and other important rays of the flux cone, the addition of constraints results in a general polyhedron which vertices are EFV, as illustrated in Figure 3. FBA searches the same polyhedron using a LP algorithm to find one solution that lies in one vertex; however, for metabolic models, the

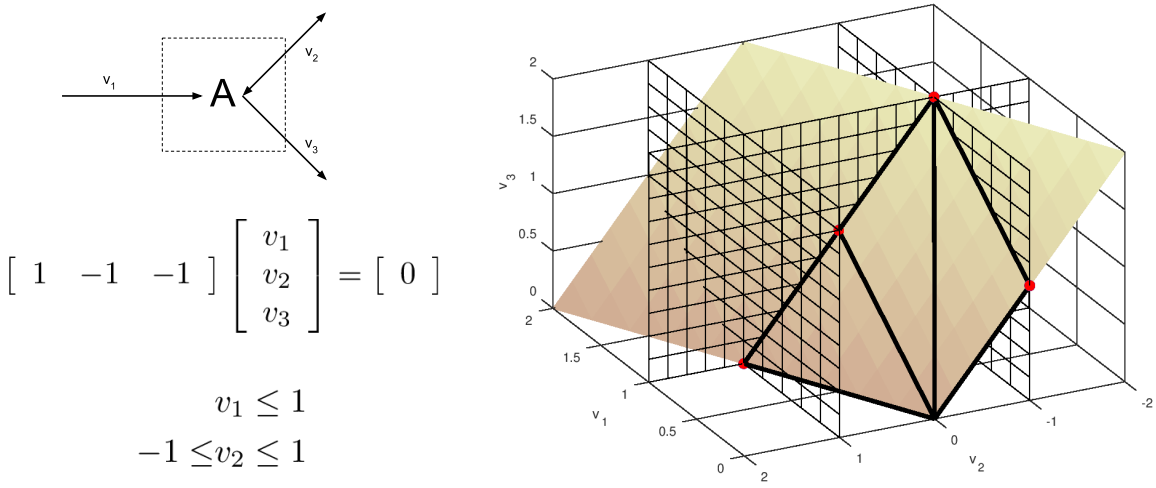

Figure 3 – Graphic representation of the EFV (red dots) of a simple metabolic network with one internal metabolite and three fluxes with bounds defined for two of them.

occurrence of multiple solutions is common. Therefore, when compared to FBA, EFV have the advantage of identifying all pathways that satisfy the optimization problem described by FBA maximizing or minimizing any chosen flux and respecting the same constraints.

The three properties that define a set of EFM, namely being unique for every metabolic network, each flux vector having the minimal number of reactions necessary to function, and being the set comprises all flux vectors that are consistent with the second property, are partially properties of EFV as well. The only difference is regarding the second property; if a reaction is removed from an EFV, it may or may not cease to function, for example, two parallel reactions might be active. However, EFV can be interpreted as minimum vectors in the sense that they represent the minimum set of reactions necessary to keep the metabolic network in steady state while respecting the imposed constraints (KLAMT et al., 2017).

Algorithms used for computing EFM are suited for calculating EFV, requiring only a different initial matrix for the iterative process; testing criteria and combination of rows follow the exact same logic. Therefore, as it is the case for EFM, enumerating EFV is computationally expensive and they cannot be computed for genome-scale networks, only for small to relatively large networks when using more efficient algorithms. Although smaller than the number of EFM due to the constraints, the number of EFV can still reach thousands (KLAMT et al., 2017).

Similarly to EFM, EFV are an important modeling technique. In fact, they have the same applications, such as identify all important reaction properties, assess robustness

of a metabolic network, and identify genetic targets, and identify pathways with maximum yield. However, because flux information can be incorporated, EFV is able to identify the maximum and minimum flux values in each reaction, which is the goal of flux variability analysis (FVA), a technique based on FBA (KLAMT et al., 2017). This information can be helpful, for example, for assessing network robustness under some fixed conditions (THIELE; GUDMUNDSSON, 2010).

Now, oppositely to EFM, EFV have not become so popular yet and there are only few works in literature using this modeling approach. Kamp and Klamt (2017) use EFV to test the feasibility of growth-coupled production of five metabolites for a small network of the core metabolism of *E. coli*. EFV has also been used to determine bounds for internal fluxes in a dynamic metabolic flux analysis (DMFA) that approximated time intervals to a pseudo steady state (FERNANDES et al., 2016). De Groot et al. (2019) show that, for metabolisms aiming optimal growth in growth-limiting situations, only a small number of EFM are active pathways or, equivalently, only one EFV.

2.1.2 Computational tools for stoichiometric modeling

Several computational tools have been developed, especially during the last 15 years, in the context of metabolic engineering. The COBRA Toolbox is probably one of the most popular tools for constraint-based modeling and analysis of metabolic network focusing on FBA. It started as a MATLAB® package (BECKER et al., 2007; SCHELLENBERGER et al., 2011), but has recently been turned into an open source project, with versions for MATLAB®, Python and Julia (HEIRENDT et al., 2019). Optflux is a standalone software developed in Java also for constrained-based modeling (ROCHA et al., 2010).

Metatool is the most popular tool for calculating elementary flux modes. Its first version was developed in C/C ++ as a standalone software, while Metatool 5.0, and later version 5.1, was implemented with a more efficient algorithm in MATLAB and Octave to facilitate the analysis of the results (PFEIFFER et al., 1999; VON KAMP; SCHUSTER, 2006). FluxModeCalculator is another tool that can calculate EFM written in MATLAB® which incorporates several solutions for improving performance (KLINKEN; DIJK, 2016).

CellNetAnalyzer is a MATLAB toolbox that performs several stoichiometric analysis, including MFA, FBA, EFM, and EFV. It is also possible to explore scenarios for minimal cut sets. This tool can be used from the command line or within an interface capable of

displaying a graphic representation of the metabolic network analyzed (KLAMT et al., 2007; KLAMT; VON KAMP, 2011; KAMP et al., 2017). COPASI is a complete tool developed for the study of metabolic fluxes capable of performing various types of analyses, including stoichiometric analysis of networks, like mass conservation and EFM, optimization of a metabolic model, and sensitivity analysis. (HOOPS et al., 2006).

3 Fundamentals

3.1 Identification of coupled and blocked reactions

Identifying coupled and block reactions is an important analysis to perform when dealing with stoichiometric models in steady state. Coupled reactions have a fixed flux ratio and are controlled by an enzyme subset, which is a group of enzymes that operate as a unit. Since they always work together with the same proportion, a single reaction can be used to represent them all. Blocked reaction have zero fluxes and can be removed from the network when working in steady state. This way, metabolic networks can be reduced before performing expensive analysis, such as EFM.

Assuming the stoichiometry matrix of internal metabolites $N \in \mathbb{R}^{m \times r}$ has full rank, matrix $K \in \mathbb{R}^{r \times r-m}$, which columns form a basis of the null space of N, also represents the space of all fluxes that keep the system at steady state, since

$$NK = 0 \tag{3.1}$$

by definition. This means that every flux distribution that can keep the system at steady state can be described as a combination of the columns of K. Each row of K corresponds to a reaction described by the columns of N. Blocked reactions can be identified by rows of K that are null vectors because for any combination of the columns of N, their coefficients are always zero. If every row K is divided by its largest coefficient, then equal rows indicate that the corresponding reactions are coupled (PFEIFFER et al., 1999).

3.2 Metabolic flux analysis

The idea of MFA is to calculate unknown intracellular fluxes from measured external fluxes. It does so by splitting the stoichiometry matrix and formulating a system of linear equations that represents the mass balances of each metabolite. Using only basic linear algebra concepts, two cases can be modeled with MFA: determined and overdetermined systems. One starts with the mass balance equations given by

$$\frac{dX_m}{dt} = r_m - \mu X_m \tag{3.2}$$

where $X_m \in \mathbb{R}_+^m$ is the concentration vector for the internal metabolites, $r_m \in \mathbb{R}_+^m$ is the vector of formation rates of internal metabolites, and $\mu \in \mathbb{R}_+$ is the biomass specific growth rate. At

this point, two hypotheses can be assumed. The first one considers intracellular metabolites to be at steady state. The other neglects the second term of equation 3.2, which represents the dilution of the metabolite pool due to growth, as it can be proved its effect is very small compared to other fluxes that affect the metabolites (STEPHANOPOULOS et al., 1998).

This way, mass balance equations are simplified to

$$r_m = 0 = Nv \tag{3.3}$$

and the formation rates of intracellular metabolites can be expressed by the product of the stoichiometry matrix, $N \in \mathbb{R}^{m \times r}$, and the flux vector with the rate of all reactions involved, $v \in \mathbb{R}^r$. This product can be split into two terms

$$Nv = N_e v_e + N_u v_u = 0 \tag{3.4}$$

$N_e \in \mathbb{R}^{m \times r_{\text{exp}}}$ and $v_e \in \mathbb{R}^{r_{\text{exp}}}$ comprise only the reactions with experimentally measured flux rates, $N_u \in \mathbb{R}^{m \times r - r_{\text{exp}}}$ and $v_u \in \mathbb{R}^{r - r_{\text{exp}}}$ consist of the stoichiometry matrix and flux vector with the unknown reactions to be determined. If the number of unknown fluxes is the same as the number of internal metabolites and N_u is invertible, the linear system is determined and the unknown flux vector can be obtained by

$$v_u = -N_u^{-1} N_e v_e \tag{3.5}$$

In cases where N_u is full rank and there are more measured fluxes than degrees of freedom in system 3.3, an estimate of the unknown flux vector can be obtained by applying the least squares method in the overdetermined system, i.e., the pseudo-inverse of Nu should be used in (3.5) instead of Nu^{-1}.

3.3 Elementary flux modes

The algorithm presented by Schuster and Hilgetag (1994) derives from an algorithm developed in convex analysis for finding generating vectors. It starts by creating an initial tableau formed by the stoichiometriy matrix $N \in \mathbb{R}^{m \times r}$ augmented with an identity matrix of appropriate size; with the reactions grouped in two blocks, one comprising the reversible reactions and the other with the irreversible reactions

$$T^{(0)} = \left[\begin{array}{c|cc} N_{\text{rev}}^T & I & 0 \\ \hline N_{\text{irr}}^T & 0 & I \end{array}\right]; \tag{3.6}$$

note that the transpose of N must be used. This is an iterative process and the number of tableaux used is equal to the number of rows in N. In the end, the elementary flux modes are represented by the rows of the right-hand part, while the left-hand part, initially N, becomes the null matrix. A new tableau, $T^{(j+1)}$, is built by combining the rows in $T^{(j)}$ with each other in a way that all new rows have zero entry at position $j+1$ in the left-hand part. If both rows are in the irreversible flux block, then

$$t_{i,j+1}^{(j)} \times t_{k,j+1}^{(j)} < 0, \tag{3.7}$$

since they can only be multiplied by positive coefficients when combined. However, when a row from the reversible flux block is involved, this row can be multiplied by a negative coefficient and inequality (3.7) does not need to hold. When adding a new row to tableau $T^{(j+1)}$, reversibility of the rows must be respected; only if both rows are reversible the new row must be added to the reversible flux block. However, only a subset of the new rows can be added to the next tableau. For each row i of the right-hand part of each $T^{(j)}$, $S(i)$ is defined as the set comprising the column indices of elements that are zero. The new rows generated from combinations and the rows that already have zero entry at $j+1$ position must fulfill the condition

$$S(i) \cap S(k) \not\subseteq S(l) \text{ with } l \neq i, k, \tag{3.8}$$

to be added to $T^{(j+1)}$.

To illustrate the algorithm just presented, consider the simple metabolic network in Figure 2 with one internal metabolite and three reactions, being the second reaction reversible. The stoichiometry matrix of this metabolic network is

$$N = \begin{bmatrix} 1 & -1 & -1 \end{bmatrix}, \tag{3.9}$$

so the initial tableau is given by

$$T^{(0)} = \left[\begin{array}{c|ccc} -1 & 1 & 0 & 0 \\ \hline 1 & 0 & 1 & 0 \\ -1 & 0 & 0 & 1 \end{array}\right], \tag{3.10}$$

with the first column in the right-hand side corresponding to v_2, the second column to v_1 and the last column to v_3. To create the next tableau, rows 1 and 2 can be summed to create a row with zero entry in the first position of the right-hand side and $S(1) \cap S(2) = \{3\}$ in the left-hand side. It can be added to $T^{(1)}$ since index 3 is not present in $S(3) = \{1, 2\}$. Because

the first row corresponds to a reversible reaction, it can be multiplied by -1 and added to row 3. This new row can also be added to the next tableau as is also satisfies 3.8. Finally, rows 2 and 3 can be combined and added to $T^{(1)}$ since they satisfy both 3.7 and 3.8, resulting in

$$T^{(1)} = \left[\begin{array}{c|ccc} 0 & 1 & 1 & 0 \\ 0 & -1 & 0 & 1 \\ 0 & 0 & 1 & 1 \end{array}\right]. \tag{3.11}$$

Since the left-hand side of 3.11 is the zero matrix, calculation is complete and the right-hand side corresponds to the set of EFM of 3.9. Because of all the EFM involve at least one irreversible reaction, they were all irreversible.

The original methodology (SCHUSTER; HILGETAG, 1994) is important for understanding in depth how the calculation of elementary flux modes works. However, ten years after it was published, Wagner (2004) proposed a different algorithm that considerably reduced computational time, called the null space approach. In this algorithm, the initial tableau is matrix $K^T \in \mathbb{R}^{r-m\times r}$, the transpose of the null space of $N \in \mathbb{R}^{m\times r}$, written in the form

$$T^{(0)} = K^T = [K' \;\; I], \tag{3.12}$$

where $K' \in \mathbb{R}^{r-m\times m}$ and $I \in \mathbb{R}^{r-m\times r-m}$. This algorithm works based on the fact that an EFM can only have $m+1$ non zero entries at most. With this method only m tableaux are generated. A new tableau $T^{(j+1)}$ starts as a copy of the previous one, and new rows are created by combining all rows of $T^{(j)}$ that have non zero entries in position $j+1$ so there is a zero entry in that position. Similarly to the original algorithm, a row can only be multiplied by a negative coefficient if all reactions in that row are reversible and a new row can be added if it satisfies (3.8). In the end of a new tableau iteration, column $j+1$ in $T^{(j+1)}$ must be the null vector. After the last tableau is computed, all rows with fluxes violating reversibility constraints must be removed.

3.4 Linear steady state data reconciliation

From a mathematical point of view, data reconciliation is a parameter estimation problem. If, for example, all external fluxes are measured, they can be modeled as

$$v_{\text{ext}} = v + \varepsilon \tag{3.13}$$

where v_{ext} is the vector of external fluxes, $v \in \mathbb{R}^{r_{\text{exp}}}$ is a flux vector representing their true values and $\varepsilon \sim \mathcal{N}(0, \Sigma)$ is vector of random errors assumed to follow a normal distribution with covariance matrix $\Sigma \in \mathbb{R}^{r_{\text{exp}} \times r_{\text{exp}}}$. Vector v is the parameters to be estimated, and formulating a least squares problem for the estimation leads to the objective function

$$\hat{v} \in \arg\min_{v} \quad (v_{\text{ext}} - v)^T W (v_{\text{ext}} - v). \tag{3.14}$$

where $W \in \mathbb{R}^{r_{\text{exp}} \times r_{\text{exp}}}$ is a weight matrix. Constraints for v are given by

$$Av = 0, \tag{3.15}$$

where $A \in \mathbb{R}^{n_{\text{bal}} \times r_{\text{ext}}}$ is a matrix with n_{bal} rows corresponding to balancing equations that represent conservation. Based on a single global equation involving all substrates and products, the rows of A can correspond to the number of carbon atoms in each metabolite and the oxidation state, for example.

For a linear system in steady state, (3.14) has an analytical solution

$$\hat{v} = v_{\text{ext}} - W^{-1} A^T (A W^{-1} A^T)^{-1} A v_{\text{ext}}, \tag{3.16}$$

where $\hat{v} \in \mathbb{R}^{r_{\text{ext}}}$ is a vector with estimates for the true value of the external fluxes. When the errors follow a normal distribution with zero mean, as it was assumed here, matrix W can be defined as the inverse of their covariance matrix. If the fluxes are considered independent from each other, Σ is a diagonal matrix with the variance of each measured flux in the corresponding entry of the diagonal. If a weight matrix is not used, W can be defined as an identity matrix of appropriate size (NARASIMHAN; JORDACHE, 1999).

3.5 Elementary flux vectors

Elementary flux vectors can be computed applying the same algorithms used for calculating elementary flux modes (KLAMT et al., 2017). The initial tableau still has the same form as Equation (3.6); however, instead of using the stoichiometry matrix N, a matrix that also takes into consideration the constraints must be used. All EFM keep the metabolic network in steady state, therefore they satisfy the equation

$$Nf = 0 \tag{3.17}$$

where $f \in \mathbb{R}^r$ is a flux vector representing an EFM.

When dealing with equality constraints, for example fixing values for external fluxes, f represents an EFV and, besides satisfying (3.17), it must also satisfy the constraints. These conditions can be written as

$$\begin{bmatrix} N & 0 \\ G & -b \end{bmatrix} \begin{bmatrix} f \\ \lambda \end{bmatrix} = 0 \tag{3.18}$$

where $G \in \mathbb{R}^{n_{\text{eq}} \times r}$ is a matrix with n_{eq} rows corresponding to equality constraints, $\lambda \in \mathbb{R}$ is an auxiliary scalar variable and $b \in \mathbb{R}^{n_{\text{eq}}}$ is the right-hand side of the equality constraints, and the matrix in the left-hand side of (3.18) is defined as $D \in \mathbb{R}^{m+n_{\text{eq}} \times r+1}$. For computing EFV, D can replace N to form the initial tableau; if, for example, the original algorithm is used, $T^{(0)} = [D \ \ I]$. After EFV are computed, if $\lambda = 0$ the corresponding EFV is unbounded, like an EFM, and if > 0, the bounded EFV is given by f/λ.

When flux bounds are added as constraints, D is slightly different. Inequalities must first be converted to equality constraints by using slack variables, which are free variables that determine how far from the bounds the fluxes are. So, the conditions that an EFV must fulfill are represented by

$$\begin{bmatrix} N & 0 & 0 \\ G & 0 & -b \\ H & I & -c \end{bmatrix} \begin{bmatrix} f \\ s \\ \lambda \end{bmatrix} = 0 \tag{3.19}$$

where $H \in \mathbb{R}^{n_{\text{ineq}} \times r}$ is a matrix with n_{ineq} rows corresponding to inequality constraints, $s \in \mathbb{R}^{n_{\text{ineq}}}$ is a vector with the slack variables and $c \in \mathbb{R}^{n_{\text{ineq}}}$ is a vector with bound values.

4 Software development

A computational tool for stoichiometry analysis of metabolic networks was developed using the C++ language. This language was chosen for being free, fast, one of the most popular languages currently in use, which consequently implies availability of many resources and community support; and object oriented, which is an important asset for structuring software. Eigen, which is a template library for C++, was used for linear algebra calculation (GUENNEBAUD et al., 2010).

4.1 Structure

This software was built using the object oriented programming paradigm, based on hierarchy, composition concepts, and polymorphism, to facilitate maintenance and addition of new functionalities. Design patterns (GAMMA et al., 1995), which are well-established solutions for common problems in software design, were implemented where applicable. This way, every feature of this software can be easily connected to the metabolic network and each other. Figure 4 presents a simplified UML diagram for this software; a central block connects a metabolic network with the modeling techniques.

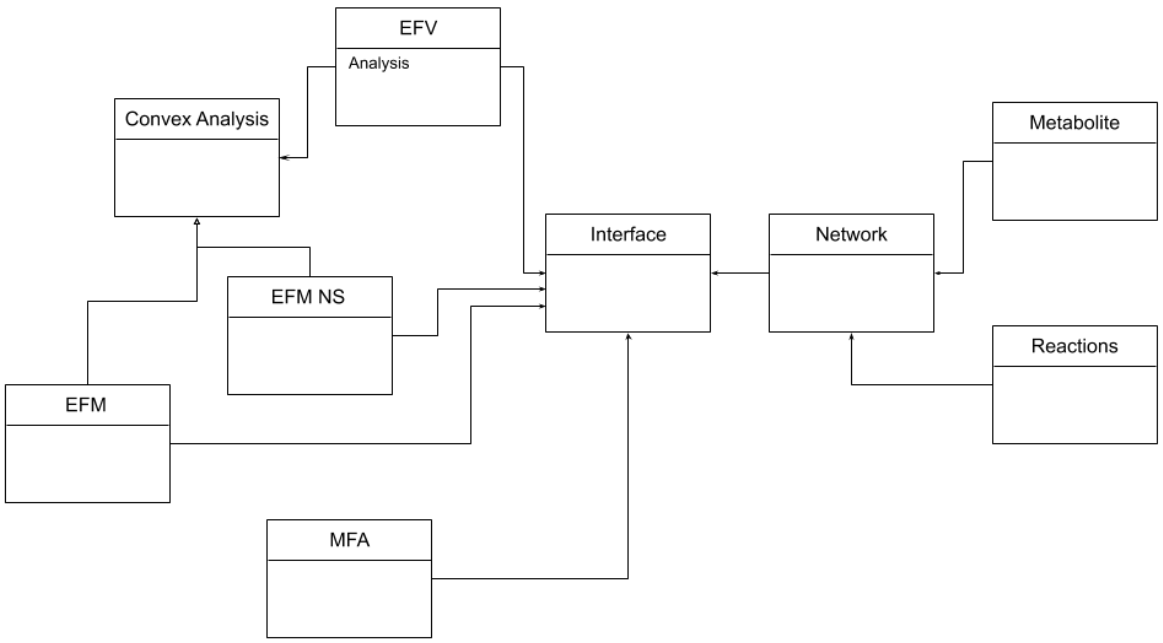

Figure 4 – Simple UML diagram of the main blocks (classes) that compose this software for stoichiometric analysis of metabolic networks.

The stoichiometric models and main supporting features implemented in this computational tool are:

- metabolic flux analysis,
- elementary flux modes,
- elementary flux vectors,
- analysis of elementary flux vectors for experimental design.

MFA was applied as described in Section 3.2 using linear algebra functions. Two algorithms were implemented for calculating EFM and EFV, the original routine (EFM) and the null space approach (EFM-NS) (SCHUSTER; HILGETAG, 1994; WAGNER, 2004). Analysis of elementary flux vectors for experimental design comprises the calculation of some properties from EFV, including a similarity measure for the flux pattern that each reaction present in the set of EFV. These properties are described with more details in the next section.

Other supporting features include

- processing the input metabolic network to verify its consistency,
- treatment of elementary flux modes to help categorize and go through the large number of EFM that metabolic networks usually have,
- identifying coupled and blocked reactions, as presented in Section 3.1, to reduce the metabolic network and, consequently, improve the computation of EFM and EFV,
- performing data reconciliation on experimental measurements used as constraints for calculating EFV as described in Section 3.4.

This last feature is necessary because EFV are a deterministic model, therefore errors in flux measurements can hamper their computation when equality constraints are used, i.e., fixed values for some fluxes. There are basically two ways to readily deal with this issue: relaxing the tolerance during EFV calculation or perform data reconciliation on flux measurements. Because some fluxes are easier to determine than others and they can present different variances, data reconciliation was implemented using carbon and redox balances. Treatment of EFM consists of removing thermodynamically infeasible EFM with no substrate uptake, calculating each EFM yield by dividing the EFM by the flux of the main substrate (defined as the first substrate listed at input), and grouping EFM with the same overall stoichiometry, which helps to identify redundant pathways of the metabolic network.

4.2 Analysis of elementary vectors for experimental design

As already mentioned, EFV can be used for extracting information about the physiological state of a metabolism that can help design experiments to detect active pathways in the metabolic network. The properties calculated by the software with that purpose are

- upper and lower bounds for each reaction, which can indicate essential and inactive reactions in the physiological state being analyzed,
- identification of sets of reactions that are completely correlated,
- cosine similarity among the groups of reactions and independent reactions.

Reactions that are completely correlated operate with a fixed relationship in every EFV. If $EV \in \mathbb{R}^{n_{\text{EFV}} \times r}$ is defined as a matrix containing all EFV thermodynamically feasible, where each row is an EFV and each column $v_i \in \mathbb{R}^{n_{\text{EFV}}}$ corresponds to a vector with the value of the i^{it} reaction in each EFV, a set of correlated reactions arises as columns with the same value up to a scalar, $v_i = \alpha v_j$. Also, if a reaction is reversible and has positive and negative values among the EFV, each direction is considered a different reaction and they belong to different sets or are independent reactions. This is done because both directions of a reversible reaction have different functions in the network and they should be analyzed according to them.

Cosine similarity is used here to identify reactions and paths in the metabolic network that are redundant and never operate together when considering minimal pathways. It is a measure of similarity between two vectors defined as

$$\text{sim}(y_1, y_2) = \frac{y_1^T y_2}{||y_1||_2 ||y_2||_2} \tag{4.1}$$

where $y_1, y_2 \in \mathbb{R}^n$ (DEHAK et al., 2010). In other words, it is the cosine of the angle between two vectors and represents how close their directions are; if the cosine is 0, they make a 90 degree angle, and if it is 1 or -1, they point to the same direction. Figure 5 shows a graphic representation of the vectors used for cosine similarity representing the flux values considering three EFV for a simple metabolic network with one metabolite and three fluxes with bounds defined for two of them. For the analysis of the cosine similarities, not every pair (v_i, v_j) is compared; only one reaction in each group and independent reactions are selected. However, these reactions must meet the condition that the upper and lower bounds either have opposite signs or one of them is zero; reactions that are active in every EFV are

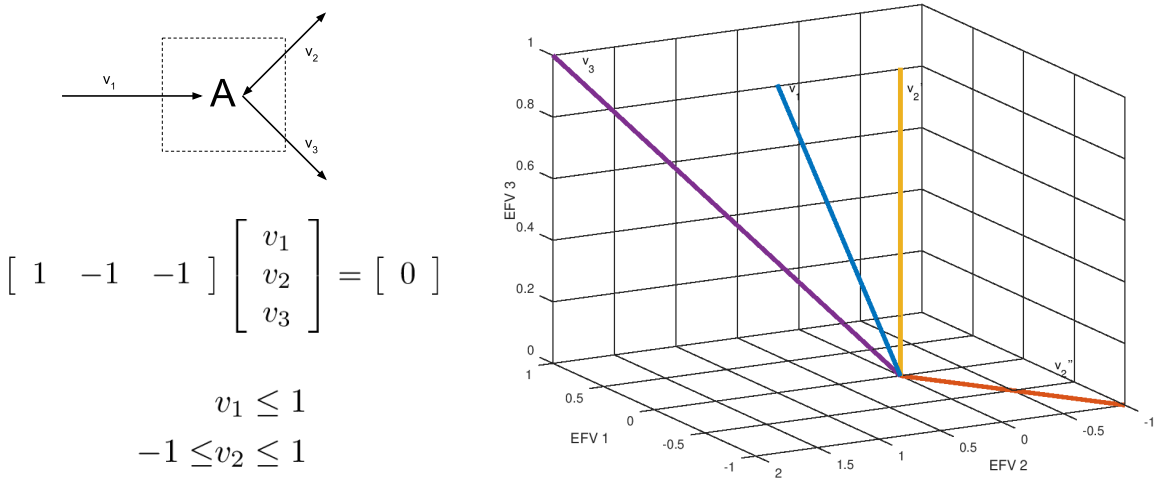

Figure 5 – Graphic representation of the flux vectors for the cosine similarity calculation obtained from three EFV of a simple metabolic network with one internal metabolite and three fluxes with bounds defined for two of them.

essential and there is no alternative for them in the metabolic network. The idea here is to identify reactions or set of reactions that have the same function in the metabolic network and help one decide where to direct effort for collecting more information to better understand the physiological state of the microorganism being analyzed.

5 Case study: *Burkholderia sacchari*

Burkholderia sacchari is a bacteria that produces PHA when an essential nutrient is limited and no-growth conditions are enforced. For this study, the core metabolism producing poly-3-hydroxybutyrate (P3HB) and poly(3-hydroxybutyrate-co-3-hydroxyhexanoate) (P3HB-co-3HHx) is analyzed using the software developed during this project. The network used to represent this metabolism consists of 54 metabolites, of which 8 are considered external, and 54 reactions, of which 12 are reversible. The input file used with the list of reactions and metabolites is presented in Appendix A.1. The metabolic network used to represent this metabolism was built based on the metabolic network used by Mendonça (2014), from where experimental measurements of external fluxes were also obtained. Figure 6 shows a graphic representation of this network, which includes the Entner–Doudoroff (ED) pathway (red) and its cyclic mode (purple), the pentose phosphate (PP) pathway (blue), the Krebs cycle (orange), the glyoxylate cycle (light green), anaplerotic reactions (yellow), transhydrogenase reactions (dark yellow), oxidative phosphorylation of NADH and $FADH_2$, and beta-oxidation of the hexanoic acid (pink). It also includes P3HB synthesis from Acetyl-CoA and two routes are considered for PHA production from hexanoic acid, two reactions encoded by the PHAJ gene (dark green) and ketoreductase (dark red).

Elementary flux modes were calculated with both implemented algorithms and with Metatool (VON KAMP; SCHUSTER, 2006) for comparison; they all resulted in the same set of 73 EFM. After removing the thermodynamically infeasible EFM with no susbstrate uptake, the remaining 70 are presented in Appendix A.2. Two conditions are considered in this case study, one using only glucose as substrate and producing P3HB and another also using hexanoic acid for the addition of the co-monomer 3HHx to P3HB leading to the synthesis of the co-polymer P(3HB-co-3HHx). From a biotechnological point of view, the synthesis of co-polymers is interesting because they can provide different material properties to the polymer according to its composition.

5.1 Synthesis of P3HB

To illustrate how the features implemented in the software can aid in pathway analysis, consider first the condition in which only P3HB is produced using only glucose. Table 1 shows the 11 possible pathways that do not consume hexanoic acid. The second row indicates

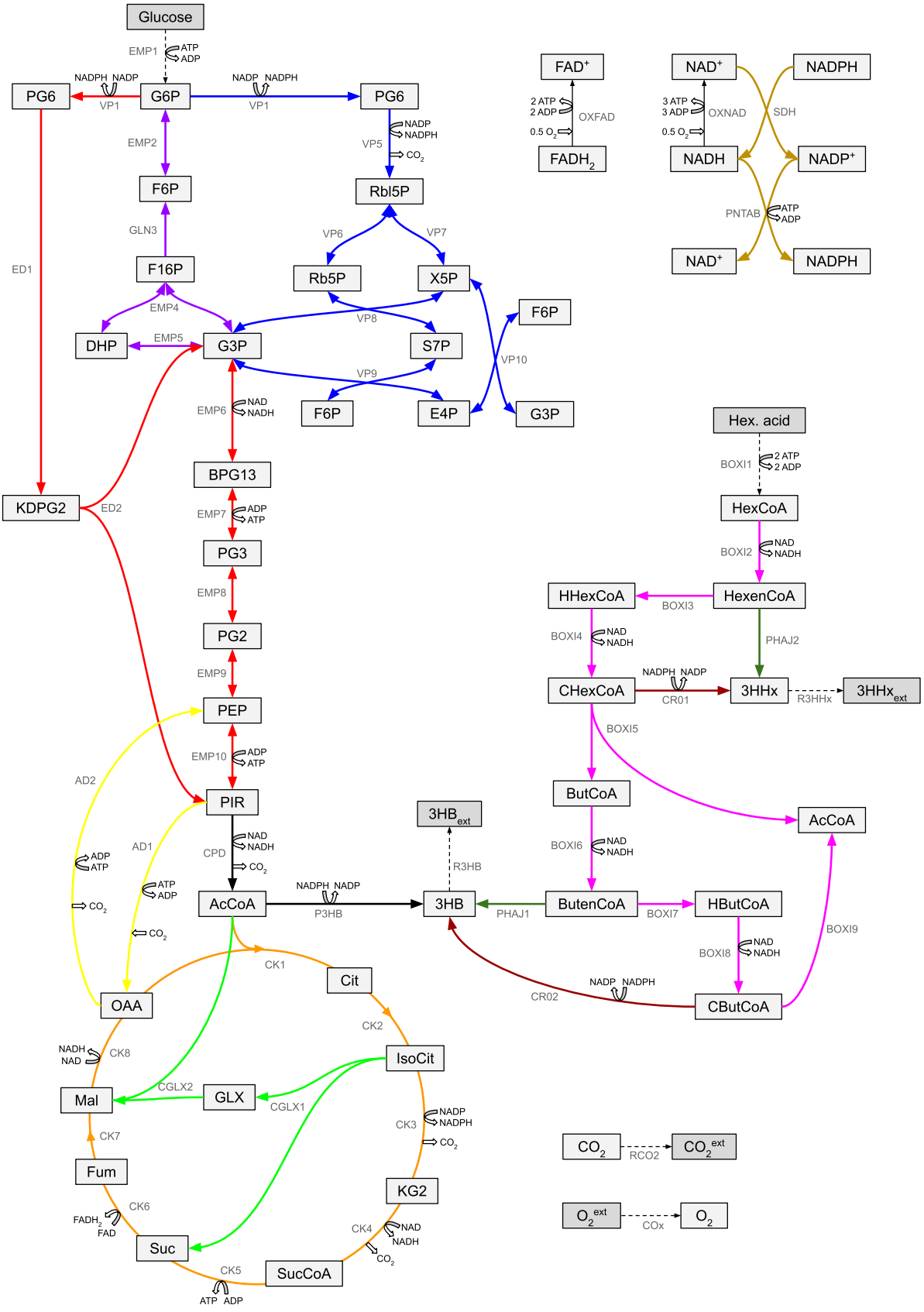

Figure 6 – Metabolic network used to represent the central metabolism of *B. sacchari* producing P3HB and P3HB-co-3HHx.

Table 1 – Subset of EFM that takes only glucose as substrate obtained for the metabolic network used to represent the core metabolism of *Burkholderia sacchari*.

EFM	**1**	**2**	**3**	**4**	**5**	**6**	**7**	**8**	**31**	**43**	**44**
Group	1	1	1	1	1	1	1	1	16	20	20
EMP2	-	-1	-3	-5	-2	-2	-	-1	-2	-1	-
EMP4	-	-1	-3	-1	-	-	-	-1	-	-1	-
EMP5	-	-1	-3	-1	-	-	-	-1	-	-1	-
EMP6	1	-	-2	-	1	1	1	-	1	-	1
EMP7	1	-	-2	-	1	1	1	-	1	-	1
EMP8	1	-	-2	-	1	1	1	-	1	-	1
EMP9	1	-	-2	-	1	1	1	-	1	-	1
VP6	-	-	-	2	1	1	-	-	1	-	-
VP7	-	-	-	4	2	2	-	-	2	-	-
VP8	-	-	-	2	1	1	-	-	1	-	-
VP9	-	-	-	2	1	1	-	-	1	-	-
VP10	-	-	-	2	1	1	-	-	1	-	-
ED1	1	2	4	-	-	-	1	2	-	2	1
ED2	1	2	4	-	-	-	1	2	-	2	1
EMP10	3	2	-	-	2	1	1	-	1	-	1
CPD	4	4	4	-	2	1	2	2	1	2	2
VP1	1	2	4	6	3	3	1	2	3	2	1
VP5	-	-	-	6	3	3	-	-	3	-	-
CK1	2	2	2	-	1	1	2	2	-	-	-
CK2	2	2	2	-	1	1	2	2	-	-	-
CK3	-	-	-	-	-	1	2	2	-	-	-
CK4	-	-	-	-	-	1	2	2	-	-	-
CK5	-	-	-	-	-	1	2	2	-	-	-
CK6	2	2	2	-	1	1	2	2	-	-	-
CK7	2	2	2	-	1	1	2	2	-	-	-
CK8	4	4	4	-	2	1	2	2	-	-	-
CGLX1	2	2	2	-	1	-	-	-	-	-	-
CGLX2	2	2	2	-	1	-	-	-	-	-	-
GLN3	-	1	3	1	-	-	-	1	-	1	-
AD1	-	-	-	-	-	-	-	-	-	-	-
AD2	2	2	2	-	1	-	-	-	-	-	-
P3HB	-	-	-	-	-	-	-	-	0,5	1	1
OXFAD	2	2	2	-	1	1	2	2	-	-	-
OXNAD	10	10	10	12	11	11	10	10	7.5	3	3
BOXI2	-	-	-	-	-	-	-	-	-	-	-
BOXI3	-	-	-	-	-	-	-	-	-	-	-
BOXI4	-	-	-	-	-	-	-	-	-	-	-
BOXI5	-	-	-	-	-	-	-	-	-	-	-
BOXI6	-	-	-	-	-	-	-	-	-	-	-
BOXI7	-	-	-	-	-	-	-	-	-	-	-
BOXI8	-	-	-	-	-	-	-	-	-	-	-
BOXI9	-	-	-	-	-	-	-	-	-	-	-
PHAJ1	-	-	-	-	-	-	-	-	-	-	-
PHAJ2	-	-	-	-	-	-	-	-	-	-	-
CR01	-	-	-	-	-	-	-	-	-	-	-
CR02	-	-	-	-	-	-	-	-	-	-	-
SDH	1	2	4	12	6	7	3	4	5.5	1	-
PNTAB	-	-	-	-	-	-	-	-	-	-	-
EMP1	1	1	1	1	1	1	1	1	1	1	1
BOXI1	-	-	-	-	-	-	-	-	-	-	-
COx	6	6	6	6	6	6	6	6	3.75	1.5	1.5
R3HB	-	-	-	-	-	-	-	-	0.5	1	1
R3HHx	-	-	-	-	-	-	-	-	-	-	-
RCO2	6	6	6	6	6	6	6	6	4	2	2

EFM with the same overall stoichiometry; they have the same group number. There are 3 EFM corresponding to pathways for 3HB synthesis, but only 2 different overall stoichiometry proportions, and 8 EFM that only release CO_2, all belonging to the same stoichiometry group. The pathways that produce 3HB use the PP or the ED pathway; the latter being either the linear or the cyclic mode. As for the EFM that release CO_2, other redundant paths arise, like the glyoxylate and Krebs cycle, and combinations among them are possible. For example, EFM 4 releases all 6 moles of CO_2 through the PP pathway, while EFM 7 uses the ED pathway and Krebs cycle.

Since the polymer is the product of interest, EFM that use the ED pathway (group 20) are the ones with optimal yield for metabolic network considered; for one mole of glucose consumed, one mole of 3HB is produced with the release of 2 moles of CO_2. Experimental data for this condition (see Table 2) show that the ratio between CO_2 and 3HB is 2.66:1; 90.2% of the glucose is used for synthesis of P3HB with maximum yield, while 9.8% is just used for respiration, which means there still is room for improvement. Understanding how a physiological state of a microorganism operates can help planning strategies that can increase product yield. One way to analyze active pathways would be performing a MFA calculation using the overall stoichiometry of each group of EFM as the unknown stoichiometry matrix and estimate the flux through each group. Since there are 4 measurements (glucose, O_2, 3HB and CO_2) and 3 groups, the problem is overdetermined and the least squares method can be applied. Table 2 shows the estimated contribution of each group of EFM. Group 16, which comprises one EFM using the PP pathway, has zero flux, implying that the production of 3HB relies on the ED pathway, either the linear or cyclic mode. The excess CO_2 is produced by one or a combination of EFM in group 1; to distinguish which pathways are being used, more information needs to be experimentally collected.

Table 2 – Overall stoichiometry of the three groups of EFM involved in metabolize glucose in the studied metabolic network. $\hat{v}_g$ is the estimated flux through each group and v_e is the experimental measured flux corresponding to consumption or production of the external metabolites (MENDONÇA, 2014).

	Group 1	Group 16	Group 20	v_e (mmol/g.h)
Glucose	-1	-1	-1	-1.97
O_2	-6	-3.75	-1.5	-3.57
3HB	0	0.5	1	1.6
CO_2	6	4	2	4.26
$\hat{v}_g$ (mmol/g.h)	0.179	0	1.65	

At first glance, one could think there are 16 minimal pathways in this metabolic network that can explain the measured fluxes, as group 1 has 8 EFM and group 8 has 2 EFM. However, when EFV are calculated fixing the values of external fluxes, 7 minimal pathways are obtained. Table 3 shows the EFV obtained from the metabolic network in Figure 6 and the experimental data in Table 2. Note that the external fluxes in the EFV, the last 6 reactions in Table 3 differ from the ones in Table 2; due to experimental errors, data reconciliation was performed and a weight matrix was not used because variance on the measurements was not available. An interesting observation is that there are two EFM that use the PP pathway and either the glyoxylate or the Krebs cycle at the same time. Those EFM are not present in the EFV set, indicating that, for this flux distribution, they all have the same function. Also, note that when the cyclic mode of the ED pathway is active, the flux through the membrane transhydrogenase (SDH) is higher to oxidize the excess NADPH produced.

Table 3 also shows independent reactions and sets of completely correlated reactions identified from EFV, as well as the maximum and minimum values of each reaction. Using this information, cosine similarity was calculated for every pair of selected reactions according to Section 4.2, which is presented in Table 4. A similarity value equal to zero, indicate that the involved reactions are redundant, i.e., have equivalent functions in the metabolic network. For example, corroborating the observation above, the PP pathway (PPP) have zero cosine similarity with the Krebs cycle (CKc) and the glyoxylate cycle (GLXc) with or without the anaplerotic reactions, which shows that their function, for the considered physiological state based on this metabolic network, is to release the remainder of the CO_2 accounted for that was not produced in the CPD reaction. Therefore, in this case, the PP pathway is not necessary for generating the co-factor NADPH used for producing 3HB; other reactions in the metabolism have enough flux to meet that demand. Other redundancies that the cosine similarity identified for this metabolic network are, for instance, the linear (EDPl) and cyclic (EDPC) modes of the ED pathway, and the Krebs and the glyoxylate cycles.

When deciding what new information should be collected, a possible reasoning would be assuming, for example, that the PP pathway, the glyoxylate cycle and the anaplerotic reactions are not active or have very little flux through them since there is no growth in the experiment from which data is being considered. Thus, excess CO_2 is assumed to be produced by the Krebs cycle and the ED pathway to be active, either the cyclic or the linear mode. How the flux is divided between them depends on co-factor and energy balances and, in this case, this can be verified by analyzing the fluxes through the ED pathway and/or the

Table 3 – Set of EFV obtained fixing the external fluxes with data from (MENDONÇA, 2014) for the experiment with 3HB production. First column corresponds to sets of reactions that operate together. The last two columns correspond to the minimum and maximum values of each reaction for this physiological state.

		EFV								
Sets	**Reactions**	**1**	**2**	**3**	**4**	**5**	**6**	**7**	**Min**	**Max**
EMP2	EMP2	-2.537	-	-1.836	-	-1.836	-2.187	-0.701	-2.537	-
EDPc	EMP4	-1.836	-	-1.836	-	-1.836	-2.187	-	-2.187	-
EDPc	EMP5	-1.836	-	-1.836	-	-1.836	-2.187	-	-2.187	-
EDPl(+) / PEP-G3P (-)	EMP6	-	1.836	-	1.836	-	-0.351	1.836	-0.351	1.836
EDPl(+) / PEP-G3P (-)	EMP7	-	1.836	-	1.836	-	-0.351	1.836	-0.351	1.836
EDPl(+) / PEP-G3P (-)	EMP8	-	1.836	-	1.836	-	-0.351	1.836	-0.351	1.836
EDPl(+) / PEP-G3P (-)	EMP9	-	1.836	-	1.836	-	-0.351	1.836	-0.351	1.836
PPP	VP6	0.351	-	-	-	-	-	0.351	-	0.351
PPP	VP7	0.701	-	-	-	-	-	0.701	-	0.701
PPP	VP8	0.351	-	-	-	-	-	0.351	-	0.351
PPP	VP9	0.351	-	-	-	-	-	0.351	-	0.351
PPP	VP10	0.351	-	-	-	-	-	0.351	-	0.351
ED	ED1	3.321	1.836	3.672	1.836	3.672	4.022	1.485	1.485	4.022
ED	ED2	3.321	1.836	3.672	1.836	3.672	4.022	1.485	1.485	4.022
EMP10	EMP10	-	1.836	-	2.187	0.351	-	1.836	-	2.187
CPD	CPD	3.321	3.672	3.672	4.022	4.022	4.022	3.321	3.321	4.022
VP1	VP1	4.373	1.836	3.672	1.836	3.672	4.022	2.537	1.836	4.373
PPP	VP5	1.052	-	-	-	-	-	1.052	-	1.052
CK / GLXc	CK1	-	0.351	0.351	0.351	0.351	0.351	-	-	0.351
CK / GLXc	CK2	-	0.351	0.351	0.351	0.351	0.351	-	-	0.351
CK	CK3	-	0.351	0.351	-	-	-	-	-	0.351
CK	CK4	-	0.351	0.351	-	-	-	-	-	0.351
CK	CK5	-	0.351	0.351	-	-	-	-	-	0.351
CK / GLXc	CK6	-	0.351	0.351	0.351	0.351	0.351	-	-	0.351
CK / GLXc	CK7	-	0.351	0.351	0.351	0.351	0.351	-	-	0.351
CK8	CK8	-	0.351	0.351	0.701	0.701	0.701	-	-	0.701
GLXc / AD	CGLX1	-	-	-	0.351	0.351	0.351	-	-	0.351
GLXc / AD	CGLX2	-	-	-	0.351	0.351	0.351	-	-	0.351
EDPc	GLN3	1.836	-	1.836	-	1.836	2.187	-	-	2.187
AD1	AD1	-	-	-	-	-	-	-	-	-
GLXc / AD	AD2	-	-	-	0.351	0.351	0.351	-	-	0.351
P3HB	P3HB	1.660	1.660	1.660	1.660	1.660	1.660	1.660	1.660	1.660
CK / GLXc	OXFAD	-	0.35	0.35	0.35	0.35	0.35	-	-	0.35
OXNAD	OXNAD	7.086	6.736	6.736	6.736	6.736	6.736	7.086	6.736	7.086
B-Ox1	BOXI2	-	-	-	-	-	-	-	-	-
B-Ox3	BOXI3	-	-	-	-	-	-	-	-	-
B-Ox3	BOXI4	-	-	-	-	-	-	-	-	-
B-Ox5	BOXI5	-	-	-	-	-	-	-	-	-
B-Ox5	BOXI6	-	-	-	-	-	-	-	-	-
B-Ox7	BOXI7	-	-	-	-	-	-	-	-	-
B-Ox7	BOXI8	-	-	-	-	-	-	-	-	-
B-Ox9	BOXI9	-	-	-	-	-	-	-	-	-
PHAJ1	PHAJ1	-	-	-	-	-	-	-	-	-
PHAJ2	PHAJ2	-	-	-	-	-	-	-	-	-
CR01	CR01	-	-	-	-	-	-	-	-	-
CR01	CR02	-	-	-	-	-	-	-	-	-
SDH	SDH	3.765	0.526	2.362	0.175	2.011	2.362	1.929	0.175	3.765
PNTAB	PNTAB	-	-	-	-	-	-	-	-	-
Gluc	EMP1	1.836	1.836	1.836	1.836	1.836	1.836	1.836	1.836	1.836
B-Ox1	BOXI1	-	-	-	-	-	-	-	-	-
Cap-O2	COx	3.543	3.543	3.543	3.543	3.543	3.543	3.543	3.543	3.543
Ext-3HB	R3HB	1.660	1.660	1.660	1.660	1.660	1.660	1.660	1.660	1.660
Ext-3HHx	R3HHx	-	-	-	-	-	-	-	-	-
Rel-CO2	RCO2	4.373	4.373	4.373	4.373	4.373	4.373	4.373	4.373	4.373

Table 4 – Cosine similarity for every pair of selected reaction (only 3HB production).

	EMP2	EDPc	PEP-G3P	EDPl	PPP	EMP10	CK / GLXc	CK	CK8	GLXc
EMP2	1	0.976	0.509	-0.094	-0.533	-0.132	-0.610	-0.302	-0.615	-0.541
EDPc	0.976	1	0.567	0	-0.336	-0.049	-0.679	-0.336	-0.684	-0.602
PEP-G3P	0.509	0.567	1	0	0	0	-0.447	0	-0.535	-0.577
EDPl	-0.094	0	0	1	0.408	0.991	0.516	0.408	0.463	0.333
PPP	-0.533	-0.336	0	0.408	1	0.380	0	0	0	0
EMP10	-0.132	-0.049	0	0.991	0.380	1	0.573	0.380	0.541	0.429
CK / GLXc	-0.610	-0.679	-0.447	0.516	0	0.573	1	0.632	0.956	0.775
CK	-0.302	-0.336	0	0.408	0	0.380	0.632	1	0.378	0
CK8	-0.615	-0.684	-0.535	0.463	0	0.541	0.956	0.378	1	0.926
GLXc	-0.541	-0.602	-0.577	0.333	0	0.429	0.775	0	0.926	1

membrane transhydrogenase. For instance, further experiments and analysis could focus on determining the activity of the membrane transhydrogenase to have a better idea of the excess NADPH being produced and analyze how it impacts this metabolic network.

5.2 Synthesis of P3HB-co-3HHx

Consider now the production of P3HB-co-3HHx using glucose and hexanoic acid as substrates. In the metabolic network considered, hexanoic acid is processed by the beta-oxidation pathway and two different sets of reactions that produce 3HB and 3HHx are chosen to be included, one using ketoreductase (CR), which is NADPH dependent, and reactions encoded by the PHAJ gene that do not require a reducing agent. As there is still uncertainty concerning whether they are both present in the genome of *Burkholderia sacchari*, the idea is to analyze scenarios with both routes that can help plan strategies to better characterize the physiological state of this microorganism and later identify targets for yield improvement.

Because fatty acids are considerably more expensive than sugars, ideally all of the hexanoic acid provided should be converted into the co-polymer, while the glucose should be used to produce PHB and maintain the cell. Table 5 shows the EFM corresponding to optimal yield for 3HHx production, every molecule of hexanoic acid consumed is converted into a molecule of 3HHx. The first 3 EFM are from the same group and do not consume glucose. The first EFM produces 3HHx using the PHAJ reaction, thus a reducing agent is not necessary. The second EFM uses ketoreductase and needs NADPH, which is generated by the membrane-bound transhydrogenase (PNTAB) from the NADH produced in the beta-oxidation pathway. The third EFM, however, uses a thermodynamically infeasible cycle to produce NADPH and, therefore, is not considered. The remaining 8 EFM represent different

Table 5 – Subset of EFM with optimal yield for 3HHx synthesis from hexanoic acid for the metabolic network used to represent the core metabolism of *Burkholderia sacchari*.

EFM	**16**	**17**	**18**	**19**	**20**	**21**	**22**	**23**	**24**	**25**	**45**
Group	5	5	5	6	7	8	9	9	10	11	21
EMP2	-	-	-1	-	-1	-	-3	-1	-2	-2	-1
EMP4	-	-	-1	-	-1	-	-3	-1	-	-	-1
EMP5	-	-	-1	-	-1	-	-3	-1	-	-	-1
EMP6	-	-	-1	1	-	1	-2	-	1	1	-
EMP7	-	-	-1	1	-	1	-2	-	1	1	-
EMP8	-	-	-1	1	-	1	-2	-	1	1	-
EMP9	-	-	-1	1	-	1	-2	-	1	1	-
VP6	-	-	-	-	-	-	-	-	1	1	-
VP7	-	-	-	-	-	-	-	-	2	2	-
VP8	-	-	-	-	-	-	-	-	1	1	-
VP9	-	-	-	-	-	-	-	-	1	1	-
VP10	-	-	-	-	-	-	-	-	1	1	-
ED1	-	-	1	1	2	1	4	2	-	-	2
ED2	-	-	1	1	2	1	4	2	-	-	2
EMP10	-	-	-	3	2	1	-	-	2	1	-
CPD	-	-	-	4	4	2	4	2	2	1	2
VP1	-	-	1	1	2	1	4	2	3	3	2
VP5	-	-	-	-	-	-	-	-	3	3	-
CK1	-	-	-	2	2	2	2	2	1	1	-
CK2	-	-	-	2	2	2	2	2	1	1	-
CK3	-	-	-	-	-	2	-	2	-	1	-
CK4	-	-	-	-	-	2	-	2	-	1	-
CK5	-	-	-	-	-	2	-	2	-	1	-
CK6	-	-	-	2	2	2	2	2	1	1	-
CK7	-	-	-	2	2	2	2	2	1	1	-
CK8	-	-	-	4	4	2	4	2	2	1	-
CGLX1	-	-	-	2	2	-	2	-	1	-	-
CGLX2	-	-	-	2	2	-	2	-	1	-	-
GLN3	-	-	1	-	1	-	3	1	-	-	1
AD1	-	-	1	-	-	-	-	-	-	-	-
AD2	-	-	1	2	2	-	2	-	1	-	-
P3HB	-	-	-	-	-	-	-	-	-	-	1
OXFAD	-	-	-	2	2	2	2	2	1	1	-
OXNAD	1	1	1	11	12	13	14	14	17	18	4
BOXI2	1	1	1	1	2	3	4	4	6	7	1
BOXI3	-	1	1	1	2	3	4	4	6	7	1
BOXI4	-	1	1	1	2	3	4	4	6	7	1
BOXI5	-	-	-	-	-	-	-	-	-	-	-
BOXI6	-	-	-	-	-	-	-	-	-	-	-
BOXI7	-	-	-	-	-	-	-	-	-	-	-
BOXI8	-	-	-	-	-	-	-	-	-	-	-
BOXI9	-	-	-	-	-	-	-	-	-	-	-
PHAJ1	-	-	-	-	-	-	-	-	-	-	-
PHAJ2	1	-	-	-	-	-	-	-	-	-	-
CR01	-	1	1	1	2	3	4	4	6	7	1
CR02	-	-	-	-	-	-	-	-	-	-	-
SDH	-	-	-	-	-	-	-	-	-	-	-
PNTAB	-	1	-	-	-	-	-	-	-	-	-
COx	0.5	0.5	0.5	6.5	7	7.5	8	8	9	9.5	2
EMP1	-	-	-	1	1	1	1	1	1	1	1
BOXI1	1	1	1	1	2	3	4	4	6	7	1
R3HB	-	-	-	-	-	-	-	-	-	-	1
R3HHx	1	1	1	1	2	3	4	4	6	7	1
RCO2	-	-	-	6	6	6	6	6	6	6	2

pathways that use glucose to generate the NADPH required by the ketoreductase, going through the cyclic mode of the ED, the PP pathway or the Krebs cycle. Most of them releases CO_2; however, the last EFM in Table 5 uses the cyclic mode of the ED pathway to generate NADPH and produces 3HB at maximal yield from glucose.

Identifying the main theoretical pathways that produce 3HHx efficiently represented by EFM 16, 17 and 45 is important to help determine where to direct efforts for further investigation. For instance, By analyzing the optimal pathways for synthesis of 3HHx, it is already possible to conclude that it would be important to determine whether the PHAJ or CR reaction is active to determine if the reducing agent is necessary and, if so, how it is provided by the metabolism. Another relevant step, though, is to analyze the physiological state with the information available, which can help achieve better understanding of this metabolism and guide later decisions. Using experimental data from Mendonça (2014), the EFV are calculated for the considered metabolic network. Table 6 shows the experimental data flux and the reconciled data used for EFV calculation. Experimental data sets are available for 4 different conditions, but since they all present similar results, only one is discussed here. It is also relevant to point out that the flux rate value for 3HHx synthesis was corrected by our collaborators to a value 25% higher than originally reported in Mendonça (2014). Originally, 3HHx flux rate corresponded to 50% efficiency for converting hexanoic acid to 3HHX, but after correction and reconciliation, the efficiency increased to approximately 70%. In addition, due to uncertainties regarding the ratio of ATP produced in both NADH and $FADH_2$ oxidation, the consumption of ATP in glucose phosphorylation, and experimental errors, the flux value for O_2 is not fixed in the EFV calculation. Since the consumption of O_2 is directly related to co-factor balances, all EFV result in the same flux rate for O_2 and this value is shown in Table 6 as the reconciled flux rate.

Table 6 – Experimental (original) and reconciled values of external fluxes obtained during the synthesis of 3HB and 3HHx using *Burkholderia sacchari*.

	Glucose	Hexanoic acid	O_2	3HB	3HHx	CO_2
v_{exp} (mmol/g.h)	1.54	0.18	3.16	1.4	0.09	3.29
v_{rec} (mmol/g.h)	1.464	0.171	2.759	1.446	0.118	3.317

The set of EFV calculated for this case study is presented in Appendix A.2. It contains 40 minimal pathways that can explain the flux data in Table 6. To assist with the EFV analysis and with identifying important parts of the metabolism that should potentially be further

investigated, the cosine similarity is calculated for every pair of selected reactions and is presented in Table 7. The sets of reactions are the same as the ones listed in Table 3. Differently from the previous case in which there was no synthesis of co-polymer, the PP pathway (PPP) is not used only for producing CO_2; the occurrence of EFV with the glyoxylate cycle (GLXc) and the PPP simultaneously active shows that the PPP is used as source of NADPH as well. Indeed, by examining the EFV, one can see that it only happens when the ketoreductase is active and for few EFV, which explains their low similarity. The membrane-bound transhydrogenase (PNTAB) has cosine similarity zero with the cyclic mode of the ED pathway (EDPc), the Krebs cycle (CK), and the PP pathway. This indicates that they have the same function in this metabolic network, namely generating NADPH. Consequently, determining which pathway is responsible for providing NADPH is important to understand the physiological state of this metabolism.

The first PHAJ associated reaction (PHAJ1) and the second ketoreductase (CR02) both produce 3HB from hexanoic acid and have cosine similarity zero. PHAJ2 and CR01 also have the same function (both produce 3HHx), but their cosine similarity is not zero. Although it has a small value, which indicates that they mostly are not active simultaneously, 3HHx synthesis is split between both reactions when NADPH would be unbalanced if only one of them was active. Besides identifying whether PHAJ or ketoreductase or even both are active, another characteristic that is important to determine is what happens to the hexanoic acid that is not converted to 3HHx. The last step of the beta-oxidation pathway (B-Ox9) has zero cosine similarity with both reactions that produce 3HB from hexanoic acid. Therefore, identifying whether this reaction is active can help determine strategies to increase 3HHx yield.

Table 7 – Cosine similarity for every pair of selected reaction (3HB and 3HHx production).

	EMP2	EDPc	PEP-G3P	EDPl	PPP	EMP10	CK / GLXc	CK	CK8	GLXc	B-Ox7	B-Ox9	PHAJ1	PHAJ2	CR01	CR02	SDH	PNTAB
EMP2	1	0.979	0.523	-0.091	-0.479	-0.104	-0.416	-0.182	-0.420	-0.389	-0.556	-0.527	-0.229	-0.295	-0.523	-0.232	-0.970	0
EDPc	0.979	1	0.570	-0.009	-0.290	-0.029	-0.450	-0.198	-0.454	-0.421	-0.516	-0.517	-0.181	-0.256	-0.477	-0.181	-0.904	0
PEP-G3P	0.523	0.570	1	0	0	0	-0.314	0	-0.358	-0.382	-0.218	-0.280	-0.167	-0.163	-0.225	0	-0.436	0
EDPl	-0.091	-0.009	0	1	0.389	0.997	0.763	0.463	0.731	0.630	0.666	0.450	0.537	0.531	0.681	0.503	0.198	0.310
PPP	-0.479	-0.290	0	0.389	1	0.364	0.014	0	0.016	0.017	0.390	0.251	0.293	0.281	0.405	0.311	0.661	0
EMP10	-0.104	-0.029	0	0.997	0.364	1	0.787	0.437	0.767	0.677	0.676	0.460	0.539	0.528	0.694	0.506	0.200	0.327
CK / GLXc	-0.416	-0.450	-0.314	0.763	0.014	0.787	1	0.573	0.969	0.848	0.746	0.610	0.468	0.515	0.727	0.431	0.378	0.300
CK	-0.182	-0.198	0	0.463	0	0.437	0.573	1	0.351	0.051	0.453	0.374	0.221	0.384	0.350	0.259	0.226	0
CK8	-0.420	-0.454	-0.358	0.731	0.016	0.767	0.969	0.351	1	0.953	0.714	0.584	0.467	0.472	0.725	0.414	0.363	0.343
GLXc	-0.389	-0.421	-0.382	0.630	0.017	0.677	0.848	0.051	0.953	1	0.615	0.502	0.427	0.379	0.660	0.358	0.314	0.366
B-Ox7	-0.556	-0.516	-0.218	0.666	0.390	0.676	0.746	0.453	0.714	0.615	1	0.779	0	0.516	0.673	0.627	0.580	0.254
B-Ox9	-0.527	-0.517	-0.280	0.450	0.251	0.460	0.610	0.374	0.584	0.502	0.779	1	0	0.468	0.479	0	0.523	0.163
PHAJ1	-0.229	-0.181	-0.167	0.537	0.293	0.539	0.468	0.221	0.467	0.427	0	0	1	0.276	0.483	0	0.290	0.091
PHAJ2	-0.295	-0.256	-0.163	0.531	0.281	0.528	0.515	0.384	0.472	0.379	0.516	0.468	0.276	1	0.027	0.242	0.379	0
CR01	-0.523	-0.477	-0.225	0.681	0.405	0.694	0.727	0.350	0.725	0.660	0.673	0.479	0.483	0.027	1	0.478	0.531	0.323
CR02	-0.232	-0.181	0	0.503	0.311	0.506	0.431	0.259	0.414	0.358	0.627	0	0	0.242	0.478	1	0.276	0.202
SDH	-0.970	-0.904	-0.436	0.198	0.661	0.200	0.378	0.226	0.363	0.314	0.580	0.523	0.290	0.379	0.531	0.276	1	0
PNTAB	0	0	0	0.310	0	0.327	0.300	0	0.343	0.366	0.254	0.163	0.091	0	0.323	0.202	0	1

6 Conclusion

In this part, stoichiometric models and their application in studying non-model microorganism and performing preliminary analysis is presented. The case studied presented here showed that, given a metabolic network representing key parts of a cellular metabolism, these models can elucidate important properties and provide information that helps guiding future experiments. Although they cannot capture non-linear behaviors intrinsic to cellular functioning, being relatively simple allows for exploring possible scenarios easily and testing different assumptions adopted for properties involving uncertainties. The case studies also illustrated that the cosine similarity can be used to inspect the elementary flux vectors and assist in the identification of redundant pathways and the corresponding functionalities that can be missed if they are manually analyzed.

Part II

Regularization of parameter estimation problems

7 Introduction

Mathematical modeling of processes is important for understanding how they operate as a unit and how each component works and interacts with each other, with the ultimate goal of making reliable predictions. In theory, one gets better representation and, consequently, predictions of a process when working with more complex and mechanistic models (GRACIANO et al., 2014). But estimating the required parameters can be challenging, if not impossible, due to the necessary amount and quality of information. When it is not possible to estimate the parameters with the information available with the desired confidence, it is said that the estimation problem is ill-conditioned or that the model is unidentifiable.

Every parameter estimation problem can be often postulated as an optimization problem with an objective function that usually aims to minimize the difference between measured and modeled data. Formally, a model is said to be identifiable if this objective function has an isolated minimum; more specifically, it is locally identifiable if this minimum is local and globally if the minimum is global (NGUYEN; WOOD, 1982). Model identifiability can be classified into two types: structural and practical. The former evaluates whether a unique parameter set can be estimated based on the model structure, regardless of measured data; the latter takes into account the quantity and quality of measured data, assessing if the available information is enough for estimating the parameters with a desired confidence (RAUE et al., 2009).

There are essentially two ways of dealing with practical unidentifiability issues. One would be collecting more data and/or decrease the uncertainty of the measurements; this approach, however, is usually expensive, in terms of labor and finance, and not always possible. The other one would be applying a mathematical strategy that can help reduce the parameter uncertainty, ideally combined with *a priori* information about the physical process, parameters or estimator. Regularization approaches are one of those mathematical strategies for dealing with ill-conditioning.

In this part, a study on how to use eigenvectors of the (reduced) Hessian as constraints of ill-conditioned parameter estimation problems is presented. This approach is first applied to parameter estimation problems of linear models, showing that eigenvector constraints effectively reduce parameter variance and can be used to identify clusters of correlated parameters. A modified elastic net formulation for sparsifying the eigenvectors is also presented; the idea is to make combinations of parameters identified by the eigenvectors

more interpretable while keeping optimal variance. The application of this regularization for linear models is demonstrated in a case study estimating kinetic parameters of enzymatic reactions in steady state. This study, presented in Chapter 9, has been published in the journal Computers & Chemical Engineering (NAKAMA et al., 2020). This regularization approach is also implemented for nonlinear parameter estimation. The implementation is first discussed in the unconstrained optimization context and a simple case study using a basic Newton's method implementation is presented. Then, the eigenvector-based regularization is implemented in a line search interior-point solver for dealing with constrained nonlinear problems with the goal of hopefully improving the quality of the search step, when compared to the most commonly used approach that adds a multiple of the identity matrix to the Hessian, and also recognize groups of correlated parameters while obtaining a solution that can describe the experimental data.

7.1 Literature review

Parameter estimation problems are often ill-conditioned due to insufficient experimental data, model overparameterization, or large measurement errors. Ill-conditioning manifests itself as high sensitivity of the parameter estimates to the observation data and high parameter variance. Several approaches have been proposed for tackling this issue for both linear and nonlinear parameter estimation problems.

7.1.1 Regularization of linear parameter estimation

Linear regression and regularization were extensively studied around 50 years ago (HELMS, 1974; LIEW, 1976; GUNST; MASON, 1979). However, with the advance of machine learning, these topics have been revisited since the 00s (FRIEDMAN et al., 2010b; LIU et al., 2011; THRAMPOULIDIS et al., 2015). Examples of applications where ill-conditioning arises in linear models include image restoration (ZHANG et al., 2015), gene selection (ANG et al., 2015), gas emission source identification (MA et al., 2017), and seasonal forecasting (DELSOLE; BANERJEE, 2017). Ill-conditioning can be addressed by using regularization strategies, of which the two main approaches are using objective penalization terms and adding constraints to the optimization model.

The three most popular regularization methods that add a penalization term to the objective function are ridge, lasso and elastic net. Ridge regression uses a term in the form of an ℓ_2 norm of the parameters to stabilize them; the squared ℓ_2 norm has the same effect as displacing the eigenvalues of the Hessian to increase the small eigenvalues responsible for large variance (HANSEN, 2005; WIERINGEN, 2015). Ridge regression is a special case of Tikhonov regularization, in which the ℓ_2 term is of a matrix L times the parameter vector; in ridge regression, L is the identity matrix (KARL, 2005). When some properties of the estimated parameters are known, it might be beneficial to use a custom matrix L (FUHRY; REICHEL, 2012).

Lasso regularization was first introduced by Santosa and Symes (1986) and later popularized by Tibshirani (1996) with the intent of reducing the estimates variance and, at the same time, improving interpretation of the parameters. The idea behind this approach is to combine these features from ridge regression and parameter subset selection. To achieve that, lasso uses an ℓ_1 norm of the parameters, which promotes continuous shrinkage of the estimates that can lead to a subset of them being zero. The number of nonzero estimates is controlled by the value of a weight parameter associated with the ℓ_1 norm penalization term. Since then, variations of the lasso method have been proposed. Group lasso selects groups of parameters or drops them out all together, and sparse group lasso also sparsifies the selected groups (YUAN; LIN, 2006; FRIEDMAN et al., 2010a). In adaptive lasso, weights are used for penalizing different coefficients in the ℓ_1 norm of the parameters penalty term (ZOU, 2006). More recently, a lasso modification that takes prior information was proposed, prior lasso adds an extra term to the objective function corresponding to a measure of the discrepancy between the prior information and the model (JIANG et al., 2016).

The elastic net regularization is similar to the lasso as it performs parameter selection and continuous shrinkage simultaneously. However, in lasso, when the number of parameters is much larger than the number of observations, the number of nonzero parameters is limited to the number of observations and, when there are sets of correlated parameters, only one of them is selected. To overcome those limitations, the elastic net adds a weighted combination of the ℓ_1 and ℓ_2 norms to the objective function (ZOU; HASTIE, 2005).

An issue associated with objective penalization is that tuning the regularization parameter is usually non-trivial (BAUER; LUKAS, 2011). Another approach that can be used to regularize an ill-conditioned problem is enforcing constraints on the parameters. Constraints have the effect of reducing the allowable parameter space to be explored. A straightforward

approach to reduce the parameter space is simply to fix a subset of parameters, which is known as parameter subset selection. However, finding an optimal set of parameters is challenging, subset selection is a combinatorial problem and an exhaustive search is expensive. Several algorithms for searching for subsets, such as greedy, branch and bound and Monte Carlo, and criteria for evaluating models, such as the Akaike information criteria (AIC) and the Bayesian information criteria (BIC), have been applied to deal with this type of problems (GEORGE, 2000).

Another popular strategy consists in using trust-region constraints, which defines a region in the parameter space by adding an inequality constraint that bounds the norm of the parameters. This region limits the space over which the parameters can be searched for (ARORA; BIEGLER, 2004). This approach, however, results in a similar behavior as regularization methods that add a penalization term to the objective function (MORÉ, 1983; CARTIS et al., 2009). For example, adding an ℓ_2 norm constraint has similar behavior as Tikhonov and ridge regression (GANDER, 1980; HANSEN, 2005).

To reduce the allowable parameter space, it is also possible to use the eigenvalue decomposition of the Hessian matrix. Park (1981) showed that one can build constraints that are optimal in the sense that they minimize the parameter covariance by using eigenvectors of the Hessian matrix. Principal component regression (JOLLIFFE, 1982) is another powerful approach that reduces the parameter subspace by using eigenvectors of the Hessian matrix. PCR selects the eigenvectors with largest eigenvalues (principal components), which correspond to directions that can explain most of the data variance, and drops the eigenvectors with associated small eigenvalues. The input data is then projected into the principal components and a reduced set of the parameters is estimated. An important feature of the principal components is that they have embedded information on correlated input data and can be used to identify these correlations (JOLLIFFE; CADIMA, 2016).

7.1.2 Ill-conditioned nonlinear parameter estimation

Instead of modifying the optimization problem directly, one way to deal with ill-conditioned problems is to use known information about the process, parameters or estimators and modify the model itself (GRACIANO et al., 2014). Model reduction is commonly used in kinetic models (NIKEREL et al., 2009; FAN et al., 2016) and it consists in using *a priori* information to simplify the model and reduce the number of equations. A classic example

is the Michaelis-Menten equation that describes enzymatic reactions (CHEN et al., 2010). From the mass balance equations of the present compounds and considering mass action kinetics, assuming that the complex enzyme-substrate is in quasi-steady-state reduces the model to one equation that depends only on the concentration of the substrate and two parameters, maximum velocity and a constant known as Michaelis constant. However, an issue associated with model reduction is that the simplification might limit the model's applicability (GRACIANO et al., 2014).

Sensitivity-based methods use the sensitivity matrix to evaluate identifiability of the parameters and identify strong correlation among parameters. A parameter is more likely to be identifiable if the model output is sensitive to small perturbation of this parameter and correlation among parameters can be assessed by analyzing linear dependency in the sensitivity matrix (MIAO et al., 2011). For instance, the eigenvalue decomposition of the sensitivity matrix can be used to detect those correlations that can identify parts of the model where reduction can be applied without compromising the performance of the model (VAJDA et al., 1985; TURANYI et al., 1989).

Automatic selection of parameters focuses on finding unidentifiable parameters to fix their values and estimate the identifiable ones. It is an iterative process that test different sets of selected parameters that are fixed at an initial value until some criteria are met. The most popular methods use sensitivity information and the Fisher information matrix (FIM) to select the parameters to be fixed and compare the performance of the model with the estimated sets of parameters. An earlier approach evaluated every possible combination from a subset of selected parameters (WEIJERS; VANROLLEGHEM, 1997). Later, other methodologies were proposed that perform eigenvalue decomposition of the sensitivity matrix to rank the parameters and avoid the combinatorial problem (LI et al., 2004; SECCHI et al., 2006). More recently, an algorithm that selects sets at a time instead of individual parameters was proposed to save computational time but the solution is not unique (ALBERTON et al., 2013).

Reparameterization is an approach similar to automatic selection of parameters as some parameters that are considered unidentifiable are fixed. However, this method deals with combinations and relations of the parameters. The idea is to perform a coordinate transformation and partition the parameter space into two parts, estimable and inestimable, in a way that they are independent. This way, the estimable parameters are not sensitive to the nominal values defined for the inestimable parameters. This coordinate transformation can be linear based on the SVD decomposition of the sensitivity matrix (SURISETTY et al.,

2010) or nonlinear using *a priori* information (BEN-ZVI, 2008). A geometric approach that does not solely rely on known information has recently been proposed (TRANSTRUM et al., 2018).

7.1.3 Regularization in nonlinear solvers

The approaches described in the previous section either require expertise to reduce or regroup parameters or are computationally expensive for large-scale problems. Thus, another option to deal with ill-conditioned parameter estimation problems is to rely on the chosen nonlinear optimization solver and their built-in functions to deal with ill-conditioning. There are two main classes of algorithms designed to solve large-scale nonlinear optimization problems: line-search and trust-region. Trust-region algorithms define a quadratic region around an initial point in the solution space and solve a quadratic subproblem in that region to determine the step and complete the iteration. When defining this quadratic region, trust-region algorithms implicitly regularize ill-conditioned problems (YUAN, 2000). FilterSQP is a solver that uses a sequential quadratic programming (SQP) trust-region algorithm (FLETCHER; LEYFFER, 1998), and other trust-region methods can be found in MATLAB® optimization toolbox (MATHWORKS, R2020a).

Line-search algorithms, on the other hand, first find a descent direction and then define the step size. In this case, regularization might be necessary to guarantee that the search direction is descent, even though regularization tends to decrease the quality of the step and increase the number of trial step computations. However, an advantage is that line-search algorithms can use any linear algebra technique to calculate the step, if this step is a descent direction, which provides flexibility to handle a variety of large-scale problems with different structures, while trust-region algorithms depend on linear solvers with some specific properties and on preconditioners that project each iterate onto the Jacobian of the constraints (CHIANG; ZAVALA, 2016).

To ensure convergence, line-search methods need a descent search direction at each iteration, which is attained by guaranteeing positive definiteness of the (reduced) Hessian matrix. SQP line-search algorithms, such as `SNOPT`, usually use an initial positive approximation of the Hessian and maintain positive definiteness by refraining from updating the Hessian approximation if the update has negative curvature (GILL et al., 2005). `Ipopt` is an interior-point line search optimization solver that regularizes ill-conditioned Hessian by

adding a sufficiently large multiple of the identity matrix so that the problem is no longer ill-conditioned. This solver uses heuristics to update this multiple efficiently whenever necessary (WÄCHTER; BIEGLER, 2006). This approach is also implemented in `LOQO`, which is also a barrier method solver (VANDERBEI, 1999). However, as the multiple of the identity matrix increases, the search direction tends to the steepest descent direction, which is known to be inefficient with very slow convergence rate (YUAN, 2006).

`KNITRO` is a package with different algorithms for nonlinear optimization, including line search and trust-region methods. The line search interior-point implementation does not modify the Hessian when it has negative curvature or is rank deficient; instead, when the algorithm detects that the Hessian is ill-conditioned, it switches to the calculation of a trust-region step that is guaranteed to make progress. The idea is to combine the efficiency of line search methods with the robustness of trust-region algorithms (BYRD et al., 2006; WALTZ et al., 2006).

Primal-dual interior point methods, i.e., those that update both the original variables and multipliers (like `Ipopt`), require the gradient of the constraints to be linearly independent. When this condition is not met, some specific regularization approaches can be implemented. Wan and Biegler (2017) propose a regularization method and compare it to two alternatives that change the structure of the problem by removing the dependent constraints. The proposed approach identifies and removes the dependent constraints during the calculation of the Newton step, which is more computationally efficient since the structure of the problem is kept and a new factorization of the system is not necessary.

Rotational or directional discrimination is a regularization approach that has not been considerably explored in literature, but could potentially be more effective for some types of problems when compared to the most common regularization method which consists in adding a multiple of the identity matrix to the Hessian. By performing the eigenvalue decomposition of the (reduced) Hessian, negative and null eigenvalues can be replaced by positive values and a new (reduced) Hessian is obtained with modifications only in the degenerating directions, leaving the original positive curvature unchanged (BARD, 1974; FARISS; LAW, 1979). However, due to the spectral decomposition, this approach is suitable for problems with relatively small degrees of freedom (WANG et al., 2013).

8 Fundamentals

8.1 Quadratic programming

Quadratic programming (QP) is a class of optimization algorithms that deals with problems with a quadratic objective function and linear constraints. Consider first the unconstrained quadratic problem

$$\min_w f(w) := \frac{1}{2} w^T Q w + c^T w \tag{8.1}$$

where $w \in \mathbb{R}^n$, $c \in \mathbb{R}^n$ and $Q \in \mathbb{R}^{n \times n}$ is a symmetric matrix. Essentially, solution w^* is a point where $f(w^*)$ is minimum. The first-order necessary condition for optimality states that $\nabla f(w^*) = 0$, in other words, w^* must be a stationary point of (8.1). If a quadratic problem is convex, w^* is a global minimum if the Hessian $\nabla^2 f(w^*)$, i.e. Q, is positive definite. If Q is positive semidefinite, (8.1) has multiple minima and if Q is indefinite, w^* is just a stationary point and nothing further can be affirmed. The requirement for positive curvature is known as the second-order necessary condition.

Now consider an equality-constrained quadratic problem of the form

$$\min_w \quad \frac{1}{2} w^T Q w + c^T w \tag{8.2a}$$

$$\text{s.t.} \quad Aw - b = 0. \tag{8.2b}$$

where $A \in \mathbb{R}^{p \times n}$ and $b \in \mathbb{R}^p$. In this case, the first order necessary conditions are not defined based on the objective function. Instead, the Lagrangian function is defined

$$\mathcal{L}(w, \lambda) := f(w) + \lambda^T (Aw - b), \tag{8.3}$$

where $\lambda \in \mathbb{R}^p$ are the Lagrange multipliers, and used to derive the first order necessary conditions

$$Qw^* + c + A^T \lambda^* = 0 \tag{8.4a}$$

$$Aw^* = b \tag{8.4b}$$

where λ^* are the Lagrange multipliers for the equality constraints (8.4b) at the solution. System (8.4) is also known as the Karush-Kuhn-Tucker (KKT) system and it can be rewritten considering $w^* = w_k + d^w$ and $\lambda^* = \lambda_k + d^\lambda$, in which a step δw is calculated from a previous value of w

$$\begin{bmatrix} Q & A^T \\ A & \end{bmatrix} \begin{bmatrix} d^w \\ d^\lambda \end{bmatrix} = - \begin{bmatrix} Qw_k + c \\ Aw_k - b \end{bmatrix}. \tag{8.5}$$

For a quadratic programming problem, a solution is reached in one iteration; since only one step needs to be calculated, $w_k = w_0$.

Differently from unconstrained optimization, solution w^* is not located at a minimum point of the Lagrangian function. Therefore, the second-order necessary conditions evaluate the the projection of the Hessian Q onto the null space of the gradient of the constraints A, represented by $Z \in \mathbb{R}^{n \times n-p}$. The conditions state that w^* is a global minimum if this projection, $Z^T QZ$, which is called the reduced Hessian, is positive definite.

8.2 Line search methods for nonlinear optimization

Line search methods are an iterative strategy for solving optimization problems. In nonlinear optimization, algorithms start with an initial guess w_0 in the variable space $\mathbb{R}^n$ and generate a sequence of $\{w_k\}_{w \in \mathbb{N}}$ until it can no longer make progress or it reaches a solution with sufficient accuracy. This type of methods first calculates a search direction and then a step size at each iteration k, which results in a new point w_{k+1} that shows some kind of improvement, e.g., reduction of the objective function.

8.2.1 Unconstrained problems

Consider the nonlinear unconstrained optimization problem

$$\min_{w} \quad f(w) \tag{8.6}$$

where $w \in \mathbb{R}^n$ and $f : \mathbb{R}^n \to \mathbb{R}$ is the nonlinear function to be minimized. Because nonlinear problems are often non convex, most methods can only guarantee to find a local minimizer, meaning that w^* is a local minimum if, in a neighborhood $\mathcal{N}$ of w^*, $f(w^*) < f(w)$ for all $w \in \mathcal{N}$. For a smooth and twice continuously differentiable $f(w)$, one can verify if a point w^* is a local minimum by checking the first and second order conditions as it was shown for QP. The gradient, $\nabla f(w^*)$, and the Hessian, $\nabla^2 f(w^*)$ of the objective function must be, respectively, zero and positive (semi)definite.

An iterate w_{k+1} is calculated by

$$w_{k+1} = w_k + \alpha d \tag{8.7}$$

where α is a scalar that determines the step length and d is the search direction. Newton's method can be used to determine a search direction by approximating a neighborhood of $f(w_k)$ to a quadratic function using Taylor's expansion as follows

$$m_k(p) := f(w_k) + d^T \nabla f(w_k) + \frac{1}{2} d^T \nabla^2 f(w_k) d \approx f(w_k + d). \tag{8.8}$$

Taking the first derivative of (8.8) with respect to d and setting it to zero leads to

$$\nabla f(w_k) + \nabla^2 f(w_k) d = 0, \tag{8.9}$$

which results in

$$d_k = -[\nabla^2 f(w_k)]^{-1} \nabla f(w_k). \tag{8.10}$$

It is important to note that to ensure that the algorithm makes progress, this direction must be descent, i.e. $f(w_k + \alpha d) < f(w_k)$, and, for that, $\nabla^2 f(w_k)$ needs to be positive definite (BARD, 1974).

Ideally, the step length parameter α would be determined by

$$\min_{\alpha} \quad f(w_k + \alpha d_k) \tag{8.11a}$$

$$\text{s.t. } \alpha > 0. \tag{8.11b}$$

However, solving an optimization subproblem at each step can be expensive; thus, there are several strategies that can be followed to find a value for α that is a good trade-off between the actual optimized step and computational cost (NOCEDAL; WRIGHT, 2006). A simple backtracking method, for instance, starts with the full step length, $\alpha = 1$, and α is iteratively updated to 0.5α until the step is accepted.

For a step to be accepted, it has to meet certain criteria. In addition to having a descent search direction, two conditions need to be satisfied

$$f(w_k + \alpha_k d_k) \leq f(w_k) + c_1 \alpha_k \nabla f(w_k)^T d_k \tag{8.12a}$$

$$\nabla f(w_k + \alpha_k d_k)^T d_k \geq c_2 \nabla f(w_k)^T d_k, \tag{8.12b}$$

for $c_1 \in (0, 1)$ and $c_2 \in (c_1, 1)$. These conditions are known as the Wolfe conditions, and typical values for c_1 and c_2 are, respectively, 10^{-4} and 0.9 (NOCEDAL; WRIGHT, 2006). The first condition defines a sufficient decrease for the objective function when choosing α and the latter ensures that the slope of the objective function in the current search direction at $\alpha = \alpha_k$ is greater than at $\alpha = 0$; otherwise f could still be significantly reduced moving further along the search direction.

8.2.2 Constrained problems

Now consider the constrained problem

$$\min_{w} \quad f(w) \tag{8.13a}$$

$$\text{s.t.} \quad h(w) = 0 \tag{8.13b}$$

where $f : \mathbb{R}^n \to \mathbb{R}$ is again the nonlinear function to be minimized and $h : \mathbb{R}^n \to \mathbb{R}^p$ is a vector function corresponding to equality constraints. Here f and h are also assumed to be smooth and twice continuously differentiable. Because inequalities constraints can be written as equality constraints using slack variables, the theory presented here can be adapted to include inequality constraints as well. Similarly to unconstrained optimization, algorithms only find local minimizers; the difference now is that the neighborhood of w^* is now limited to the feasible region, i.e., values of w that satisfy the constraints $h(w) = 0$.

Similarly to QP, the Lagrange function is defined as

$$\mathcal{L}(w, \lambda) := f(w) + \sum_{i=1}^{p} \lambda_i h_i(w), \tag{8.14}$$

where λ_i is the Langrange multiplier for the i^{th} constraint. The first-order necessary conditions states that, if the gradient of the constraints at w^* are linearly independent, there exists a vector λ^* such that

$$\nabla_w \mathcal{L}(w^*, \lambda^*) = 0 \tag{8.15a}$$

$$h_i(w^*) = 0 \quad \text{for all } i \in \{1, \ldots, p\}. \tag{8.15b}$$

A stationary point w^* of $f(w)$ subject to $h(w)$ is a stationary point of $\mathcal{L}(w, \lambda)$. To guarantee that w^* is a local minimizer, one needs to check the reduced Hessian of the Lagrange function at w^*, that is, the projection of $\nabla^2_{ww}\mathcal{L}(w^*, \lambda^*)$ onto the null space of $\nabla h(w^*)^T$, Z. The point (w^*, λ^*) is a local minimum if it satisfies (8.15) and the reduced Hessian, $Z^T \nabla^2_{ww}\mathcal{L}(w^*, \lambda^*)Z$, is positive (semi)definite.

To calculate a search direction, Newton-based algorithms use Newton's method for nonlinear equations, which approximates the neighborhood region to a linear model. Applying it to (8.15) gives

$$\nabla^2_{ww}\mathcal{L}(w_k, \lambda_k)d^w_k + \sum_{i=1}^{p} \lambda_i \nabla h_i(w_k) d^\lambda_k + \nabla_w \mathcal{L}(w_k, \lambda_k) = 0 \tag{8.16a}$$

$$\nabla h_i(w_k) d^w_k + h_i(w_k) = 0 \quad \text{for all } i \in 1, \ldots, p, \tag{8.16b}$$

where d_k^w and d_k^λ are the search direction for the current step k for w and λ respectively. The KKT system can also be written in matrix notation as follows

$$\begin{bmatrix} \nabla^2_{ww}\mathcal{L}(w_k,\lambda_k) & \nabla h(w_k)^T \\ \nabla h(w_k) & \end{bmatrix}\begin{bmatrix} d_k^w \\ d_k^\lambda \end{bmatrix} = -\begin{bmatrix} \nabla_w \mathcal{L}(w_k,\lambda_k) \\ h(w_k) \end{bmatrix}. \tag{8.17}$$

Further details on how to actually solve problem (8.13), such as how the step length is determined, criteria for accepting a step and how to deal with variable bounds, depend on each algorithm implementation. Here, for constrained optimization, an interior point algorithm is considered.

8.2.2.1 Interior point methods

An overview of the most important aspects of an interior point implementation is presented in this section, describing key features of the solver `Ipopt`; a complete description of the algorithm can be found in (WÄCHTER; BIEGLER, 2006). First, consider the problem

$$\min_w \quad f(w) \tag{8.18a}$$

$$\text{s.t.} \quad h(w) = 0 \tag{8.18b}$$

$$w \geq 0 \tag{8.18c}$$

The interior point method is a barrier method, in which (8.18) is reformulated as

$$\min_w \quad \varphi(w,\mu) := f(w) - \mu \sum_{i=1}^{n} \log w^i \tag{8.19a}$$

$$\text{s.t.} \quad h(w) = 0, \tag{8.19b}$$

where the term added to the objective function is a barrier term that prevents w from becoming too small, and μ is the barrier parameter. As $w^i \to 0$, $-\log w^i$ becomes considerably large, and constraints for variable bounds can be eliminated. Equivalently, this can be interpreted as using a homotopy approach and the first-order conditions are given by

$$\nabla f(w) + \nabla h(w)^T \lambda - z = 0 \tag{8.20a}$$

$$h(w) = 0 \tag{8.20b}$$

$$W\mathcal{Z}e - \mu e = 0, \tag{8.20c}$$

where $z \in \mathbb{R}^n$ is a non negative vector with the Lagrange multipliers for the bounds, $W \in \mathbb{R}^{n\times n}$ and $\mathcal{Z} \in \mathbb{R}^{n\times n}$ are diagonal matrices with w and z in the main diagonal respectively, and e is

a vector of ones of appropriate size. This optimization is solved by solving (8.19) multiple times with decreasing values of μ. For each μ_j, (8.20) is satisfied to an accuracy proportional to the value of μ_j.

Applying Newton's method to (8.20) and writing it in matrix notation leads to

$$\begin{bmatrix} H_k & \nabla h_i(w_k)^T & -I \\ \nabla h_i(w_k) & & \\ \mathcal{Z}_k & & W_k \end{bmatrix} \begin{bmatrix} d_k^w \\ d_k^\lambda \\ d_k^z \end{bmatrix} = - \begin{bmatrix} \nabla_w \mathcal{L}(w_k, \lambda_k, z_k) \\ h_i(w_k) \\ W_k \mathcal{Z}_k e - \mu_j e \end{bmatrix} \tag{8.21}$$

where $\mathcal{L}(w, \lambda, z) := f(w) + h(w)^T - z$ and $H_k := \nabla^2_{ww} \mathcal{L}(w_k, \lambda_k, z_k)$. The matrix in the left-hand side of (8.21) can be reduced to a symmetric matrix, for which there are several efficient linear solvers, by removing the last row and column, resulting in

$$\begin{bmatrix} H_k + \Sigma_k & \nabla h(w_k)^T \\ \nabla h(w_k) & \end{bmatrix} \begin{bmatrix} d_k^w \\ d_k^\lambda \end{bmatrix} = - \begin{bmatrix} \nabla_w \varphi(w_k, \mu_j) + \nabla h(w_k)^T \lambda_k \\ h(w_k) \end{bmatrix} \tag{8.22}$$

where $\Sigma_k := W_k^{-1} \mathcal{Z}_k$ and $\varphi(w_k, \mu_j)$ is the objective function with the barrier term, and d_k^z can be recovered from $d_k^z = \mu_j W_k^{-1} e - z_k - \Sigma_k d_k^w$. When the reduced Hessian is positive definite, a descent search direction can obtained by solving (8.22).

The step length α_k can be calculated using a backtracking algorithm similar to the unconstrained case. However, to guarantee that w will not violate its bounds, the maximum value for α is defined as

$$\alpha_k^{\max} := \max\{\alpha \in (0, 1] : w_k + \alpha d_k^w \geq (1 - \tau_j) w_k\} \tag{8.23}$$

where $\tau_j < 1$ is a parameter that is a function of μ_j and limits how close to the bound w can get.

A filter method can be used to decide whether a step is acceptable (NOCEDAL; WRIGHT, 2006). At each step, the value of the objective function with the barrier term, $\varphi(w_k, \mu_j)$, and the constraint violation, $\rho(w_k) := \|h(w_k)\|$, should decrease; thus, a step is acceptable if, for a trial $\alpha_{k,l}$, either value is improved, measured by

$$\rho(w_k + \alpha_{k,l} d_k^w) \leq (1 - \gamma_\rho) \rho(w_k) \tag{8.24a}$$

$$\varphi(w_k + \alpha_{k,l} d_k^w, \mu_j) \leq \varphi(w_k, \mu_j) - \gamma_\varphi \rho(w_k) \tag{8.24b}$$

where $\gamma_\rho, \gamma_\varphi \in (0, 1)$. However, if $\rho(w_k) \leq \rho_{\min}$, only the value of $\varphi(w_k)$ is evaluated based on a condition similar to (8.12a) for unconstrained algorithms.

8.3 Reduced Hessian

The straightforward approach to obtain the reduced Hessian would be calculating a basis for the null space of A, Z, and performing $Z^T QZ$. However, obtaining Z can be expensive for large problems. Instead, the reduced Hessian, $Z^T QT$, can be calculated performing backsolves using the KKT system. Suppose the set of variables $w \in \mathbb{R}^n$ in a constrained optimization problem contains state variables, $x \in \mathbb{R}^p$, and parameters, $\theta \in \mathbb{R}^m$. Also, suppose this problem has p constraints, $h_i(x, \theta) = 0$ with $i = 1, ..., p$ and, thus, m degrees of freedom. Dropping the iteration index for clarity, the KKT system (8.17) can be written as

$$\begin{bmatrix} \nabla^2_{xx}\mathcal{L}(x,\theta,\lambda) & \nabla^2_{x\theta}\mathcal{L}(x,\theta,\lambda) & \nabla_x h(x,\theta)^T \\ \nabla^2_{\theta x}\mathcal{L}(x,\theta,\lambda) & \nabla^2_{\theta\theta}\mathcal{L}(x,\theta,\lambda) & \nabla_\theta h(x,\theta)^T \\ \nabla_x h(x,\theta) & \nabla_\theta h(x,\theta) & \end{bmatrix} \begin{bmatrix} d^x \\ d^\theta \\ d^\lambda \end{bmatrix} = - \begin{bmatrix} \nabla_x \mathcal{L}(x,\theta,\lambda) \\ \nabla_\theta \mathcal{L}(x,\theta,\lambda) \\ h(x,\theta) \end{bmatrix}. \tag{8.25}$$

Zavala (2008) shows that the reduced Hessian can be obtained by changing the right-hand side of the KKT system and solving it. Considering the parameters θ as the independent variables and solving the modified system

$$\begin{bmatrix} \nabla^2_{xx}\mathcal{L}(x,\theta,\lambda) & \nabla^2_{x\theta}\mathcal{L}(x,\theta,\lambda) & \nabla_x h(x,\theta)^T \\ \nabla^2_{\theta x}\mathcal{L}(x,\theta,\lambda) & \nabla^2_{\theta\theta}\mathcal{L}(x,\theta,\lambda) & \nabla_\theta h(x,\theta)^T \\ \nabla_x h(x,\theta) & \nabla_\theta h(x,\theta) & \end{bmatrix} \begin{bmatrix} D^x \\ D^\theta \\ D^\lambda \end{bmatrix} = \begin{bmatrix} 0 \\ I_m \\ 0 \end{bmatrix} \tag{8.26}$$

results in the inverse of the Reduced Hessian given by D^θ, i.e., $D^\theta = (Z^T QZ)^{-1}$.

9 Linear parameter estimation

Consider a set of input observations $x_\ell \in \mathbb{R}^m$ and output observations $\eta_\ell \in \mathbb{R}$, where the observation index is given by $\ell = 1, ..., L$. Suppose the correspondence between them follows a linear model response

$$\eta_\ell = \theta^T x_\ell + \epsilon_\ell \tag{9.1}$$

where $\theta \in \mathbb{R}^m$ is a set of parameters to be estimated and $\epsilon_\ell \sim \mathcal{N}(0, \sigma^2)$ are independent and identically distributed random variables representing noise. In matrix notation, 9.1 is $\eta = X\theta + \varepsilon$, where $X \in \mathbb{R}^{s\times m}$ is the input data matrix, $\eta \in \mathbb{R}^L$ is the response data vector, and $\varepsilon \sim \mathcal{N}(0, \sigma^2 I)$.

Applying the least squares method leads to a quadratic programming problem defined by

$$\hat{\theta} \in \arg\min_\theta \frac{1}{2}(\eta - X\theta)^T(\eta - X\theta). \tag{9.2}$$

The first-order optimality conditions result in

$$\hat{\theta} = K^{-1}X^T\eta. \tag{9.3}$$

where $\hat{\theta} \in \mathbb{R}^m$ is known as the least squares estimator and $K := X^TX \in \mathbb{R}^{m\times m}$ is the Hessian matrix that here is also called kernel matrix and encodes all information from X and associated impact on the estimated parameters. Since η are Gaussian variables and the estimated parameters $\hat{\theta}$ are a linear transformation of η, they are also normally distributed with covariance matrix

$$\mathbb{V}[\hat{\theta}] = \sigma^2 K^{-1}. \tag{9.4}$$

Note from (9.3) that $\hat{\theta}$ exist, are unique, and a minimum of 9.2 if and only if the input data matrix X has full rank, which implies that K is nonsingular and positive definite. Also, from (9.4) it is possible to observe that the inverse of K has direct effect on the covariance matrix $\mathbb{V}[\hat{\theta}]$. If the inverse of K is rewritten as $K^{-1} = V\Lambda^{-1}V^T$, with $V \in \mathbb{R}^{m\times m}$ being the matrix with the eigenvectors of K and $\Lambda \in \mathbb{R}^{m\times m}$ the diagonal matrix with its eigenvalues, the kernel matrix can be expressed as $K = \sum_{j=1}^m \lambda_j v_j v_j^T$ and its Frobenius norm as $\|K\|_F = \|\Lambda\|_F = \sqrt{\sum_{j=1}^m \lambda_j^2}$. Since the eigenvalues of $\mathbb{V}[\hat{\theta}]$ indicate the level of confidence in the parameters, as the eigenvalues of K decrease, the parameters become less reliable and, when variance is high, the problem is said to be ill-conditioned.

9.1 Constraint-based regularization

When input data is insufficient to estimate the parameters with sufficient confidence, it is necessary to regularize the problem. Constrained-based regularization strategies are formulated as

$$\tilde{\theta} \in \arg\min_{\theta} \frac{1}{2}(\eta - X\theta)^T(\eta - X\theta) \tag{9.5a}$$

$$\text{s.t. } R\theta = r, \tag{9.5b}$$

here $R \in \mathbb{R}^{p\times m}$ is a given regularization constraint matrix and $r \in \mathbb{R}^p$ is a given constraint right-hand side vector. The QP problem has now $m - p$ degrees of freedom, which shows that the parameter subspace dimension is reduced from m to $m - p$. Subset selection, for example, can be seen as a constrained-based regularization if R is a matrix with one unity per row in the position corresponding to the fixed components of θ and the right-hand side is a vector with the values to be fixed. On the other hand, each row of R can also represent a combination of the parameters, which provides more flexibility since the parameters themselves are not fixed, only their relationship.

The constrained estimator, $\tilde{\theta} \in \mathbb{R}^m$, is obtained from the Lagrange function, $\mathcal{L}(\theta, \lambda)$,

$$\tilde{\theta} \in \arg\min_{\theta,\lambda} \frac{1}{2}(\eta - X\theta)^T(\eta - X\theta) + \lambda^T(R\theta - r) \tag{9.6}$$

where $\lambda \in \mathbb{R}^p$ are the Lagrange multipliers. From the first-order conditions,

$$-X^T\eta + X^TX\theta + R^T\lambda = 0 \tag{9.7a}$$

$$R\tilde{\theta} - r = 0. \tag{9.7b}$$

Multiplying (9.7a) by K^{-1} leads to

$$\theta = K^{-1}X^T\eta - K^{-1}R^T\lambda, \tag{9.8}$$

which inserted into the second condition results in

$$RK^{-1}X^T\eta - RK^{-1}R^T\lambda - r = 0, \tag{9.9}$$

and thus,

$$\lambda = (RK^{-1}R^T)^{-1}RK^{-1}X^T\eta - (RK^{-1}R^T)^{-1}r. \tag{9.10}$$

Substituting (9.10) into (9.8) gives

$$\tilde{\theta} = K^{-1}X^T\eta - K^{-1}R^T(RK^{-1}R^T)^{-1}RK^{-1}X^T\eta + K^{-1}R^T(RK^{-1}R^T)^{-1}r, \tag{9.11}$$

which can be written as a function of the unconstrained estimator (9.3),

$$\begin{aligned}\tilde{\theta} &= \hat{\theta} - K^{-1}R^T(RK^{-1}R^T)^{-1}R\hat{\theta} + K^{-1}R^T(RK^{-1}R^T)^{-1}r \\ &= \Gamma\hat{\theta} + \tilde{r},\end{aligned} \tag{9.12}$$

where $\Gamma := I - K^{-1}R^T(RK^{-1}R^T)^{-1}R$ and $\tilde{r} := K^{-1}R^T(RK^{-1}R^T)^{-1}r$. Since Γ and $\tilde{r}$ are constants, the covariance matrix for the constraint estimator is given by

$$\begin{aligned}\mathbb{V}[\tilde{\theta}] &= \mathbb{V}[\Gamma\hat{\theta}] + \mathbb{V}[\tilde{r}] \\ &= \Gamma\mathbb{V}[\hat{\theta}]\Gamma^T \\ &= \sigma^2K^{-1} - \sigma^2K^{-1}R^T(RK^{-1}R^T)^{-1}RK^{-1}.\end{aligned} \tag{9.13}$$

Note that the constraint right-hand side r influences the value of the estimated parameters but does not affect the parameter covariance. Moreover, the covariance $\mathbb{V}[\tilde{\theta}]$ can be controlled by selecting a suitable constraint matrix R.

9.1.1 Regularization using eigenvector constraints

Park (PARK, 1981) noticed that a matrix R (of rank $q \leq m$) that minimizes covariance can be obtained from the eigenvalue decomposition of the kernel matrix K. Consider the eigenvalue decomposition of the kernel matrix

$$K = [V_1 \mid V_2]\left[\begin{array}{c|c} \Lambda_1 & \\ \hline & \Lambda_2 \end{array}\right]\left[\begin{array}{c} V_1^T \\ \hline V_2^T \end{array}\right] \tag{9.14}$$

where $\Lambda_1 \in \mathbb{R}^{m-q\times m-q}$ is a diagonal matrix with the $(m-q)$-largest eigenvalues of K with associated eigenvectors $V_1 \in \mathbb{R}^{m\times m-q}$, and $\Lambda_2 \in \mathbb{R}^{q\times q}$ is also a diagonal matrix with q smallest eigenvalues with eigenvectors $V_2 \in \mathbb{R}^{m\times q}$. It is relevant to point out that the kernel matrix can be expressed as $K^{-1} = V_1\Lambda_1^{-1}V_1^T + V_2\Lambda_2^{-1}V_2^T$ and that V_1 and V_2 are orthogonal, therefore $V_1^TV_2 = 0$ and $V_2^TV_1 = 0$, and $V_2^TV_2 = \mathbb{I}$. Taking $R = \sqrt{\Lambda_2}V_2^T$ gives

$$\begin{aligned}RK^{-1}R^T &= \sqrt{\Lambda_2}V_2^T(V_1\Lambda_1^{-1}V_1^T + V_2\Lambda_2^{-1}V_2^T)V_2\sqrt{\Lambda_2} \\ &= \sqrt{\Lambda_2}V_2^TV_2\Lambda_2^{-1}V_2^TV_2\sqrt{\Lambda_2} \\ &= \mathbb{I},\end{aligned}$$

which in turn leads to

$$\begin{aligned} K^{-1}R^T(RK^{-1}R^T)^{-1}RK &= (V_1\Lambda_1^{-1}V_1^T + V_2\Lambda_2^{-1}V_2^T)V_2\sqrt{\Lambda_2}\mathbb{I}\sqrt{\Lambda_2}V_2^T(V_1\Lambda_1^{-1}V_1^T + V_2\Lambda_2^{-1}V_2^T) \\ &= (V_1\Lambda_1^{-1}V_1^T + V_2\Lambda_2^{-1}V_2^T)V_2\Lambda_2V_2^T(V_1\Lambda_1^{-1}V_1^T + V_2\Lambda_2^{-1}V_2^T) \\ &= V_2V_2^T(V_1\Lambda_1^{-1}V_1^T + V_2\Lambda_2^{-1}V_2^T) \\ &= V_2\Lambda_2^{-1}V_2^T. \end{aligned}$$

Upon substitution in (9.13), the covariance matrix of estimator calculated with eigenvector constraints is given by

$$\begin{aligned} \mathbb{V}[\tilde{\theta}] &= \sigma^2(V_1\Lambda_1^{-1}V_1^T + V_2\Lambda_2^{-1}V_2^T) - \sigma^2V_2\Lambda_2^{-1}V_2^T \\ &= \sigma^2(V_1\Lambda_1^{-1}V_1^T). \end{aligned} \tag{9.15}$$

Consequently, enforcing the constraint $R\theta = r$ (with $R = \sqrt{\Lambda_2}V_2^T$) minimizes the effect of the damaging (small) eigenvalues of K on the covariance matrix since only their components are removed in (9.15); in particular, note that $\|\mathbb{V}[\tilde{\theta}]\|_F = \sigma^2\sum_{j=1}^{m-q}\lambda_j^{-2}$.

9.1.2 Principal component regression

Originally, principal component regression projects the input data matrix X onto the space of the $(m-q)$ largest eigenvectors as $XV_1 \in \mathbb{R}^{n\times m-q}$ and estimates a reduced parameter set $\gamma \in \mathbb{R}^{m-q}$ by solving

$$\hat{\gamma} \in \arg\min_{\gamma} \frac{1}{2}(\eta - XV_1\gamma)^T(\eta - XV_1\gamma). \tag{9.16}$$

Therefore, an estimator for the reduced parameter set is given by $\hat{\gamma} = (V_1^TX^TXV_1)^{-1}V_1^TX^T\eta$ and a solution in the original parameter space is recovered from $\hat{\theta} = V_1\hat{\gamma}$. However, PCR can also be seen as a constrained QP defined by

$$(\hat{\theta}, \hat{\gamma}) \in \arg\min_{\gamma,\theta} \frac{1}{2}(\eta - X\theta)^T(\eta - X\theta) \tag{9.17a}$$

$$\text{s.t.} \quad V_1^T\theta = \gamma \tag{9.17b}$$

Note that the coefficient matrix is $R = V_1^T$ and $r = \gamma$.

The covariance of $\hat{\gamma}$ is given by

$$\begin{aligned} \mathbb{V}[\hat{\gamma}] &= \sigma^2(V_1^TX^TXV_1)^{-1} \\ &= \sigma^2(V_1^T(V_1\Lambda_1V_1^T + V_2\Lambda_2V_2^T)V_1)^{-1} \\ &= \sigma^2\Lambda_1^{-1}. \end{aligned} \tag{9.18}$$

Since Λ_1 is a diagonal matrix, the reduced parameters are uncorrelated. The covariance of the full parameter estimate $\hat{\theta}$ is

$$\begin{aligned}\mathbb{V}[\hat{\theta}] &= V_1 \mathbb{V}[\hat{\gamma}] V_1^T \\ &= \sigma^2 V_1 \Lambda_1^{-1} V_1^T. \end{aligned} \tag{9.19}$$

This shows that using eigenvector constraints and PCR have the same regularization effect; they eliminate the effect of the small eigenvalues from the kernel matrix. However, they follow different implementation mechanisms, which are exemplified in Figure 7. Specifically, PCR projects X onto V_1 (Figure 7a) and creates a reduced set of parameters $\gamma = V_1^T \theta$ that are linear combinations of the original parameters, which can be interpreted as parameter clusters, and seeks to find cluster values $\hat{\gamma}$ that minimize the model error. Eigenvectors of the kernel matrix provide the coefficients for the clusters that minimize the parameter covariance and constrain the search space (Figure 7b). Therefore, this scheme provides a mechanism to optimally cluster parameters when individual parameters cannot be estimated with high confidence given the available data.

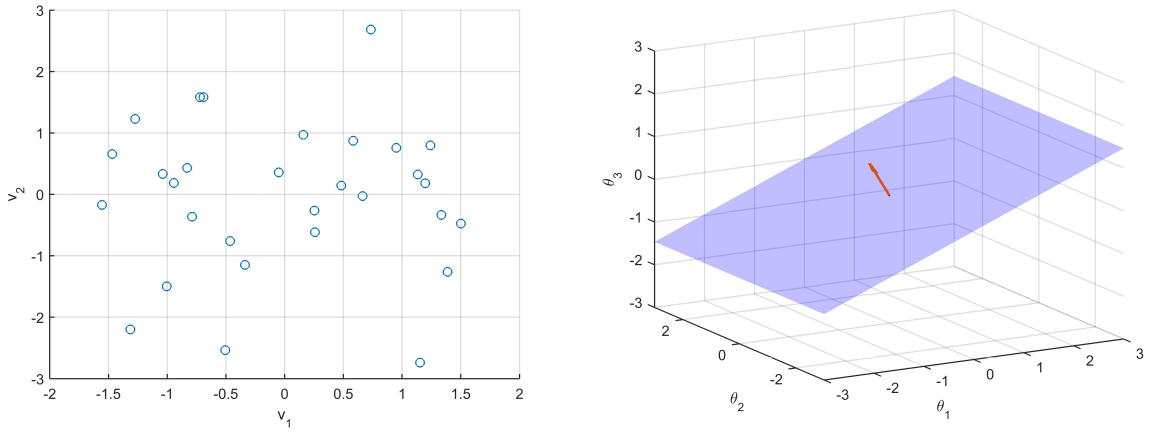

(a) PCR (b) Eigenvector constraints

Figure 7 – Three parameter example of how PCR and using eigenvector constraints regularize an estimation problem; PCR projects the data onto the 2 leading eigenvectors, while using eigenvector constraints creates a hyperplane where the solution is contained.

9.1.3 Sparse principal component regression

As demonstrated in the previous section, PCR can be interpreted as estimating an optimal set of parameter clusters $\gamma = V_1^T \theta$. Unfortunately, the coefficients of these clusters,

the eigenvectors V_1, are dense and every cluster depends on all parameters, which might make interpreting the clusters challenging. Sparsifying these clusters can help identifying more dominant parameters in each cluster. This can be done by using an elastic net approach, also known as sparse PC. Zou et al. (2006) shows that sparse approximations of the leading p eigenvectors of $K = X^T X$ can be obtained from the solution of the elastic net problem,

$$\tilde{v}_i \in \arg\min_v \frac{1}{2}\|Xv_i - Xv\|_2^2 + \kappa_2\|v\|_2^2 + \kappa_1\|v\|_1 \tag{9.20}$$

for $i = 1, ..., p$ and $\tilde{v}_i \leftarrow \tilde{v}_i/\|\tilde{v}_i\|_2$, where $\tilde{v}_i \in \mathbb{R}^m$ is the sparse approximation of the eigenvector v_i. This approach is derived based on the observation that the p leading eigenvectors $v_i,\ j = 1, ..., p$ of $X^T X$ can be recovered from the solution of the problem,

$$\tilde{v}_i = \arg\min_v \frac{1}{2}\|Xv_i - Xv\|_2^2 + \kappa_2\|v\|_2^2 \tag{9.21}$$

for any value of $\kappa_2 \in \mathbb{R}_+$. The tuning parameter κ_1 is used to control the sparsity of the eigenvectors $\tilde{V}_1$.

It is important to note that the sparse PC approach does not provide eigenvalue information. However, since PCR and eigenvector constraints are equivalent, one can implement optimal constraint regularization in the form of PCR using the sparse eigenvector approximation. A larger issue with using the sparse PC approach, however, is that the sparse eigenvectors might fail to reduce the parameter variance, which is the goal when applying regularization techniques. Consider the PC regression problem with sparse eigenvectors

$$\tilde{\gamma} \in \arg\min_\gamma \frac{1}{2}(\eta - X\tilde{V}_1\gamma)^T(\eta - X\tilde{V}_1\gamma), \tag{9.22}$$

with $\tilde{\theta} = \tilde{V}_1\tilde{\gamma}$. The parameter covariance is given by

$$\begin{aligned}\mathbb{V}[\tilde{\theta}] &= \sigma^2\tilde{V}_1(\tilde{V}_1^T X^T X\tilde{V}_1)^{-1}\tilde{V}_1^T \\ &= \sigma^2\tilde{V}_1(\tilde{V}_1^T(V_1\Lambda_1 V_1^T + V_2\Lambda_2 V_2^T)\tilde{V}_1)^{-1}\tilde{V}_1^T.\end{aligned} \tag{9.23}$$

Because $\tilde{V}_1$ is not necessarily orthogonal to V_2, the effect of the small eigenvalues of K is not eliminated. To keep the variance close to optimal, a new elastic net formulation with orthogonality constraints can be applied

$$\tilde{v}_i = \arg\min_v \quad \frac{1}{2}\|Xv_i - Xv\|_2^2 + \kappa_2\|v\|_2^2 + \kappa_1\|v\|_1 \tag{9.24a}$$

$$\text{s.t.} \quad v^T v_j = 0,\ j = m - q + 1, ..., m \quad \text{and} \quad j \neq i \tag{9.24b}$$

$$v^T v_j = 1,\ j = i \tag{9.24c}$$

which is solved for $i = 1, ..., m - q$ and with $\tilde{v}_i \leftarrow \tilde{v}_i / \|\tilde{v}_i\|_2$ to construct the sparse eigenvector matrix $\tilde{V}_1$.

9.2 Illustrative examples

9.2.1 Collineatities in the input data

The studied eigenvector regularization approach is applied to an ill-conditioned linear model in which the input data present near collinearities. A synthetic model is built with $m = 6$ parameters and $L = 15$ data points. To induce collinearities, the input data is generated as follows

$$x_1 \sim \mathcal{N}(0, 1) \tag{9.25a}$$

$$x_2 \sim \mathcal{N}(0, 1) \tag{9.25b}$$

$$x_3 \sim \mathcal{N}(0, 1) \tag{9.25c}$$

$$x_4 = x_1 \tag{9.25d}$$

$$x_5 = x_2 \tag{9.25e}$$

$$x_6 = x_1 + x_2, \tag{9.25f}$$

implying dependencies between parameters $\theta_1, \theta_4, \theta_6$ and between parameters $\theta_2, \theta_5, \theta_6$. No collinearities are induced by the third input. The kernel matrix is shown in Table 8 and Table 9 presents the eigenvectors and eigenvalues of $X^T X$.

Table 8 – Kernel matrix corresponding to the first example.

$K = X^T X$					
15.02	-1.69	6.09	15.02	-1.69	13.33
-1.69	11.16	-3.2	-1.68	11.16	9.48
6.09	-3.2	17.33	6.08	-3.2	2.88
15.02	-1.68	6.08	15.03	-1.68	13.33
-1.69	11.16	-3.2	-1.68	11.15	9.47
13.33	9.48	2.88	13.33	9.47	22.8

Inspecting the eigenvalues of K, one can conclude that most of the variance of the inputs can be captured by the $m - q = 3$ leading eigenvalues. This highlights, as expected, that only three parameters can be estimated, e.g., the two clusters and an additional parameter. The eigenvector matrix V_1 is shown in Table 10, which also presents the

Table 9 – Eigenvectors and corresponding eigenvalues of $X^T X$ from the first example.

X_1	-0.502	-0.253	0.244	0.051	-0.587	0.527
X_2	-0.138	0.554	-0.222	-0.346	0.324	0.633
X_3	-0.224	-0.409	-0.884	0	0	0
X_4	-0.502	-0.252	0.244	-0.661	0.298	-0.316
X_5	-0.138	0.554	-0.222	-0.264	-0.614	-0.422
X_6	-0.639	0.302	0.023	0.610	0.290	-0.211
Λ	48.8	31.4	12.3	1.6e-5	5.8e-6	1.9e-6

sparse eigenvectors obtained with both the elastic net and the elastic net with orthogonality constraints approaches. Figure 8 shows the parameter covariance when using unregularized estimation and PCR. It is clear that the problem is ill-conditioned, due to the large entries in the covariance matrix of the unregularized estimation, and regularization is needed to stabilize the estimates.

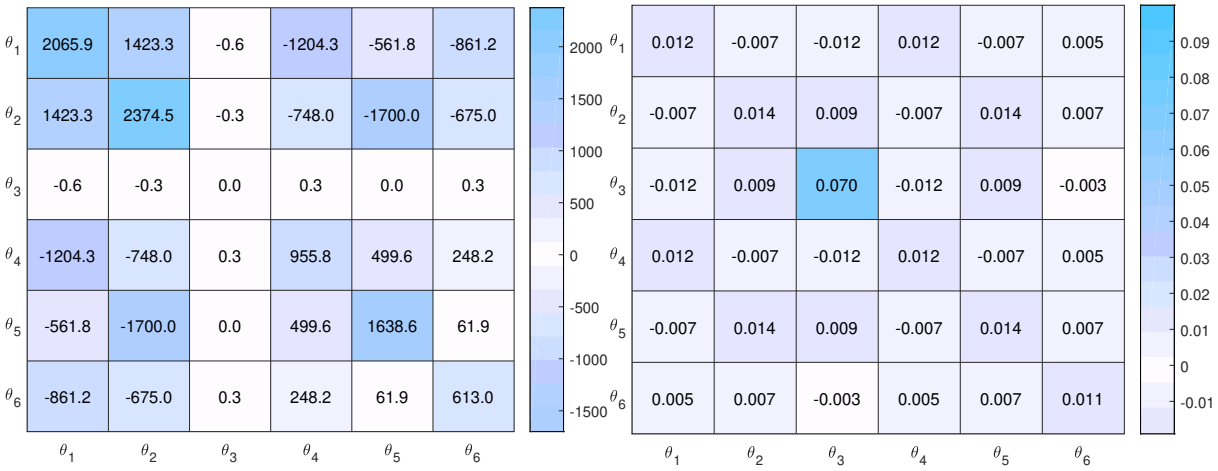

(a) Unregularized (b) PCR

Figure 8 – Covariance matrix for estimated parameters $\mathbb{V}[\hat{\theta}]$ from the first example.

Table 10 – Eigenvectors V_1 and sparse eigenvectors $\tilde{V}_1$ obtained with elastic net (EN) and elastic net with orthogonality constraints (EN-OC) (First example).

	V_1			$\tilde{V}_1$ (EN)			$\tilde{V}_1$ (EN-OC)		
	v_1	v_2	v_3	$\tilde{v}_1$	$\tilde{v}_2$	$\tilde{v}_3$	$\tilde{v}_1$	$\tilde{v}_2$	$\tilde{v}_3$
X_1	-0.502	-0.253	0.244	0	0	0	-0.577	0	0
X_2	-0.138	0.554	-0.222	0	0.950	-0.354	0	0.577	0
X_3	-0.224	-0.409	-0.884	-0.009	-0.285	-0.820	0	0	-1.0
X_4	-0.502	-0.252	0.244	-0.577	0	0.451	-0.577	0	0
X_5	-0.138	0.554	-0.222	0	0.127	0	0	0.577	0
X_6	-0.639	0.302	0.023	-0.817	0	0	-0.577	0.577	0

A comparison of the effect of regularization using PCR with the elastic net (EN) approach directly and with the elastic net with orthogonality constraints (EN-OC) is conducted by exploring the performance of EN and EN-OC employing different values for the tuning parameters κ_1. Since $L > m$, κ_2 can be set to zero as this parameter does not affect the solution in this case (ZOU et al., 2006). Tuning parameter κ_1 controls the sparsity of the vector; note that $\kappa_1 = 0$ is equivalent to PCR with dense eigenvectors and that κ_1 can affect the parameter variance. Figure 9b shows the Frobenius norm of the covariance matrix as a function of κ_1. For EN, the variance increases as $\tilde{V}_1$ becomes sparser (the numbers in parenthesis are the number of nonzeros in each eigenvector) and the quality of the eigenvectors degrades. For a large value of κ_1 we observe that all eigenvectors only contain one entry (denoted as $(1, 1, 1)$). Figure 9b also shows that EN-OC keeps the parameter variance at the minimum (optimal) value obtained with dense PCR; the variance does not increase with κ_1 but the sparsity does increase. This result is surprising, as it indicates that one can improve sparsity without compromising optimality. However, it is important to observe that EN-OC cannot fully sparsify the eigenvectors; for instance, in the limit the eigenvectors have $(3, 6, 1)$ nonzero entries. This limitation happens because the orthogonality constraints only allow spanning a limited subspace of X.

The dense eigenvectors V_1 and sparse eigenvectors $\tilde{V}_1$ calculated with EN and EN-OC are presented in Table 10. The value of κ_1 for EN was chosen based on the trade-off between variance and sparsity while for EN-OC limiting value at which sparsity is no longer affected was used. An interesting observation is that the sparsity structure of the eigenvectors of EN-OC reveals the clusters of parameters associated with the dependent columns of the input matrix (parameters $\theta_1, \theta_4, \theta_6$, parameters $\theta_2, \theta_5, \theta_6$, and parameter θ_3). This shows how sparse eigenvectors can help reveal parameter clusters, while PCR using the dense eigenvectors and using $\tilde{V}_1$ of EN are not able to identify these clusters.

Figure 9a shows the Frobenius norm of the covariance matrix obtained under parameter subset selection for all possible combinations with $m - q = 3$ fixed parameters, and the norm obtained with PCR. It is possible to see that none of the subset selections reach the minimum variance of PCR, corroborating that PCR is optimal and that subset selection is inherently suboptimal. Another interesting observation is that the variance of the sparsest eigenvectors found with EN (one nonzero entry per eigenvector) is similar to that of the best subset selection, which might indicate that one can find a suitable subset by using EN and avoid a combinatorial search.

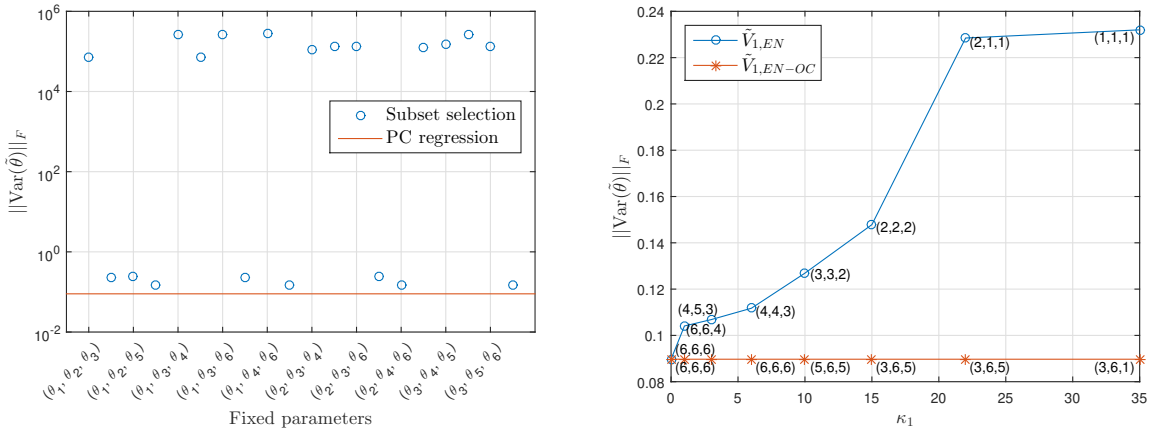

(a) (b)

Figure 9 – (a) Frobenius norm of parameter covariance matrix obtained with all possible subset selections with $p = 3$ (circles) and obtained with PCR (red line). (b) Frobenius norm of the covariance matrix obtained with sparse PCR with elastic net (EN) and elastic net with orthogonality constraints (EN-OC). The sparsest eigenvectors (with one nonzero entry) is equivalent to fixing parameters θ_1, θ_4 and θ_5.

9.2.2 Fewer input observations than parameters

A simple setting with more parameters than data points, $m > L$, is now analyzed. Since in this case the kernel matrix $K = X^T X$ is singular, unregularized estimation cannot be directly used. Results using ridge regularization and PCR with dense and sparse eigenvectors are compared. The results presented here use a random matrix $X \in \mathbb{R}^{L \times m}$ with $m = 8$, $L = 5$ and model $\eta = X\theta + \varepsilon$, with $\varepsilon \sim \mathcal{N}(0, \sigma^2 I)$ and $\sigma^2 = 1 \times 10^{-4}$.

Table 11 – Eigenvectors and corresponding eigenvalues of $X^T X$ from the second example.

X_1	0.462	0.355	0.010	0.106	-0.484	0.621	-0.115	0.131
X_2	0.246	0.675	0.412	-0.201	0.350	-0.242	0.277	0.125
X_3	-0.371	0.450	-0.066	0.056	-0.545	-0.479	-0.354	-0.011
X_4	0.441	-0.319	-0.123	-0.482	-0.319	-0.389	0.082	0.443
X_5	0.468	-0.178	0.295	0.333	-0.221	-0.333	0.0904	-0.619
X_6	0.350	0.258	-0.795	0.070	0.305	-0.153	-0.136	-0.198
X_7	-0.116	0.075	-0.045	-0.754	-0.132	0.203	0.052	-0.590
X_8	-0.198	0.100	-0.299	0.168	-0.291	0	0.865	0
Λ	19.0	16.7	5.8	3.9	0.5	0	0	0

Sparse and dense PCR can deliver parameter estimates with a SSE of zero regardless of the sparsity level used. Again it is possible to observe that orthogonality constraints are essential to control the variance of the parameters. In particular, using orthogonality

constraints maintains a minimum variance regardless of the number of nonzeros in the eigenvector matrix, as it can be seen in Figure 10a. When comparing PCR performance with ridge regularization, the latter can only achieve the same level of variance as the former by sacrificing SSE (see Figure 10b), which suggests that PCR offers different regularization behavior than objective regularization.

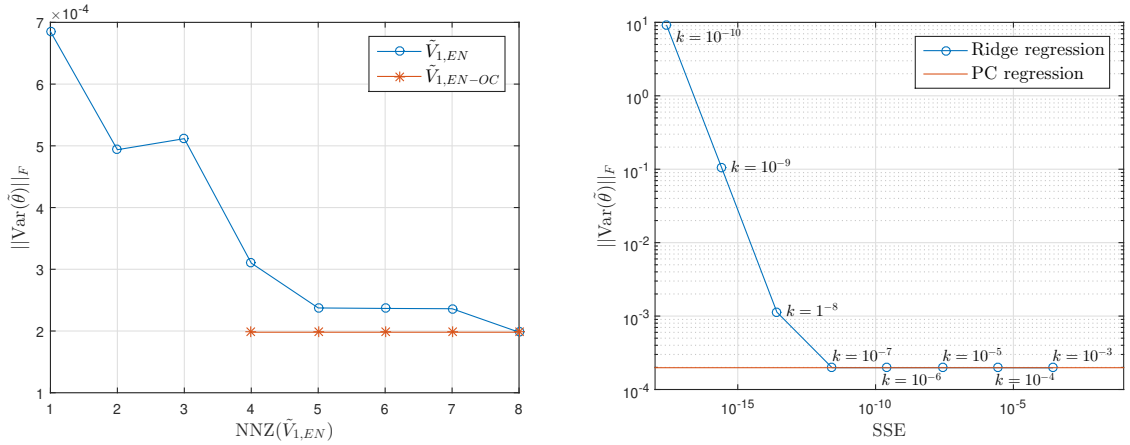

(a) (b)

Figure 10 – (a) Frobenius norm of the covariance matrix of the estimated parameters calculated with sparse PC regression (both approaches) as a function of the number of nonzero entries (NNZ) in each eigenvector in $\tilde{V}_1$. (b) Frobenius norm of the covariance matrix of the estimated parameters (circles) and sum of the squared errors (SSE) of $\hat{\eta}$ (stars) using Ridge regression as a function of its parameter (Second example).

9.3 Case study: Enzymatic reactions

Enzymatic reactions can be represented by elementary steps and described by the mass action kinetics. A simple mechanism with one substrate S and one enzyme E resulting in one product P can be expressed as

$$\mathrm{E} \quad + \quad \mathrm{S} \underset{k_{-1}}{\overset{k_1}{\rightleftharpoons}} \mathrm{ES} \xrightarrow{k_2} \mathrm{EP} \underset{k_{-3}}{\overset{k_3}{\rightleftharpoons}} \mathrm{E} \quad + \quad \mathrm{P}.$$

Suppose, for example, that the rate of reaction of the first step in both directions is many orders of magnitude higher than the following steps. This implies that the substrate-enzyme binding and dissociation step is considerably faster, which is said to be in a *quasi-equilibrium* state. Michaelis-Menten is the most used model for describing enzymatic reactions and is derived under a quasi-equilibrium assumption. Using the same principles, other expressions

have been developed to account for additional conditions, such as inhibition and activation. Employing this type of equations require knowledge about the enzymatic reactions being modeled and manual selection of the appropriate equation describing such reactions. In this case study, the idea is to apply the sparse PC regularization approach to identify steps in quasi-equilibrium and estimate kinetic constants using the complete mass action description and concentration data without further assumptions.

Consider the simple enzymatic reaction just described in an open steady-state system

$$-k_1 x_E x_S + k_{-1} x_{ES} + F(x_S^{in} - x_S) = 0 \tag{9.26a}$$

$$-k_1 x_E x_S + k_{-1} x_{ES} + k_3 x_{EP} - k_{-3} x_E x_P + F(x_E^{in} - x_E) = 0 \tag{9.26b}$$

$$k_1 x_E x_S - k_{-1} x_{ES} - k_2 x_{ES} + F(x_{ES}^{in} - x_{ES}) = 0 \tag{9.26c}$$

$$k_2 x_{ES} - k_3 x_{EP} + k_{-3} x_E x_P + F(x_{EP}^{in} - x_{EP}) = 0 \tag{9.26d}$$

$$k_3 x_{EP} - k_{-3} x_E x_P + F(x_P^{in} - x_P) = 0 \tag{9.26e}$$

where k_j is the kinetic constant of the forward reaction of the j^{th} step, k_{-j} is the kinetic constant of the backward reaction of the j^{th} step, x_i is the volume concentration of the i^{th} species, x_i^{in} is the concentration of the i^{th} species in the inlet and F is the volume flow rate divided by the volume of the system. It is important to note that steady state data does not provide enough information for individually identifying steps with considerably larger kinetic constants that operate in a different timescale. Assuming that all species are measured and F and x^{in} are known makes the system a linear model with respect to the parameters. X is generated with 10 data points by varying F from 0.01 to 2.5, fixing the inlet flow to contain only enzyme and substrate in equal concentrations, and calculating all species concentration in steady state. k_1 and k_{-1} are set to be 9 orders of magnitude larger than k_2, k_3 and k_{-3}, which creates a quasi-equilibrium for the first step.

Table 12 – Complete set of eigenvectors V_1 and V_2 and sparse eigenvectors $\tilde{V}_1$ obtained with elastic net with orthogonality constraints (EN-OC).

	V_1				V_2	$\tilde{V}_1$ (EN-OC)			
	v_1	v_2	v_3	v_4	v_5	$\tilde{v_1}$	$\tilde{v_2}$	$\tilde{v_3}$	$\tilde{v_4}$
k_1	0.102	-0.587	-0.224	0.066	0.768	0	-0.640	0	0
k_{-1}	-0.122	0.705	0.268	-0.079	0.640	0	0.768	0	0
k_2	0.073	0.377	-0.905	0.181	0	0	0	-1	0
k_3	-0.755	-0.073	0.039	0.651	0	-1	0	0	0
k_{-3}	0.632	0.100	0.238	0.730	0	0	0	0	1
Λ	4.335	1.921	0.495	0.033	2.2e-16				

The eigenvalues and eigenvectors of the kernel matrix are shown in Table 12. Because of the last eigenvalue close to zero, K is ill-conditioned and the coefficients of the covariance matrix corresponding to k_1 and k_{-1} are large (see Figure 11). PCR with dense and sparse EN-OC eigenvectors provide the same reduced variance and estimates. However, EN-OC, in its sparsest form, has the advantage of explicitly identifying steps in quasi-equilibrium, as shown by the second sparse eigenvector (see Table 12).

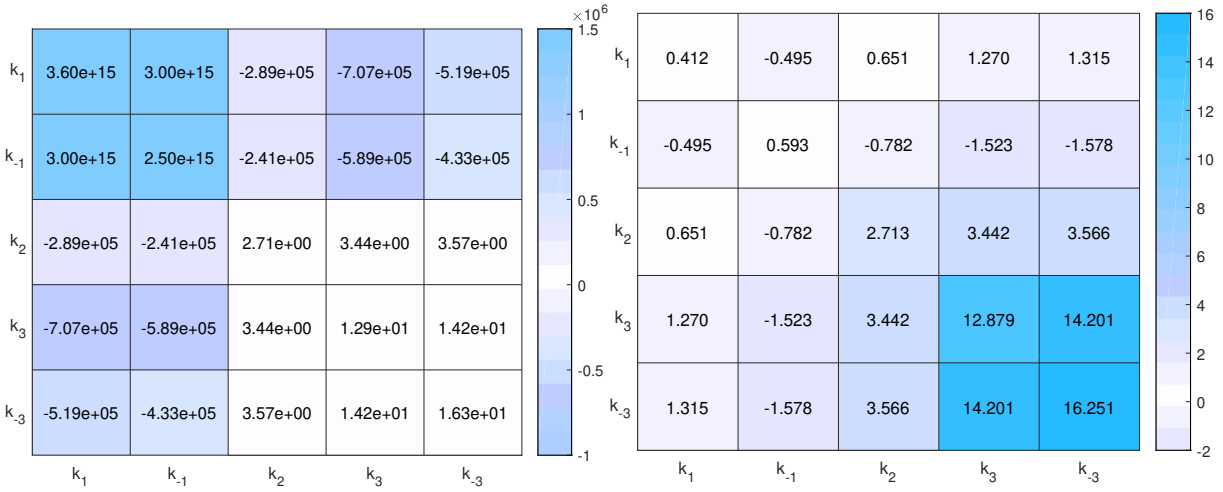

(a) Unregularized (b) PC regression

Figure 11 – Covariance matrix for estimated kinetic constants $\mathbb{V}[\hat{\theta}]$.

This approach is also applied for the general modifier mechanism of Botts and Morales (VARÓN et al., 2002):

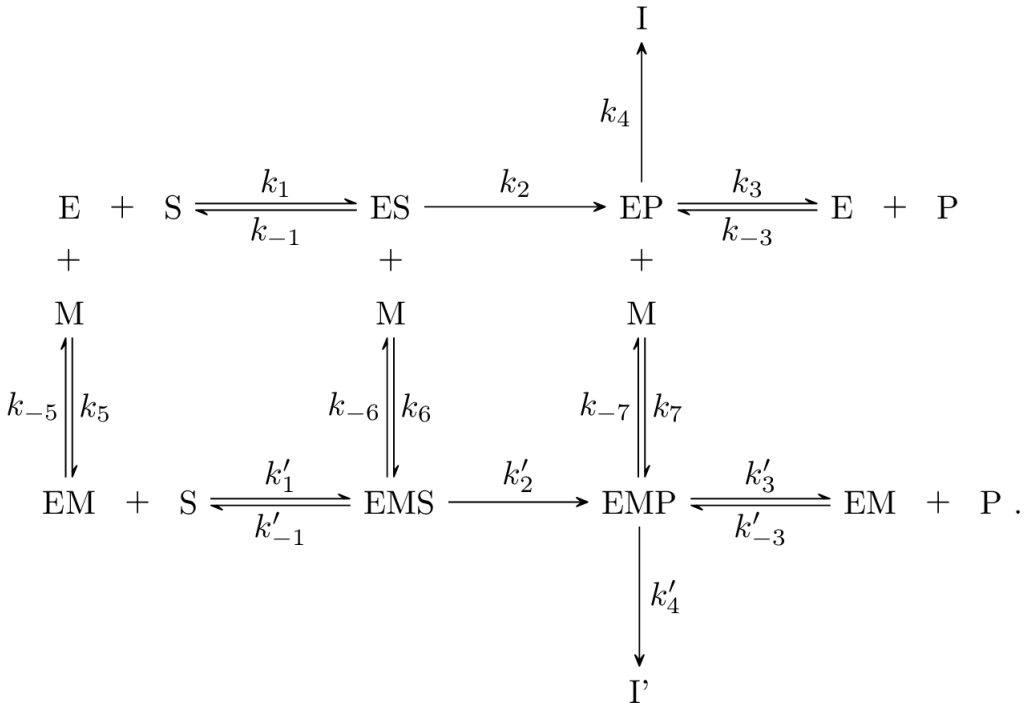

Table 13 – Dense eigenvectors V_1 for Botts-Morales example.

	V_1										
k_1	0.294	-0.544	-0.084	-0.152	0.001	-0.064	0.03	-0.084	0.264	0.0	0.076
k_{-1}	-0.294	0.544	0.084	0.152	-0.001	0.064	-0.03	0.084	-0.264	0.0	-0.076
k_2	-0.054	0.304	-0.227	-0.829	0.036	-0.216	0.209	-0.222	-0.037	0.115	0.1
k_3	-0.066	0.011	0.032	0.296	-0.056	-0.602	-0.078	-0.658	-0.111	-0.264	0.146
k_{-3}	0.017	-0.002	-0.008	-0.077	0.012	0.208	0.007	0.189	-0.182	-0.54	0.768
k_4	0.001	-0.015	0.021	0.224	-0.089	-0.077	0.964	0.075	0.001	-0.026	-0.0
k'_1	-0.069	-0.201	-0.495	0.042	-0.13	-0.017	-0.021	0.075	-0.413	-0.013	-0.119
k'_{-1}	0.069	0.201	0.495	-0.042	0.13	0.017	0.021	-0.075	0.413	0.013	0.119
k'_2	0.001	-0.009	0.267	-0.194	-0.836	-0.225	-0.082	0.259	0.037	-0.213	-0.148
k'_3	0.0	0.0	0.0	0.0	0.0	0.0	0.0	0.0	0.0	0.0	0.0
k'_{-3}	0.001	0.0	0.011	-0.038	-0.332	0.695	0.078	-0.616	-0.024	-0.091	-0.105
k'_4	0.0	0.0	0.0	0.0	0.0	0.0	0.0	0.0	0.0	0.0	0.0
k_5	0.632	0.217	0.021	0.035	0.007	-0.015	-0.007	-0.001	-0.215	-0.013	-0.066
k_{-5}	-0.632	-0.217	-0.021	-0.035	-0.007	0.015	0.007	0.001	0.215	0.013	0.066
k_6	0.065	0.264	-0.43	0.158	-0.126	0.001	-0.041	0.036	0.432	-0.093	0.041
k_{-6}	-0.065	-0.264	0.43	-0.158	0.126	-0.001	0.041	-0.036	-0.432	0.093	-0.041
k_7	0.034	0.019	-0.005	0.168	-0.336	-0.012	-0.046	-0.048	-0.073	0.744	0.542
k_{-7}	0.0	0.0	0.0	0.0	0.0	0.0	0.0	0.0	0.0	0.0	0.0

Depending on the values of the parameters, species M can act as an inhibitor or as an activator. Usually, quasi-equilibrium is assumed for the reversible reactions so that Michaelis-Menten type of equations can be used. The goal is to use concentration data for all species to identify quasi-equilibrium steps and the actual role of M. Considering a reaction with non-competitive linear inhibition, zero rate of reaction for steps 1', 2', 3', 4' and 7 is set, and kinetic constants for steps 1, 5 and 6 are defined to be much larger than for steps 2, 4 and 3. This time, 250 points for F ranging from 0.01 to 2.5 are used, which generate a data matrix X with 2500 rows. Note that the sparse eigenvectors of EN-OC identify steps 1, 1', 5, and 6 to be in quasi-equilibrium (see Table 14). In contrast, PCR correctly estimates reaction steps with zero rate but does not reveal quasi-equilibrium states (see Table 13). Other configurations were also tested, such as cases with essential activation and competitive inhibition, and EN-OC correctly identified steps that are in a different timescale and those with zero rate of reaction.

9.4 Conclusion

In this study, strategies to regularize ill-posed parameter estimation problems of linear models by using constraints were explored, showing that optimal constraints that minimize parameter covariance can be constructed by exploiting information from the kernel matrix. A modified elastic net strategy to sparsify the constraints and facilitate their interpretability is

Table 14 – Sparse eigenvectors $\tilde{V}_1$ or Botts-Morales example calculated with elastic net with orthogonality constraint.

	$\tilde{V}_1$ (EN-OC)										
k_1	0.0	-0.707	0.0	0.0	0.0	0.0	0.0	0.0	0.0	0.0	0.0
k_{-1}	0.0	0.707	0.0	0.0	0.0	0.0	0.0	0.0	0.0	0.0	0.0
k_2	0.0	0.0	0.0	-1.0	0.0	0.0	0.0	0.0	0.0	0.0	0.0
k_3	0.0	0.0	0.0	0.0	0.0	0.0	0.0	-1.0	0.0	0.0	0.0
k_{-3}	0.0	0.0	0.0	0.0	0.0	0.0	0.0	0.0	0.0	0.0	1.0
k_4	0.0	0.0	0.0	0.0	0.0	0.0	1.0	0.0	0.0	0.0	0.0
k'_1	0.0	0.0	-0.707	0.0	0.0	0.0	0.0	0.0	0.0	0.0	0.0
k'_{-1}	0.0	0.0	0.707	0.0	0.0	0.0	0.0	0.0	0.0	0.0	0.0
k'_2	0.0	0.0	0.0	0.0	-1.0	0.0	0.0	0.0	0.0	0.0	0.0
k'_3	0.0	0.0	0.0	0.0	0.0	0.0	0.0	0.0	0.0	0.0	0.0
k'_{-3}	0.0	0.0	0.0	0.0	0.0	1.0	0.0	0.0	0.0	0.0	0.0
k'_4	0.0	0.0	0.0	0.0	0.0	0.0	0.0	0.0	0.0	0.0	0.0
k_5	0.707	0.0	0.0	0.0	0.0	0.0	0.0	0.0	0.0	0.0	0.0
k_{-5}	-0.707	0.0	0.0	0.0	0.0	0.0	0.0	0.0	0.0	0.0	0.0
k_6	0.0	0.0	0.0	0.0	0.0	0.0	0.0	0.0	0.707	0.0	0.0
k_{-6}	0.0	0.0	0.0	0.0	0.0	0.0	0.0	0.0	-0.707	0.0	0.0
k_7	0.0	0.0	0.0	0.0	0.0	0.0	0.0	0.0	0.0	1.0	0.0
k_{-7}	0.0	0.0	0.0	0.0	0.0	0.0	0.0	0.0	0.0	0.0	0.0

also presented. An interesting finding is that this approach can identify clusters of parameters in an effective manner. In the next chapter, this eigenvector-based regularization approach is applied to nonlinear estimation problems by using regularization inside an interior-point optimization solver.

10 Nonlinear parameter estimation

Consider a set of state variables $x_\ell \in \mathbb{R}^p$ and output observations $\eta_\ell \in \mathbb{R}^s$ with $\ell = 1, \ldots, L$ experiments. Suppose the output observations can be modeled as $\bar{\eta}_\ell = \phi(x_\ell, \theta)$ where $\bar{\eta}_\ell \in \mathbb{R}^s$ are the modeled observations and $\theta \in \mathbb{R}^m$ are unknown parameters. Assuming that the error $\epsilon_\ell = \eta_\ell - \bar{\eta}_\ell$ is a Gaussian variable $\epsilon_\ell \sim \mathcal{N}(0, \mathbb{V}_\ell)$ with covariance $\mathbb{V}_\ell \in \mathbb{R}^{s\times s}$, the likelihood function is given by

$$L_H(\theta) := (2\pi)^{-sL/2} \prod_{\ell=1}^{L} (\det \mathbb{V}_\ell)^{(-1/2)} \exp\left(-\frac{1}{2} \sum_{\ell=1}^{L} \epsilon_\ell^T \mathbb{V}_\ell^{-1} \epsilon_\ell \right). \tag{10.1}$$

In maximum likelihood estimation (MLE), the idea is to find an estimate $\hat{\theta}$ for the parameters that maximize the likelihood function. Because the natural logarithm is a monotone function, maximizing the likelihood function is equivalent to maximizing the log likelihood function. Assuming that errors from different experiments are independent and that every experiment ℓ has the same covariance matrix $\mathbb{V}$, the log likelihood function is

$$\log L_H(\theta) = -\frac{sL}{2} \log 2\pi - \frac{L}{2} \log \det \mathbb{V} - \frac{1}{2} \sum_{\ell=1}^{L} \epsilon_\ell^T \mathbb{V}_\ell^{-1} \epsilon_\ell. \tag{10.2}$$

Maximizing $\log L_H(\theta)$ is equivalent to minimizing $-\log L_H(\theta)$ and, since only ϵ_ℓ depends on the parameters, the MLE estimate is given by

$$\hat{\theta} \in \arg\min_\theta \ \frac{1}{2} \sum_{\ell=1}^{L} (\eta_\ell - \bar{\eta}_\ell)^T \mathbb{V}^{-1} (\eta_\ell - \bar{\eta}_\ell). \tag{10.3}$$

If the errors within each experiment are also independent, $\mathbb{V}$ is diagonal and MLE is equivalent to the weighted least squares estimation with the $\mathbb{V}$ as the weight matrix. Bard (1974) shows that for a single equation model, MLE is equivalent to the unweighted least squares method.

When the state variables x are known exactly and there are no constraints on the parameters, the estimation problem can be formulated as an unconstrained optimization problem

$$\hat{\theta} \in \arg\min_\theta \ \frac{1}{2} \sum_{\ell=1}^{L} \left(\eta_\ell - \phi(x_\ell, \theta)\right)^T \mathbb{V}^{-1} \left(\eta_\ell - \phi(x_\ell, \theta)\right) \tag{10.4}$$

where $\phi(x_\ell, \theta)$ is a nonlinear mapping function between the problem variables and the output observation, and solved according to Section 8.2.1. However, if the states variables are not directly measured or are subjected to errors, they can also be treated as random variables

to be estimated. Models that represent their behavior can be used as constraints in the formulated optimization problem as follows

$$(\hat{\theta}, \hat{x}) \in \arg\min_{\theta,x} \frac{1}{2} \sum_{\ell=1}^{L} (\eta_\ell - \phi(x_\ell, \theta))^T \mathbb{V}^{-1} (\eta_\ell - \phi(x_\ell, \theta)) \tag{10.5a}$$

$$\text{s.t.} \quad h_\ell(x_\ell, \theta) = 0 \quad \text{for } \ell = 1, \ldots, L \tag{10.5b}$$

where $\phi(x_\ell, \theta)$ is a mapping function between the problem variables and the output observation and $h_\ell(x_\ell, \theta)$ corresponds to the p model equations for the ℓ^{th} experiment.

Whether the estimation problem is an unconstrained or a constrained optimization, positive definiteness of the Hessian or the reduced Hessian, respectively, is a required condition for convergence to a local minimum, if the problem is non-convex. If, for example, during the iterative solution using a line search interior point algorithm, they are singular or indefinite, a regularization approach is necessary.

10.1 Hessian modification

A common strategy for regularizing ill-conditioned (reduced) Hessian in line search interior point algorithms is modifying the Hessian of the Lagrange function by adding a multiple of the identity matrix. `Ipopt` and `LOQO`, for example, are two solvers that implement this approach (WÄCHTER; BIEGLER, 2006; VANDERBEI, 1999).

Consider the KKT system (8.22) for iteration k in a line search interior point algorithm. If the reduced Hessian is not positive definite, the KKT matrix is modified as follows

$$\begin{bmatrix} H_k + \Sigma_k + \delta_H I & \nabla h(w_k)^T \\ \nabla h(w_k) & -\delta_h I \end{bmatrix} \begin{bmatrix} d_k^w \\ d_k^\lambda \end{bmatrix} = - \begin{bmatrix} \nabla_w \varphi(w_k, \mu_j) + \nabla h(w_k)^T \lambda_k \\ h(w_k) \end{bmatrix} \tag{10.6}$$

where $\delta_H \geq 0$ is a scalar chosen in a way that the reduced Hessian becomes positive definite and $\delta_h \geq 0$ is used when $\nabla h(w_k)$ are linearly dependent, which implies that the KKT matrix is singular. In each iteration, `Ipopt` uses a heuristic for choosing δ_H that increases δ_H gradually so that it can be approximately the smallest necessary value. A nonzero value is also set to δ_h whenever the KKT matrix is singular; it is always assumed that, in this case, ill-conditioning is due to rank-deficient constraint gradients, the occurrence of singularity in reduced Hessian is not verified (WÄCHTER; BIEGLER, 2006).

10.2 Eigenvector-based regularization

An eigenvector-based regularization inspired by rotational discrimination (FARISS; LAW, 1979) and PCR (JOLLIFFE, 1982) is presented. The idea is to decompose the (reduced) Hessian into eigenvalues and eigenvectors, and to remove directions from the solution space associated with near zero eigenvalues, i.e., directions with small curvature, at iterations that require regularization due to (near) singularity in the reduced Hessian. The advantage of this approach is that convex directions are kept unchanged, while directions that do not significantly influence the objective value in the iterate neighborhood are removed. In addition, groups of correlated parameters can be identified by inspecting the eigenvectors of the reduced Hessian.

10.2.1 Unconstrained problems

Consider the unconstrained estimation problem

$$\min_{\theta} \; f(\theta) := \frac{1}{2} \sum_{\ell=1}^{L} (\eta_\ell - \phi(x_\ell, \theta))^T (\eta_\ell - \phi(x_\ell, \theta)) \tag{10.7}$$

where $\eta_\ell \in \mathbb{R}$ is an output observation and $x_\ell \in \mathbb{R}^p$ is a known state variable for the L^{th} experiment, $\theta \in \mathbb{R}^m$ are the unknown parameters and $\phi(x_\ell, \theta)$ is a nonlinear mapping function between the state variable and parameters and the output observation. Here the focus is on the calculation of the search direction, since it is the step of the iteration calculation that is directly influenced by ill-conditioning of the Hessian. Equation 8.10 can be rewritten using the eigenvalue decomposition of $\nabla^2 f(\theta_k)$ as

$$(V \Lambda V^T) d_k = -\nabla f(\theta_k), \tag{10.8}$$

where $V \in \mathbb{R}^{m \times m}$ is the eigenvectors and $\Lambda \in \mathbb{R}^{m \times m}$ is a diagonal matrix with the eigenvalues of the Hessian. $V \Lambda V^T$ can be split into a term with large eigenvalues $\Lambda_1 \in \mathbb{R}^{m-q \times m-q}$ and their associated eigenvectors $V_1 \in \mathbb{R}^{m \times m-q}$ and a term with (near) zero eigenvalues $\Lambda_2 \in \mathbb{R}^{q \times q}$, defined by a threshold β, and their associated eigenvectors $V_2 \in \mathbb{R}^{m \times q}$, resulting in

$$(V_1 \Lambda_1 V_1^T + V_2 \Lambda_2 V_2^T) d_k = -\nabla f(\theta_k). \tag{10.9}$$

Dropping the second term of the eigenvalue decomposition leads to

$$\begin{aligned}(V_1\Lambda_1 V_1^T)d_k &= -\nabla f(\theta_k)\\ \Lambda_1 V_1^T d_k &= -V_1^T\nabla f(\theta_k)\\ V_1^T d_k &= -\Lambda^{-1}V_1^T\nabla f(\theta_k),\end{aligned} \tag{10.10}$$

which is the search direction projected onto V_1. In the original coordinates, the search direction is $d_k = -V_1\Lambda^{-1}V_1^T\nabla f(\theta_k)$. Therefore, the PCR-like method decomposes the Hessian into eigenvalues and eigenvectors, calculates a search direction in the space spanned by the eigenvectors associated with large eigenvalues, and then projects this search direction back onto the original coordinates.

Because nonlinear problems are often nonconvex, it is also important to address how to deal with negative curvature in the Hessian. Instead of perturbing the complete matrix, as done by the Hessian modification method, one can change only the directions associated with negative eigenvalues, since the eigenvalue decomposition is already performed. Here, two approaches are considered: (i) using the absolute value of negative eigenvalues, and (ii) replacing them by a small positive value, which is similar to the Hessian modification as it can be seen as adding a scalar to negative eigenvalues large enough for them to become positive and greater than zero. While the former simply realigns the search direction downwards, the latter defines a large step in the direction of the negative eigenvalue. These approaches can be implemented in Equation (10.10) by redefining Λ_1. The first approach changes negative entries of Λ_1 by assuming their absolute values,

$$\lambda_j = |\lambda_j| \quad \text{for } j = 1,\ldots,m-q, \tag{10.11}$$

while the second approach modifies negative eigenvalues as follows

$$\lambda_j = \beta \quad \text{if } \lambda_j < -\beta \quad \text{for } j = 1,\ldots,m-q \tag{10.12}$$

where β is a small positive scalar, the same used as threshold for determining Λ_2.

10.2.1.1 Case study

A simple Newton's method algorithm is implemented in Python following the description in Section 8.2.1 and using Casadi (ANDERSSON et al., 2019) for the computation of first and second derivatives. This algorithm is used to solve the simple unconstrained parameter

estimation problem presented here. The problem, obtained from Bard (1974), consists of a least squares estimation of two parameters from a single compound chemical reaction model starting from initial conditions $\eta_0 = 1$ and $t_0 = 0$, which is given by

$$\bar{\eta} = \exp\left(-\theta_1 t \exp\left(-\frac{\theta_2}{T} \right) \right) \tag{10.13}$$

where $\bar{\eta} \in \mathbb{R}$ is the modeled remaining fraction of the reacting compound, $\theta \in \mathbb{R}^2$ are the parameters, $t \in \mathbb{R}$ is time ellapsed (s) and $T \in \mathbb{R}$ is temperature (K). The input data used for this estimation problem are listed in Table 15. This problem is not actually ill-conditioned, but it is a good example to analyze how the regularization approach based on eigenvalue decomposition deals with non convexity in the solution space.

Table 15 – Input data for the unconstrained least squares case study from Bard (1974).

Experiment ℓ	t **(s)**	T **(K)**	η
1	0.1	100	0.980
2	0.2	100	0.983
3	0.3	100	0.955
4	0.4	100	0.979
5	0.5	100	0.993
6	0.05	200	0.626
7	0.1	200	0.544
8	0.15	200	0.455
9	0.2	200	0.225
10	0.25	200	0.167
11	0.02	300	0.566
12	0.04	300	0.317
13	0.06	300	0.034
14	0.08	300	0.016
15	0.1	300	0.066

A three dimensional graph and a contour plot of the solution space are presented in Figure 12, which shows that the problem is not convex and has small curvature mostly along axis θ_1. The eigenvector-based regularization approach is compared with the Hessian modification method. The former is combined with both approaches described in Section (10.2.1) to deal with negative eigenvalues, namely (i) using the absolute value of negative eigenvalues to rewrite the Hessian, and (ii) setting a small positive value equal to the threshold β to replace negative eigenvalues.

For the eigenvector-based regularization approach, a threshold $\beta = 10^{-6}$ is used and, for the Hessian modification, constant δ is calculated in a way that the smallest eigenvalue bellow this threshold has the same value as β. 20 different initial points for θ are used to

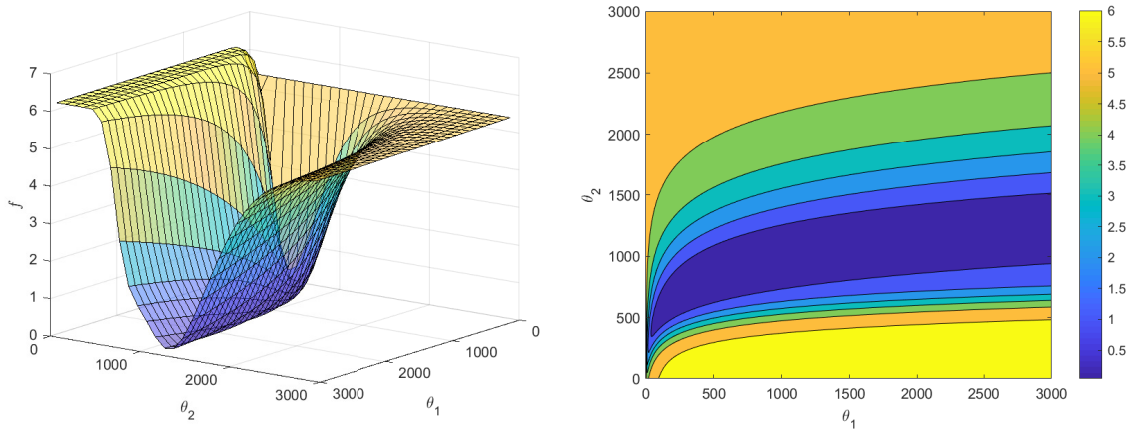

Figure 12 – 3D graph and contour plot of the space of allowable solutions for the unconstrained parameter estimation case study.

assess the regularization methods; $\theta_{1,0}$ and $\theta_{2,0}$ are uniform and randomly selected from a range from 200 to 2000. Figure 13 compares the number of iterations using both eigenvalue based regularization approach and the Hessian modification method; note that the three regularization methods perform similarly. The red circles correspond to problems that are not able to leave the initial point neighborhood using the approach that sets negative eigenvalues to a small positive value. All estimation problems that converge to a solution find the estimate $\theta^{*T} = [\ 813.9 \quad 961.0\ ]$. However, they do not necessarily follow the same path, as evidenced by the different number of iterations; Figure 14 shows an example of the calculation path using the three different regularization approaches. Nonetheless, due to the expensive task of performing an eigenvalue decomposition, it is possible to conclude that, in this case, the Hessian modification method is more efficient when it comes to dealing with negative curvature.

An important observation is that the threshold β must be carefully chosen to ensure that the algorithm makes progress when using the eigenvector-based regularization method. For instance, the eigenvalues of the Hessian matrix at $\theta_k^T = [\ 1000 \quad 200\ ]$ are $\Lambda_k = [\ -1.25 \times 10^{-9} \quad -9.81 \times 10^{-8}\ ]$. If $\beta = 10^{-6}$, as used in this example, and those values were chosen as initial guess, for example, the algorithm would not be able to determine a search direction and calculation would cease without finding a solution. Therefore, if one also considers that the Hessian modification method is more efficient when dealing with negative curvature, the eigenvector-based regularization approach is more suitable for application during the last iterations, when the algorithm gets close to a solution, in a convex region, corroborating the remarks made by Wang et al. (2013).

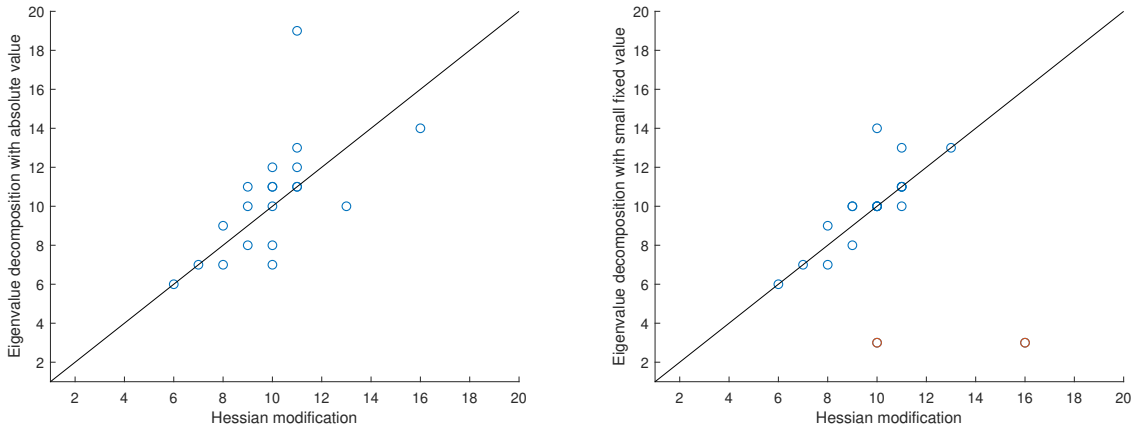

Figure 13 – Comparison between both eigenvalue decomposition regularization approaches and the Hessian modification method regarding the necessary number of iterations used to solve the unconstrained parameter estimation problem with 20 different initial guesses.

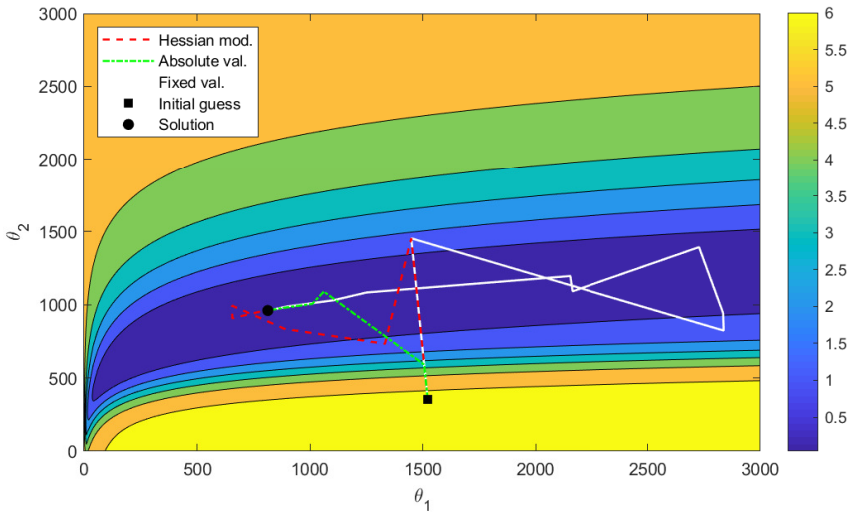

Figure 14 – Example of paths when both eigenvalue decomposition regularization approaches and the Hessian modification method are used for the unconstrained parameter estimation problem with same initial guess.

10.2.2 Constrained problems

Due to the presence of constraints, reducing the space of allowable solutions is not as simple as just using selected eigenvectors of the Hessian matrix as it can be done with unconstrained problems. However, this reduction can be done by enforcing specific constraints using eigenvectors of the reduced Hessian. As described in Section 8.2.2, Newton's method approximates the KKT system of the current point w_k to a linear model. Therefore, calculating an iteration step is equivalent to solving a linear system and an

analogy can be made between QP and calculating an iteration in nonlinear programming (NLP) by comparing Equations (8.5) and (8.17). In this section, it is first demonstrated that adding a constraint of the form $V_2^T\theta = 0$ in an equality-constrained quadratic problem is equivalent to performing the eigenvalue decomposition of the reduced Hessian and removing the directions corresponding to V_2. Then, based on this observation and on the results from unconstrained parameter estimation, the implementation of this regularization approach in an interior point solver for nonlinear optimization is described. The main advantage of this regularization method is that, besides dealing with nearly flat regions in the neighborhood of the solution, the eigenvectors can be used to recognize groups of correlated parameters providing valuable information for identifiability analysis.

10.2.2.1 Equality-constrained quadratic problems

Consider the QP problem for one experiment

$$\min_{x,\theta} \quad \frac{1}{2}(\eta - (Cx + D\theta))^T(\eta - (Cx + D\theta)) \tag{10.14a}$$

$$\text{s.t.} \quad h(x,\theta) := Ax + B\theta = 0 \tag{10.14b}$$

where $\eta \in \mathbb{R}^s$ are output observations, $x \in \mathbb{R}^p$ are state variables and $\theta \in \mathbb{R}^m$ are parameters. The expression $Cx + D\theta$ is a linear mapping between the state variables and parameters, and the output observations with $C \in \mathbb{R}^{s\times p}$ and $D \in \mathbb{R}^{s\times m}$, and $h(x,\theta)$ are equality constraints where $A \in \mathbb{R}^{p\times p}$ is a nonsingular square matrix and $B \in \mathbb{R}^{p\times m}$. Note that this problem has m degrees of freedom, as there are the same number of constraints and state variables. From equation (8.5), the KKT system for this optimization problem is given by

$$\begin{bmatrix} C^TC & C^TD & A^T \\ D^TC & D^TD & B^T \\ A & B & \end{bmatrix}\begin{bmatrix} d^x \\ d^\theta \\ \lambda \end{bmatrix} = -\begin{bmatrix} C^TCx_0 + C^TD\theta_0 + c_x \\ D^TCx_0 + D^TD\theta_0 + c_\theta \\ Ax_0 + B\theta_0 \end{bmatrix}. \tag{10.15}$$

where $\lambda \in \mathbb{R}^p$ are the Lagrange multipliers, d are the steps for the state variables and parameters, x_0 and θ_0 are the initial value for the state variables and the parameters, and $c_x := \eta^T C$ and $c_\theta := \eta^T D$.

The reduced Hessian can be obtained by calculating the null space of $\nabla h(x,\theta)$, $Z \in \mathbb{R}^{n\times m}$ with $n = m + p$, and performing Z^TQZ, where $Q \in \mathbb{R}^{n\times n}$ is the Hessian matrix. Matrix Z is not unique; however, a pertinent way of calculating it is to consider the state variables x

as dependent variables and the parameters θ as independent variables, as shown in Section 8.3, and calculate

$$Z = \begin{bmatrix} -A^{-1}B \\ I_p \end{bmatrix} \tag{10.16}$$

where $\mathbb{I}_p$ is the identity matrix of dimension p. The Hessian matrix, Q, is the 2×2 top right block in the KKT matrix in (10.15). By calculating $Z^T QZ$, the reduced Hessian is given by

$$Z^T QZ = D^T D - D^T CA^{-1}B - B^T(A^{-1})^T C^T D + B^T(A^{-1})^T C^T CA^{-1}B. \tag{10.17}$$

The KKT system (10.15) can be analytically solved. Rearranging the third equation leads to

$$d^x = -A^{-1}(Bd^\theta + B\theta_0 + Ax_0), \tag{10.18}$$

and substituting it into the first equation gives

$$\lambda = -A^{-T}(C^T D - C^T CA^{-1}B)d^\theta + A^{-T}C^T CA^{-1}(B\theta_0 + Ax_0) - \quad A^{-T}(C^T D\theta_0 + C^T Cx_0) - A^{-T}c_x. \tag{10.19}$$

Substituting λ and d^x into the second equation and rearranging all terms result in

$$Z^T QZd^\theta = -Z^T QZ\theta_0 + B^T A^{-T}c_x - c_\theta. \tag{10.20}$$

Once d^θ is obtained, the dependent variable step d^x and the Lagrange multipliers λ can be then calculated.

If the reduced Hessian is (near) singular, this problem can be regularized in a PCR-like approach. The eigenvalue decomposition of the reduced Hessian can be used for that end. After defining a threshold β, $Z^T QZ$ can be split into two terms according to its eigenvalues as follows

$$Z^T QZ = V_1 \Lambda_1 V_1^T + V_2 \Lambda_2 V_2^T, \tag{10.21}$$

where V_2 are the q eigenvectors associated with the (near) zero eigenvalues Λ_2 and V_1 are the $m - q$ eigenvectors associated with the large eigenvalues Λ_1. Then, dropping the term with Λ_2 in the left-hand side, equation (10.20) becomes

$$V_1 \Lambda_1 V_1^T d^\theta = -Z^T QZ\theta_0 + B^T A^{-T}c_x - c_\theta. \tag{10.22}$$

Multiplying both sides by V_1^T and then by Λ_1^{-1} respectively leads to

$$V_1^T d^\theta = -\Lambda_1^{-1} V_1^T (Z^T Q Z \theta_0 + B^T A^{-T} c_x - c_\theta), \tag{10.23}$$

which is the reduced set of variables corresponding to the step of the independent variables d^θ in V_1 coordinates. Projecting it back to the original coordinates gives the expression

$$d^\theta = -V_1 \Lambda_1^{-1} V_1^T (Z^T Q Z \theta_0 + B^T A^{-T} c_x - c_\theta). \tag{10.24}$$

Alternatively, an ill-conditioned problem of the form (10.14) can be solved by adding new constraints that fix the parameter relationships present in V_2, the eigenvectors associated with the damaging eigenvalues from the reduced Hessian. Modifying the KKT system (10.15) and enforcing the constraint $V_2^T d^\theta = 0$ result in

$$\begin{bmatrix} C^T C & C^T D & A^T & \\ D^T C & D^T D & B^T & V_2 \\ A & B & & \\ & V_2^T & & \end{bmatrix} \begin{bmatrix} d^x \\ d^\theta \\ \lambda \\ \nu \end{bmatrix} = - \begin{bmatrix} C^T C x_0 + C^T D \theta_0 + c_x \\ D^T C x_0 + D^T D \theta_0 + c_\theta \\ A x_0 + B \theta_0 \\ 0 \end{bmatrix}, \tag{10.25}$$

where ν are the Lagrange multipliers corresponding to the new constraints. Comparing (10.25) to (10.15), it is possible to see that equations one and three are both unchanged, so d^x and λ are also described by the same expressions (10.18) and (10.19). The second equation from (10.25), however, has a new term when compared to (10.20), and when (10.18) and (10.19) are substituted into it, the new expression is

$$Z^T Q Z d^\theta + V_2 \nu = -Z^T Q Z \theta_0 + B^T A^{-T} c_x - c_\theta. \tag{10.26}$$

Again, splitting $Z^T Q Z$ into two terms according to its eigenvalues, as in (10.21), and multiplying by V_1^T leads to

$$V_1^T (V_1 \Lambda_1 V_1^T + V_2 \Lambda_2 V_2^T) d^\theta + V_1^T V_2 \nu = -V_1^T (Z^T Q Z \theta_0 + B^T A^{-T} c_x - c_\theta). \tag{10.27}$$

Because V_1 and V_2 are orthogonal, $V_1^T V_2 \Lambda_2 V_2^T d^\theta$ and the second term on the letf-hand side are both zero, which results in (10.23). This shows that adding the set of constraints $V_2^T d^\theta = 0$ with eigenvectors of the reduced Hessian is equivalent to reducing the space of allowable solutions in a PCR-like approach.

10.2.2.1.1 Illustrative example

An example is now presented to illustrate that adding new constraints using the eigenvectors of the reduced Hessian, and performing a principal component reduction in the space of solution are equivalent. The results are also compared to the Hessian modification approach, which adds a diagonal matrix to the top left block of the KKT matrix. A simple synthetic ill-conditioned QP problem in the same form as (10.14) is created. The model is built with $m = 5$ parameters θ and $p = 1$ state variable . To induce correlations among the parameters, the columns of D are generated as follows

$$\begin{aligned}
\eth_1 &\sim \mathcal{N}(0, 1) \\
\eth_2 &\sim \mathcal{N}(0, 1) \\
\eth_3 &\sim \mathcal{N}(0, 1) \\
\eth_4 &= \eth_1 + \varepsilon \\
\eth_5 &= 2\eth_2 + \varepsilon
\end{aligned}$$

where $\eth_i \in \mathbb{R}^s$ is the i^{th} column of D and $\varepsilon \sim \mathcal{N}(0, I \cdot 10^{-12})$ is a small perturbation. In this case, $C \sim \mathcal{N}(0, I)$ is a column vector, and η is generated from the mapping function, with the original parameters and state variable in Table 17 and the addition of an error $\epsilon \sim \mathcal{N}(0, I \cdot 10^{-2})$. The equality constraint $h(x, \theta)$ is defined by $A = [-1]$ and $B = [\ 1.3 \quad 1 \quad 1 \quad 1 \quad 1\ ]$.

The reduced Hessian is calculated following the methodology described in Section 8.3. The eigenvalue decomposition is presented in Table 16. The presence of a small eigenvalue indicates that the equality constraint is not able to provide all the information necessary to uniquely determine the parameters with high confidence, as shown in the previous chapter; there is still one direction V_2 that keeps the problem ill-conditioned.

Table 16 – Eigenvectors of the reduced Hessian calculated from the KKT matrix of the illustrative example for equality-constrained quadratic problem.

	V_2	V_1			
θ_1	-0.639	0.206	0.251	-0.686	0.129
θ_2	0.383	0.773	0.043	-0.015	0.504
θ_3	0.000	-0.101	-0.914	-0.323	0.223
θ_4	0.639	-0.391	0.273	-0.599	0.073
θ_5	-0.192	-0.444	0.158	0.258	0.822
Λ	2.24e-12	0.91	10.95	30.92	116.64

Table 17 shows the original parameters and state variable, as well as estimations computed with the PCR-like approach (10.24), by adding the new constraint $V_2^T\theta = 0$, and by adding $\delta_H I$ to the Hessian with $\delta_H = 10^{-6}$. The same initial values for x and θ is used. It is possible to see that reducing the space of allowable solution according to the eigenvalue decomposition and adding new constraint built with the eigenvectors associated with the smallest eigenvalues generate equivalent steps. Also, the Hessian modification method resulted in a different estimate for θ, which shows that this regularization approach provides a different search direction than regularization based on the eigenvalue decomposition of the reduced Hessian. An advantage of the latter approach is that parameters that cannot be individually estimated and are, therefore, correlated can be singled out by the entries of the eigenvectors in V_2.

Table 17 – Original and estimated state variable and parameters of the illustrative example for equality-constrained quadratic problem.

	x	θ_1	θ_2	θ_3	θ_4	θ_5
Original variables	2	1	1.5	-0.5	0.7	-1
PCR-like	1.999	0.980	1.462	-0.471	0.710	-0.975
Constraint V_2	1.998	0.979	1.463	-0.471	0.709	-0.975
Hessian modification	1.998	1.812	0.963	-0.471	-0.125	-0.725

10.2.2.2 Interior point implementation

The eigenvector-based regularization method is implemented in an existing interior point solver developed with Pynumero (RODRIGUEZ et al., 2018), which is a framework for developing NLP optimization algorithms in Python. Pyomo (HART et al., 2017; HART et al., 2011) is used as the mathematical modeling language. Since it has interfaces with tools for automatic differentiation, Pyomo provides exact first and second derivatives. This interior point implementation is based on the `Ipopt` algorithm and, thus, follows the same steps as described in Section 8.2.2.1. For later reference, the KKT system (8.22) can be rewritten

defining $W_k := H_k + \Sigma_k$ and splitting the complete vector of variables into state variables and parameters as follows

$$\begin{bmatrix} W_k^{xx} & W_k^{x\theta} & \nabla_x h(x_k,\theta_k)^T \\ W_k^{\theta x} & W_k^{\theta\theta} & \nabla_\theta h(x_k,\theta_k)^T \\ \nabla h_x(x_k,\theta_k) & \nabla h_\theta(x_k,\theta_k) & \end{bmatrix} \begin{bmatrix} d_k^x \\ d_k^\theta \\ d_k^\lambda \end{bmatrix} = - \begin{bmatrix} \nabla_x \varphi(x_k,\theta_k,\mu_j) + \nabla_x h(x_k,\theta_k)^T \lambda_k \\ \nabla_\theta \varphi(x_k,\theta_k,\mu_j) + \nabla_\theta h(x_k,\theta_k)^T \lambda_k \\ h(x_k,\theta_k) \end{bmatrix}. \tag{10.29}$$

To calculate a step, the interior point algorithm provides the KKT system to a linear solver. First, the linear solver factorizes the KKT matrix and, then, performs backsolves using the right-hand side. After the factorization step, some solvers, such as MA27, MA57 and MUMPS (AMESTOY et al., 2001; STFC, 2020), return the inertia of the factorized matrix, i.e, the number of positive, negative and zero eigenvalues. For the reduced Hessian to be positive definite, the KKT matrix must have n positive, p negative, and no zero eigenvalues (CHIANG; ZAVALA, 2016), where n is the total number of variables and p is the number of constraints. Therefore, when there are more than p negative eigenvalues, the reduced Hessian is not positive definite, and when there are zero eigenvalues, the matrix is not invertible and there are infinite possible values for the step. In both cases, regularization is needed. The interior point algorithm used relies on the inertia information to decide when to regularize the KKT matrix.

The default precision to determine if an eigenvalue is zero is machine precision, but a different value can be provided to the linear solver. To implement the eigenvector-based regularization method, a threshold β_ε is defined to identify iterations at which the reduced Hessian might have nearly flat directions. However, based on the results from Section 10.2.1.1, this regularization approach is ideally applied close to the solution, thus the threshold β_ε is only defined when the barrier parameter μ_j is smaller than a specified value β_μ.

The eigenvector-based regularization uses the KKT matrix to calculate the reduced Hessian using the approach described in Section 8.3 and performs its eigenvalue decompo-

sition. A new set of constraints built with the eigenvectors associated with the eigenvalues smaller than β_ε, V_2, is added, resulting in a new KKT system of the form

$$\begin{bmatrix} W_k^{xx} & W_k^{x\theta} & \nabla_x h(x_k,\theta_k)^T & \\ W_k^{\theta x} & W_k^{\theta\theta} & \nabla_\theta h(x_k,\theta_k)^T & V_2 \\ \nabla h_x(x_k,\theta_k) & \nabla h_\theta(x_k,\theta_k) & & \\ & V_2^T & & \end{bmatrix} \begin{bmatrix} d_k^x \\ d_k^\theta \\ d_k^\lambda \\ d_k^\nu \end{bmatrix} = - \begin{bmatrix} \nabla_x \varphi(x_k,\theta_k,\mu_j) + \nabla_x h(x_k,\theta_k)^T \lambda_k \\ \nabla_\theta \varphi(x_k,\theta_k,\mu_j) + \nabla_\theta h(x_k,\theta_k)^T \lambda_k \\ h(x_k,\theta_k) \\ 0 \end{bmatrix}. \tag{10.30}$$

This system is then solved by the linear solver to compute the regularized step. A summary of the step computation with the eigenvector-based regularization method implementation is presented in Algorithm 1.

Algorithm 1 Step computation in the interior point algorithm used to implement the eigenvector-based regularization method.

```
if μ_j < β_μ then
    set linear solver precision to β_ε
    perform KKT matrix factorization
    if number of zero eigenvalues > 0 and number of negative eigenvalues == p then
        set linear solver precision to 0
        perform KKT matrix factorization
        calculate reduced Hessian
        perform eigenvalue decomposition of the reduced Hessian
        add new constraints V_2 to the KKT system
        perform KKT matrix factorization
    end
else
    perform KKT matrix factorization
    if number of zero eigenvalues > 0 then
        set a value to δ_h
        modify the Hessian
        if number of negative eigenvalues == p then
            perform KKT matrix factorization
        end
    end
end
if number of negative eigenvalues > p then
    while number of negative eigenvalues > p do
        set a value to δ_H
        modify the Hessian
        perform KKT matrix factorization
    end
end
calculate new step with backsolves
```

10.3 Case studies

Two case studies are presented in this section. The case study estimating the parameters of a simple enzymatic reaction from last chapter is revisited with a nonlinear optimization problem formulation. The other case study is the parameter estimation problem of a dynamic kinetic model with ordinary differential equations (ODE) as constraints. Both problems are solved using the interior point algorithm in Pynumero with the implementation of the eigenvector-based regularization and the MUMPS linear solver.

10.3.1 Enzymatic reaction

Consider again the mechanism for a simple enzymatic reaction

$$\mathrm{E} + \mathrm{S} \underset{k_{-1}}{\overset{k_1}{\rightleftharpoons}} \mathrm{ES} \xrightarrow{k_2} \mathrm{EP} \underset{k_{-3}}{\overset{k_3}{\rightleftharpoons}} \mathrm{E} + \mathrm{P}$$

and the corresponding model (9.26). If just a subset of the participating species is measured and a positive constraint is imposed to all variables, the parameter estimation problem becomes nonlinear. Suppose the same conditions are valid: the system is in steady state, k_1 and k_{-1} are set to be 9 orders of magnitude larger than k_2, k_3 and k_{-3}, and the inlet has only enzyme and substrate in the same concentration. Measurements are available for $L = 8$ different values of the volume flow rate F, ranging from 0.05 to 2.5. However, in this case, only concentrations for substrate x_S, product x_P and enzyme x_E, are considered known. The optimization problem is then formulated as follows

$$(\hat{x}, \hat{k}) \in \underset{x,k}{\arg\min} \sum_{i \in \mathcal{M}} \sum_{\ell=1}^{L} \left(x_{i\ell}^{\mathsf{exp}} - x_{i\ell}\right)^2 \tag{10.31a}$$

$$\text{s.t.} \quad -k_1 x_E x_S + k_{-1} x_{ES} + F(x_S^{in} - x_S) = 0 \tag{10.31b}$$

$$-k_1 x_E x_S + k_{-1} x_{ES} + k_3 x_{EP} - k_{-3} x_E x_P + F(x_E^{in} - x_E) = 0 \tag{10.31c}$$

$$k_1 x_E x_S - k_{-1} x_{ES} - k_2 x_{ES} + F(x_{ES}^{in} - x_{ES}) = 0 \tag{10.31d}$$

$$k_2 x_{ES} - k_3 x_{EP} + k_{-3} x_E x_P + F(x_{EP}^{in} - x_{EP}) = 0 \tag{10.31e}$$

$$k_3 x_{EP} - k_{-3} x_E x_P + F(x_P^{in} - x_P) = 0 \tag{10.31f}$$

$$k_j \geq 0 \quad \text{for } j = 1, -1, 2, 3, -3 \tag{10.31g}$$

$$x_i \geq 0 \quad \text{for } i \in \mathcal{S} \tag{10.31h}$$

where $x_{i\ell} \in \mathbb{R}$ is the concentration of the i^{th} specie for experiment ℓ, $k_j \in \mathbb{R}$ is kinetic parameter associated with the j^{th} reaction, $\mathcal{S}$ is the set of all species and $\mathcal{M}$ is the subset of measured species.

For this case study, the eigenvector-based regularization approach is used when $\mu_j < \beta_\mu = 10^{-5}$ and the threshold for selecting small eigenvalues is $\beta_\varepsilon = 10^{-12}$. The Pyomo model has $n = 85$ variables and $p = 80$ equality constraints, and thus $m = 5$ degrees of freedom and parameters. Table 18 presents the value of the estimates and residuals (objective function) when using only the Hessian modification regularization approach and when combining it with the eigenvector-based method. Note that the residual is the essentially same using both approaches; however, their estimation for k_3 and k_{-3} differ, which already shows the presence of flat regions and that the problem has identifiability issues.

Table 18 – Estimates and residuals for the nonlinear enzymatic reaction estimation problem when using Hessian modification regularization and eigenvector-based regularization.

	$\hat{k}_1$	$\hat{k}_{-1}$	$\hat{k}_2$	$\hat{k}_3$	$\hat{k}_{-3}$	**Residual**
Hessian modification	5.86e5	3.61e5	0.562	2.13e6	2.10e6	6.23e-3
Eigenvector-based	5.84e5	3.63e5	0.563	2.56e5	2.54e5	6.23e-3

Figure 15 shows the progression of the objective value, the value of μ, and the value of δ_H in the case where the Hessian modification regularization is used; the top graph corresponds to the solution using only the Hessian modification method and the bottom graph refers to the solution when the eigenvector-based regularization is implemented (the thicker dotted line shows that this regularization was used in the corresponding iterations, from the 30$^{\text{th}}$ onward in this case). Table 19 shows the number of numeric factorizations used in the last iterations comparing both approaches. Hessian modification chooses δ_H gradually and it might take several attempts to find a suitable value, e.g., iteration 37 performed 4 numeric factorizations. Using the eigenvector-based regularization always requires 3 numeric factorizations per iteration. However, in this case, even when most iterations using the Hessian modification approach used only 2 factorizations, the total number of numeric factorizations required for the eigenvector-based regularization is still smaller.

Different initial guesses for the parameters are also used as shown in Table 20. When applying the eigenvector-based regularization method, the optimization problem converges to a solution for every tested set of initial guesses (adjusting the value of β_μ), while using only the Hessian modification method do not converge in 200 iterations when all parameters

started with value 0.25 and, when three other initial guesses are used, it is not able to satisfy the optimization tolerance set to 10^{-8} (indicated by a dash). Note that, in this case, reducing the solution space using the eigenvectors of the reduced Hessian resulted in a smaller number of iterations necessary for convergence, indicating that enforcing these constraints can help the algorithm achieve convergence when the neighborhood around the solution is nearly flat.

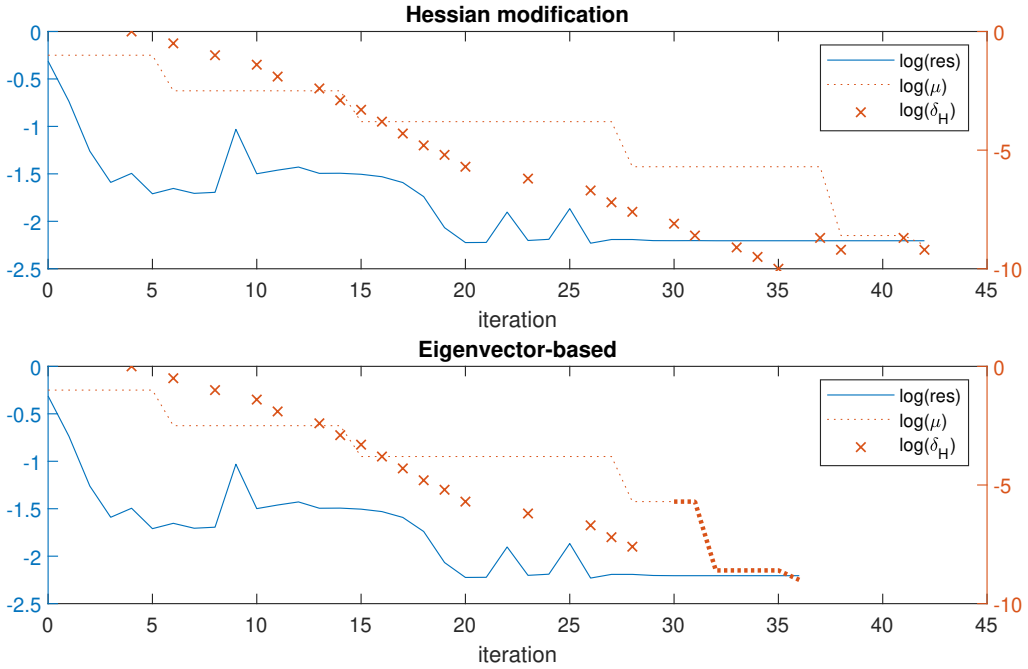

Figure 15 – Progression of the nonlinear enzymatic reaction estimation problem employing the Hessian modification and the eigenvector-based regularization approaches.

Table 19 – Comparison of the number of factorizations for the final iterations when the eigenvector-based regularization is used and when only Hessian modification is employed.

Iteration	**29**	**30**	**31**	**32**	**33**	**34**	**35**	**36**	**37**	**38**	**39**	**40**	**41**	**42**	**Total**
Hessian modification	1	2	2	1	2	2	2	1	4	2	1	1	3	2	26
Eigenvector-based	1	3	3	3	3	3	3	3							22

Another advantage of using the eigenvector-based regularization approach is that the eigenvalue decomposition of the reduced Hessian can indicate correlated parameters. Table 21 shows the eigenvectors and eigenvalues obtained in the last iteration during the calculation of the estimates. Note that each vector in V_2 shows a pair of kinetic constants that are correlated, namely k_1 and k_{-1}, and k_3 and k_{-3}. As evidenced by the eigenvalues Λ_2, changing the values of these parameters while keeping their ratio fixed does not significantly

Table 20 – Number of iterations for the nonlinear enzymatic reaction estimation problem when using Hessian modification regularization and eigenvector-based regularization starting from different initial guesses.

Initial guess for every parameter	Number of iterations for Hessian modification	Number of iterations for eigenvector-based	β_μ
0.1	–	49	10e-3
0.25	iteration limit	43	10e-3
0.5	83	44	10e-5
1	42	36	10e-5
10	–	66	10e-3
100	–	39	10e-3

influence the residual value. Inspecting all eigenvectors shows that k_2 is independently estimated, since its corresponding entries are zero in all eigenvectors but the last one, which is the only nonzero entry.

Table 21 – Eigenvalue decomposition of the reduced Hessian in the last iteration of the calculation using the eigenvector-based regularization for the enzymatic reaction estimation problem.

	V_2		V_1		
k_1	0.0	0.845	0.473	-0.249	0.0
k_{-1}	0.0	0.534	-0.736	0.416	0.0
k_2	0.0	0.0	0.0	0.0	1.0
k_3	0.711	-0.010	0.341	0.615	0.0
k_{-3}	0.703	0.010	-0.345	-0.622	0.0
Λ	-7.60e-19	2.77e-14	1.87e-12	7.45e-12	1.30

10.3.2 Dynamic kinetic model

A dynamic kinetic model is also solved using both regularization methods being tested and a similar analysis as carried out for the nonlinear enzymatic reaction estimation problem is performed. For this example, the mechanism of the hydrogen-bromine reaction is considered

$$\mathrm{Br_2} + \mathrm{Cat} \underset{k_2}{\overset{k_1}{\rightleftharpoons}} 2\,\mathrm{Br} + \mathrm{Cat}$$

$$\mathrm{Br} + \mathrm{H_2} \underset{k_4}{\overset{k_3}{\rightleftharpoons}} \mathrm{H} + \mathrm{HBr}$$

$$\mathrm{H} + \mathrm{Br_2} \xrightarrow{k_5} \mathrm{Br} + \mathrm{HBr}.$$

This kinetic model and the supporting data were obtained from Vajda et al. (1985). Initial conditions are $x_{Br_2}(0) = x_{H_2}(0) = 10$, Br, H and HBr are not present at the beginning, and $x_{\text{Cat}} = 10^4$ is kept constant. Considering that only Br_2, H_2, and HBr are measured, the parameter estimation problem is given by

$$(\hat{x}, \hat{k}) \in \underset{x,k}{\arg\min} \sum_{i \in \mathcal{M}} \sum_{t \in \mathcal{T}} \left(x_i^{\text{exp}}(t) - x_i(t)\right)^2 \tag{10.32a}$$

$$\text{s.t.} \quad \frac{dx_{Br_2}}{dt} = -k_1 x_{Br_2} x_{\text{Cat}} + k_2 x_{Br}^2 x_{\text{Cat}} - k_5 x_H x_{Br_2} \tag{10.32b}$$

$$\frac{dx_{Br}}{dt} = k_1 x_{Br_2} x_{\text{Cat}} - k_2 x_{Br}^2 x_{\text{Cat}} - k_3 x_{Br} x_{H_2} + k_4 x_H x_{HBr} + k_5 x_H x_{Br_2} \tag{10.32c}$$

$$\frac{dx_{H_2}}{dt} = -k_3 x_{Br} x_{H_2} + k_4 x_H x_{HBr} \tag{10.32d}$$

$$\frac{dx_H}{dt} = k_3 x_{Br} x_{H_2} - k_4 x_H x_{HBr} - k_5 x_H x_{Br_2} \tag{10.32e}$$

$$\frac{dx_{HBr}}{dt} = k_3 x_{Br} x_{H_2} - k_4 x_H x_{HBr} + k_5 x_H x_{Br_2} \tag{10.32f}$$

$$k_j \geq 0 \quad \text{for } j = 1, \ldots, 5 \tag{10.32g}$$

$$x_i \geq 0 \quad \text{for } i \in \mathcal{S} \tag{10.32h}$$

where $x_i(t) \in \mathbb{R}$ is the concentration of the i^{th} specie at time t, $k_j \in \mathbb{R}$ is kinetic parameter associated with the j^{th} reaction, $\mathcal{T}$ is the set of times of the measurements, $\mathcal{S}$ is the set of all species and $\mathcal{M}$ is the subset of measured species. Pyomo can automatically discretize differential equations; thus, in this case, orthogonal collocation is used with 10 finite elements and 3 collocation points. For this estimation problem, points corresponding to the finite elements are considered measured for the species in $\mathcal{M}$, thus 10 equally spaced concentration points for 3 species and initial condition for every species are known. The Pyomo model has $n = 465$ variables and $p = 460$ equality constraints, resulting in $m = 5$ degrees of freedom. For this case study, $\beta_\mu = 10^{-8}$ and $\beta_\varepsilon = 10^{-12}$ as set in the previous case study.

Table 22 – Estimates and residuals for the dynamic kinetic model estimation problem when using Hessian modification regularization and eigenvector-based regularization.

	$\hat{k}_1$	$\hat{k}_2$	$\hat{k}_3$	$\hat{k}_4$	$\hat{k}_5$	**Residual**
Hessian modification	6.26e-4	1.56e-3	2.61	1.77e3	1.49e4	3.06e-8
Eigenvector-based	6.27e-4	1.56e-3	2.61	3.20e2	2.69e3	1.18e-6

Estimates presented in Table 22 indicates that there is a nearly flat direction involving k_4 and k_5, since the other parameters have the same estimates and they differ in one order

of magnitude when comparing both solutions. Different from the previous case study, the objective values (residuals) are not the same; however, they are both small and Figure 16 shows that both estimates can successfully simulate the measured data, note that they essentially deliver the same result.

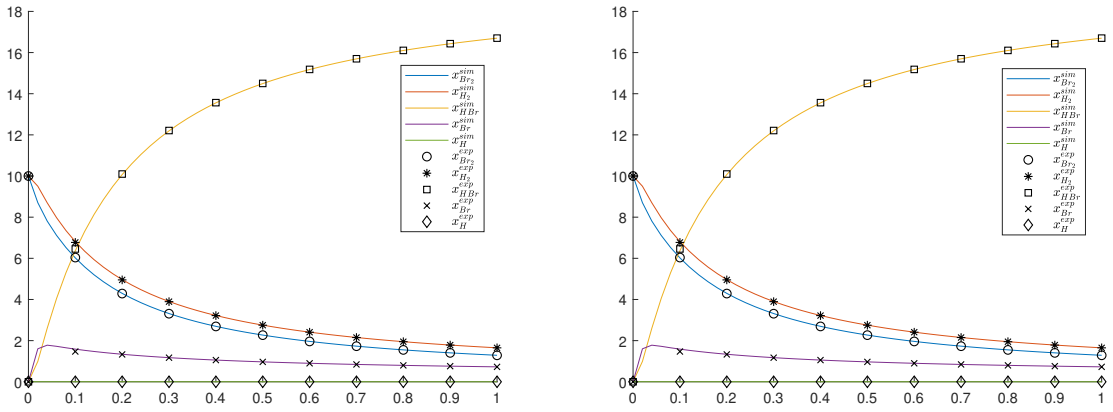

(a) Hessian modification regularization

(b) Eigenvector-based regularization

Figure 16 – Measured data points used for estimation and simulation using both sets of estimates for the nonlinear parameter estimation of the dynamic kinetic model.

Figure 17 shows the progression of the optimization problem calculation. Analyzing when regularization is applied during the computation of the estimates, one can observe that, even though $\mu_j < \beta_\mu$ from iteration 6 onward, the Hessian modification method is still used in most iterations, which indicates that the algorithm is exploring regions with small negative curvature, as the residual does not change significantly for many of those iterations. Once a convex region is reached, progress is made and the eigenvector-based regularization is only used in the last two iterations. In this case study, this regularization helps find a solution in neighborhood with nearly flat directions by fixing a relationship between parameters and also reduces the number of iterations required.

The eigenvalue decomposition of the reduced Hessian presented in Table 23 also shows that parameters k_4 and k_5 are correlated and cannot be individually estimated with confidence from the available data. This finding corroborates the results presented in Vajda et al. (1985). By analyzing the eigenvectors associated with small eigenvalues of the sensitivity matrix, the authors conclude that k_4 and k_5 should have a fixed ratio.

Table 23 – Eigenvalue decomposition of the reduced Hessian in the last iteration of the calculation using the eigenvector-based regularization for the dynamic kinetic model estimation problem.

	V_2	V_1			
k_1	0.0	0.0	0.0	-0.936	-0.353
k_2	0.0	0.0	-0.001	0.353	-0.936
k_3	0.0	-0.003	-1.0	0.0	0.001
k_4	-0.118	-0.993	0.003	0.0	0.0
k_5	-0.993	0.118	0.0	0.0	0.0
Λ	9.81e-13	9.23e-6	6.64e-1	4.03e8	1.43e5

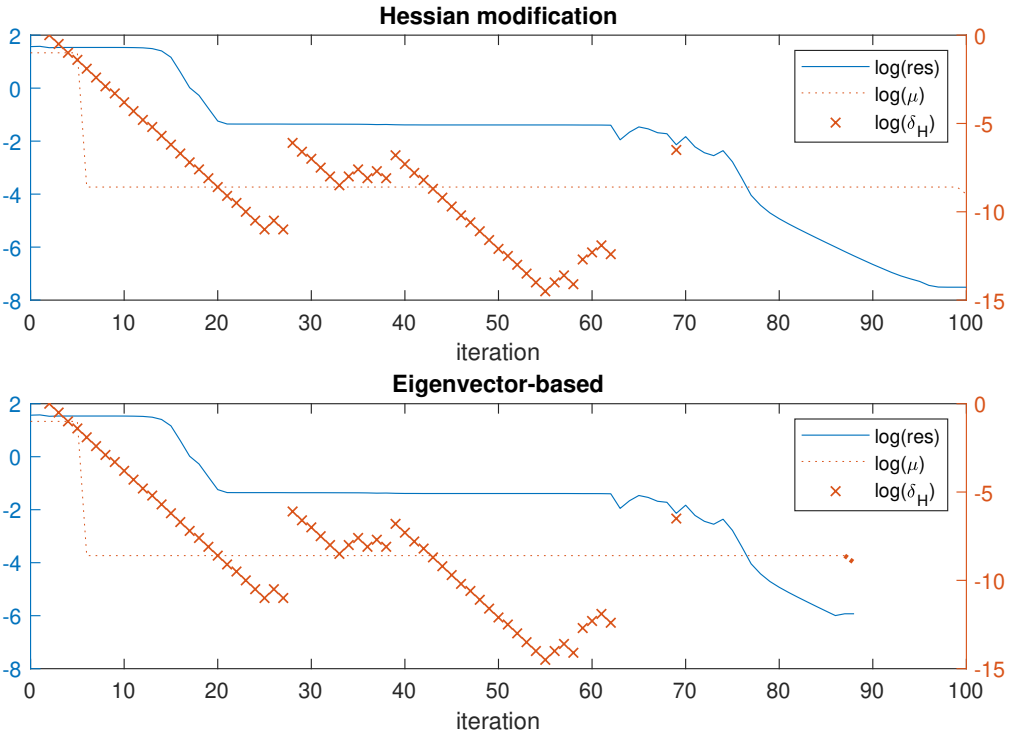

Figure 17 – Progression of the dynamic kinetic model estimation problem employing the Hessian modification and the eigenvector-based regularization approaches.

10.4 Conclusion

In this chapter, a regularization approach for line search interior point algorithms based on the eigenvalue decomposition of the (reduced) Hessian for solving nonlinear parameter estimation problems is presented. Although its application for dealing with negative curvature does not show practical improvement when compared to the Hessian modification method, enforcing constraints built from the eigenvectors of the (reduced) Hessian can be beneficial when dealing with nearly flat regions in the neighborhood of the solution, as indi-

cated by the results from the case studies. Another advantage of using the eigenvector-based regularization is that the constraints actually represent sets of correlated parameters, which is important information for identifiability analysis and for suggesting some phenomenological simplifications in the model.

11 Concluding remarks

Stoichiometric modeling has been an important tool for metabolic engineering since this field has emerged in the 1990s based on metabolic flux analysis. Over the past 30 years, improvement in computational power and development of different modeling techniques have enabled highly detailed *in silico* models, especially for extensively investigated organisms. However, non-model organisms, such as *Burkholderia sacchari*, still need effort towards experimental work to develop more complex models that could potentially simulate their metabolism. Part I of this thesis illustrates that stoichiometric models based on small to medium metabolic networks are still a valuable tool that can help elucidate properties of microorganisms and guide the design of experiments. In addition, they are a good starting point for metabolic engineering; since stoichiometric models are linear, they can be relatively simple (especially for small networks), which helps build the connection between biology and mathematical modeling concepts more clearly.

Mechanistic models for describing cellular metabolism are challenging mainly due to the amount and quality of data required, which are difficult to collect (if not impossible). This obstacle gives rise to identifiability issues, which are evidenced by the high uncertainty of the estimates. Regularization is a mathematical strategy that can successfully reduce parameter variance, as discussed in Part II. Moreover, designing regularization methods based on the eigenvalue decomposition of the (reduced) Hessian matrix is optimal for linear problems and helpful for nonlinear problems with nearly flat neighborhood around the solution. However, an important and valuable property of eigenvector-based regularization in both cases is that these approaches also recognize correlated parameters, allowing for better understanding the identifiability sources.

11.1 Recommendations for future work

- An interesting work for the near future is to continue with the analysis of the *Burkholderia sacchari* metabolism and perform experiments that can elucidate the co-factor balance to help plan for strategies that increase the conversion of fatty acid into co-polymer, ideally to 100%.
- A recommendation of work related to modeling of metabolic networks is studying kinetic model frameworks and their inherent identifiability issues. How regularization

methods based on eigenvalue decomposition would impact these frameworks is worth investigating. Starting with the ensemble modeling technique would be a good strategy since it is a popular more consolidated framework.

- The implementation of the eigenvector-based regularization method in a linear search interior point algorithm can continue; some details of implementation can be further investigated to require less manual input. For instance, the definition of the threshold for deciding when a direction is considered flat and the algorithm for deciding whether the eigenvector-based regularization should be used are two points that have room for improvement.
- It would also be interesting to use the eigenvector-based regularization method in larger nonlinear problems and verify whether the sparse principal components with orthogonality constraints can also group sets of parameters with larger correlation.
- Another interesting idea that could be investigated is whether this eigenvector-based regularization method could be extended to general optimization problems and if it would be relevant doing so. A straightforward obstacle is how to define a good set of independent variables. For parameter estimation problems, the choice of the parameters is obvious, but they still have to be selected by the user.

Bibliography

ALBERTON, K. P. et al. Accelerating the parameters identifiability procedure: set by set selection. *Computers & chemical engineering*, Elsevier, v. 55, p. 181–197, 2013.

AMESTOY, P. et al. A fully asynchronous multifrontal solver using distributed dynamic scheduling. *SIAM Journal on Matrix Analysis and Applications*, v. 23, n. 1, p. 15–41, 2001.

ANDERSSON, J. A. E. et al. CasADi – A software framework for nonlinear optimization and optimal control. *Mathematical Programming Computation*, Springer, v. 11, n. 1, p. 1–36, 2019.

ANG, J. C. et al. Supervised, unsupervised, and semi-supervised feature selection: a review on gene selection. *IEEE/ACM transactions on computational biology and bioinformatics*, IEEE, v. 13, n. 5, p. 971–989, 2015.

ANTONIEWICZ, M. R. Methods and advances in metabolic flux analysis: a mini-review. *Journal of Industrial Microbiology and Biotechnology*, v. 42, n. 3, p. 317–325, 2015.

ARMENGAUD, J. et al. Non-model organisms, a species endangered by proteogenomics. *Journal of proteomics*, Elsevier, v. 105, p. 5–18, 2014.

ARORA, N.; BIEGLER, L. T. Parameter estimation for a polymerization reactor model with a composite-step trust-region nlp algorithm. *Industrial & engineering chemistry research*, ACS Publications, v. 43, n. 14, p. 3616–3631, 2004.

BARD, Y. *Nonlinear Parameter Estimation*. [S.l.]: Academic Press, 1974.

BAUER, F.; LUKAS, M. A. Comparing parameter choice methods for regularization of ill-posed problems. *Mathematics and Computers in Simulation*, Elsevier, v. 81, n. 9, p. 1795–1841, 2011.

BECKER, S. A. et al. Quantitative prediction of cellular metabolism with constraint-based models: the cobra toolbox. *Nature protocols*, Nature Publishing Group, v. 2, n. 3, p. 727–738, 2007.

BEN-ZVI, A. Reparameterization of inestimable systems with applications to chemical and biochemical reactor systems. *AIChE journal*, Wiley Online Library, v. 54, n. 5, p. 1270–1281, 2008.

BONARIUS, H. P. et al. Metabolic flux analysis of hybridoma cells in different culture media using mass balances. *Biotechnology and bioengineering*, Wiley Online Library, v. 50, n. 3, p. 299–318, 1996.

BYRD, R. H.; NOCEDAL, J.; WALTZ, R. A. Knitro: An integrated package for nonlinear optimization. In: *Large-scale nonlinear optimization*. [S.l.]: Springer, 2006. p. 35–59.

CARLSON, R.; SRIENC, F. Fundamental Escherichia coli Biochemical Pathways for Biomass and Energy Production: Identification of Reactions. *Biotechnology and Bioengineering*, v. 85, n. 1, p. 1–19, 2004.

CARTIS, C.; GOULD, N. I.; TOINT, P. L. Trust-region and other regularisations of linear least-squares problems. *BIT Numerical Mathematics*, Springer, v. 49, n. 1, p. 21–53, 2009.

CHEN, W. W.; NIEPEL, M.; SORGER, P. K. Classic and contemporary approaches to modeling biochemical reactions. *Genes & development*, Cold Spring Harbor Lab, v. 24, n. 17, p. 1861–1875, 2010.

CHIANG, N.-Y.; ZAVALA, V. M. An inertia-free filter line-search algorithm for large-scale nonlinear programming. *Computational Optimization and Applications*, Springer, v. 64, n. 2, p. 327–354, 2016.

CONG, L. et al. Multiplex Genome Engineering Using CRISPR/VCas Systems. *Science*, v. 339, n. 6121, p. 819–823, 2013.

COVERT, M. W. et al. Integrating high-throughput and computational data elucidates bacterial networks. *Nature*, v. 429, n. 6987, p. 92–96, 2004.

DE GROOT, D. H. et al. The number of active metabolic pathways is bounded by the number of cellular constraints at maximal metabolic rates. *PLoS computational biology*, Public Library of Science, v. 15, n. 3, p. e1006858, 2019.

DEHAK, N. et al. Cosine similarity scoring without score normalization techniques. In: *Odyssey*. [S.l.: s.n.], 2010. p. 15.

DELSOLE, T.; BANERJEE, A. Statistical seasonal prediction based on regularized regression. *Journal of Climate*, v. 30, n. 4, p. 1345–1361, 2017.

DIETRICH, K. et al. Producing phas in the bioeconomy—towards a sustainable bioplastic. *Sustainable production and consumption*, Elsevier, v. 9, p. 58–70, 2017.

FAN, Y. et al. Model reduction of kinetic equations by operator projection. *Journal of Statistical Physics*, Springer, v. 162, n. 2, p. 457–486, 2016.

FARISS, R.; LAW, V. An efficient computational technique for generalized application of maximum likelihood to improve correlation of experimental data. *Computers & Chemical Engineering*, Elsevier, v. 3, n. 1-4, p. 95–104, 1979.

FERNANDES, S. et al. Application of dynamic metabolic flux convex analysis to cho-dxb11 cell fed-batch cultures. *IFAC-PapersOnLine*, Elsevier, v. 49, n. 7, p. 466–471, 2016.

FERREIRA, A. R. et al. Projection to latent pathways (PLP): a constrained projection to latent variables (PLS) method for elementary flux modes discrimination. *BMC systems biology*, v. 5, n. 1, p. 181, 2011.

FLETCHER, R.; LEYFFER, S. User manual for filtersqp. *Numerical Analysis Report NA/181, Department of Mathematics, University of Dundee, Dundee, Scotland*, v. 35, 1998.

FORSTER, J. et al. Genome-scale reconstruction of the Saccharomyces cerevisiae metabolic network. *Genome Research*, n. 13, p. 244–253, 2003.

FRIEDMAN, J.; HASTIE, T.; TIBSHIRANI, R. A note on the group lasso and a sparse group lasso. *arXiv preprint arXiv:1001.0736*, 2010.

FRIEDMAN, J.; HASTIE, T.; TIBSHIRANI, R. Regularization paths for generalized linear models via coordinate descent. *Journal of statistical software*, NIH Public Access, v. 33, n. 1, p. 1, 2010.

FUHRY, M.; REICHEL, L. A new tikhonov regularization method. *Numerical Algorithms*, Springer, v. 59, n. 3, p. 433–445, 2012.

GAGNEUR, J.; KLAMT, S. Computation of elementary modes: a unifying framework and the new binary approach. *BMC bioinformatics*, v. 5, n. 1, p. 175, 2004.

GAMMA, E. et al. *Design Patterns: Elements of Reusable Object-oriented Software*. [S.l.]: Addison-Wesley Longman Publishing Co., Inc., 1995. ISBN 0-201-63361-2.

GANDER, W. Least squares with a quadratic constraint. *Numerische Mathematik*, Springer, v. 36, n. 3, p. 291–307, 1980.

GEORGE, E. I. The variable selection problem. *Journal of the American Statistical Association*, Taylor & Francis Group, v. 95, n. 452, p. 1304–1308, 2000.

GERSTL, M. P.; JUNGREUTHMAYER, C.; ZANGHELLINI, J. TEFMA: Computing thermodynamically feasible elementary flux modes in metabolic networks. *Bioinformatics*, v. 31, n. 13, p. 2232–2234, 2015.

GILL, P. E.; MURRAY, W.; SAUNDERS, M. A. Snopt: An sqp algorithm for large-scale constrained optimization. *SIAM review*, SIAM, v. 47, n. 1, p. 99–131, 2005.

GRACIANO, J.; MENDOZA, D.; ROUX, G. A. L. Performance comparison of parameter estimation techniques for unidentifiable models. *Computers & Chemical Engineering*, Elsevier, v. 64, p. 24–40, 2014.

GUAMÁN, L. P. et al. Engineering xylose metabolism for production of polyhydroxybutyrate in the non-model bacterium burkholderia sacchari. *Microbial cell factories*, BioMed Central, v. 17, n. 1, p. 74, 2018.

GUENNEBAUD, G.; JACOB, B. et al. *Eigen v3*. 2010. Disponível em: <http://eigen.tuxfamily-.org>.

GUIL, F.; HIDALGO, J. F.; GARCÍA, J. M. Boosting the extraction of elementary flux modes in genome-scale metabolic networks using the linear programming approach. *Bioinformatics*, 2020.

GUNST, R. F.; MASON, R. L. Some considerations in the evaluation of alternate prediction equations. *Technometrics*, Taylor & Francis, v. 21, n. 1, p. 55–63, 1979.

GUO, W.; SHENG, J.; FENG, X. 13C-Metabolic Flux Analysis: An Accurate Approach to Demystify Microbial Metabolism for Biochemical Production. *Bioengineering*, v. 3, n. 1, p. 3, 2015.

HANSEN, P. C. *Rank-deficient and discrete ill-posed problems: numerical aspects of linear inversion*. [S.l.]: Siam, 2005. v. 4.

HART, W. E. et al. *Pyomo–optimization modeling in python*. Second. [S.l.]: Springer Science & Business Media, 2017. v. 67.

HART, W. E.; WATSON, J.-P.; WOODRUFF, D. L. Pyomo: modeling and solving mathematical programs in python. *Mathematical Programming Computation*, Springer, v. 3, n. 3, p. 219–260, 2011.

HEIRENDT, L. et al. Creation and analysis of biochemical constraint-based models using the cobra toolbox v. 3.0. *Nature protocols*, Nature Publishing Group, v. 14, n. 3, p. 639–702, 2019.

HELMS, R. W. The average estimated variance criterion for the selection-of-variables problem in general linear models. *Technometrics*, Taylor & Francis Group, v. 16, n. 2, p. 261–273, 1974.

HONG, S. H.; LEE, S. Y. Metabolic flux analysis for succinic acid production by recombinant Escherichia coli with amplified malic enzyme activity. *Biotechnology and bioengineering*, v. 74, n. 2, p. 89–95, 2001.

HOOPS, S. et al. COPASI - A COmplex PAthway SImulator. *Bioinformatics*, v. 22, n. 24, p. 3067–3074, 2006.

JIANG, Y.; HE, Y.; ZHANG, H. Variable selection with prior information for generalized linear models via the prior lasso method. *Journal of the American Statistical Association*, Taylor & Francis, v. 111, n. 513, p. 355–376, 2016.

JOLLIFFE, I. T. A note on the use of principal components in regression. *Journal of the Royal Statistical Society: Series C (Applied Statistics)*, Wiley Online Library, v. 31, n. 3, p. 300–303, 1982.

JOLLIFFE, I. T.; CADIMA, J. Principal component analysis: a review and recent developments. *Philosophical Transactions of the Royal Society A: Mathematical, Physical and Engineering Sciences*, The Royal Society Publishing, v. 374, n. 2065, p. 20150202, 2016.

KAMP, A. von; KLAMT, S. Growth-coupled overproduction is feasible for almost all metabolites in five major production organisms. *Nature communications*, Nature Publishing Group, v. 8, n. 1, p. 1–10, 2017.

KAMP, A. von et al. Use of cellnetanalyzer in biotechnology and metabolic engineering. *Journal of biotechnology*, Elsevier, v. 261, p. 221–228, 2017.

KARL, W. C. Regularization in image restoration and reconstruction. In: BOVIK, A. (Ed.). *Handbook of Image and Video Processing*. Second edition. [S.l.]: Academic Press, 2005, (Communications, Networking and Multimedia). p. 183 – V.

KLAMT, S.; GAGNEUR, J.; KAMP, A. von. Algorithmic approaches for computing elementary modes in large biochemical reaction networks. *IEE Proceedings-Systems Biology*, v. 152, n. 4, p. 249–255, 2005.

KLAMT, S.; HÄDICKE, O.; KAMP, A. von. Stoichiometric and constraint-based analysis of biochemical reaction networks. In: *Large-Scale Networks in Engineering and Life Sciences*. [S.l.]: Springer, 2014. p. 263–316.

KLAMT, S. et al. From elementary flux modes to elementary flux vectors: Metabolic pathway analysis with arbitrary linear flux constraints. *PLoS computational biology*, Public Library of Science, v. 13, n. 4, 2017.

KLAMT, S.; SAEZ-RODRIGUEZ, J.; GILLES, E. D. Structural and functional analysis of cellular networks with cellnetanalyzer. *BMC systems biology*, v. 1, n. 1, p. 2, 2007.

KLAMT, S.; STELLING, J. Two approaches for metabolic pathway analysis? *Trends in biotechnology*, v. 21, n. 2, p. 64–69, 2003.

KLAMT, S.; VON KAMP, A. An application programming interface for cellnetanalyzer. *Biosystems*, v. 105, n. 2, p. 162–168, 2011.

KLINKEN, J. B. V.; DIJK, K. Willems van. Fluxmodecalculator: an efficient tool for large-scale flux mode computation. *Bioinformatics*, Oxford University Press, v. 32, n. 8, p. 1265–1266, 2016.

LI, R.; HENSON, M. A.; KURTZ, M. J. Selection of model parameters for off-line parameter estimation. *IEEE Transactions on control systems technology*, IEEE, v. 12, n. 3, p. 402–412, 2004.

LIEW, C. K. Inequality constrained least-squares estimation. *Journal of the American Statistical Association*, Taylor & Francis, v. 71, n. 355, p. 746–751, 1976.

LIU, X. et al. Image interpolation via regularized local linear regression. *IEEE Transactions on Image Processing*, IEEE, v. 20, n. 12, p. 3455–3469, 2011.

MA, D. et al. Parameter identification for continuous point emission source based on tikhonov regularization method coupled with particle swarm optimization algorithm. *Journal of hazardous materials*, Elsevier, v. 325, p. 239–250, 2017.

MATHWORKS. *Constrained Nonlinear Optimization Algorithms*. R2020a. Disponível em: <https://www.mathworks.com/help/optim/ug/constrained-nonlinear-optimization-algorithms.html>.

MENDONÇA, T. T. *Estudo de bactérias recombinantes e análise de fluxos metabólicos para a biossíntese do copolímero biodegradável poli(3-hidroxibutirato-co-3-hidroxihexanoato)[p(3hb-co-3hhx)]*. Tese (Doutorado) — Universidade de São Paulo, 2014.

MIAO, H. et al. On identifiability of nonlinear ode models and applications in viral dynamics. *SIAM review*, SIAM, v. 53, n. 1, p. 3–39, 2011.

MORÉ, J. J. Recent developments in algorithms and software for trust region methods. In: *Mathematical programming The state of the art*. [S.l.]: Springer, 1983. p. 258–287.

MOTZKIN, T. S. et al. The double desciption method. In: KUHN, H. W.; TUCKER, A. W. (Ed.). *Contributions to theory of games*. [S.l.]: Princeton University Press, 1953. v. 2, p. 51–73.

NAKAMA, C. S.; ROUX, G. A. L.; ZAVALA, V. M. Optimal constraint-based regularization for parameter estimation problems. *Computers & Chemical Engineering*, Elsevier, v. 139, p. 106873, 2020.

NARASIMHAN, S.; JORDACHE, C. *Data reconciliation and gross error detection: An intelligent use of process data*. [S.l.]: Elsevier, 1999.

NGUYEN, V.; WOOD, E. Review and unification of linear identifiability concepts. *SIAM review*, SIAM, v. 24, n. 1, p. 34–51, 1982.

NIELSEN, J. et al. Engineering synergy in biotechnology. *Nature Chemical Biology*, v. 10, n. 5, p. 319–322, 2014.

NIKEREL, I. E. et al. Model reduction and a priori kinetic parameter identifiability analysis using metabolome time series for metabolic reaction networks with linlog kinetics. *Metabolic engineering*, Elsevier, v. 11, n. 1, p. 20–30, 2009.

NOCEDAL, J.; WRIGHT, S. *Numerical optimization*. [S.l.]: Springer Science & Business Media, 2006.

NOOKAEW, I. et al. Identification of flux regulation coefficients from elementary flux modes: A systems biology tool for analysis of metabolic networks. *Biotechnology and bioengineering*, v. 97, n. 6, p. 1535–1549, 2007.

ODDSDÓTTIR, H. Æ. et al. Robustness analysis of elementary flux modes generated by column generation. *Mathematical biosciences*, Elsevier, v. 273, p. 45–56, 2016.

ORTH, J. D.; THIELE, I.; PALSSON, B. Ø. O. What is flux balance analysis? *Nature biotechnology*, v. 28, n. 3, p. 245–248, 2010.

PAPIN, J. A. et al. Comparison of network-based pathway analysis methods. *Trends in Biotechnology*, v. 22, n. 8, p. 400–405, 2004.

PARK, S. H. Collinearity and optimal restrictions on regression parameters for estimating responses. *Technometrics*, Taylor & Francis Group, v. 23, n. 3, p. 289–295, 1981.

PERES, S. et al. How important is thermodynamics for identifying elementary flux modes? *PloS one*, Public Library of Science, v. 12, n. 2, 2017.

PFEIFFER, T. et al. METATOOL: For studying metabolic networks. *Bioinformatics*, v. 15, n. 3, p. 251–257, 1999.

POBLETE-CASTRO, I. et al. In-silico-driven metabolic engineering of Pseudomonas putida for enhanced production of poly-hydroxyalkanoates. *Metabolic Engineering*, Elsevier, v. 15, n. 1, p. 113–123, 2013.

POOLMAN, M. G. et al. A method for the determination of flux in elementary modes, and its application to Lactobacillus rhamnosus. *Biotechnology and Bioengineering*, v. 88, n. 5, p. 601–612, 2004.

QUEK, L.-E.; NIELSEN, L. K. A depth-first search algorithm to compute elementary flux modes by linear programming. *BMC systems biology*, BioMed Central, v. 8, n. 1, p. 94, 2014.

RAUE, A. et al. Structural and practical identifiability analysis of partially observed dynamical models by exploiting the profile likelihood. *Bioinformatics*, Oxford University Press, v. 25, n. 15, p. 1923–1929, 2009.

ROCHA, I. et al. Optflux: an open-source software platform for in silico metabolic engineering. *BMC systems biology*, v. 4, n. 1, p. 45, 2010.

RODRIGUEZ, J. S. et al. *PyNumero: Python Numerical Optimization.* [S.l.], 2018.

ROLLIÉ, S.; MANGOLD, M.; SUNDMACHER, K. Designing biological systems: Systems Engineering meets Synthetic Biology. *Chemical Engineering Science*, v. 69, n. 1, p. 1–29, 2012.

RUCKERBAUER, D. E.; JUNGREUTHMAYER, C.; ZANGHELLINI, J. Predicting genetic engineering targets with Elementary Flux Mode Analysis: A review of four current methods. *New Biotechnology*, v. 32, n. 6, p. 534–546, 2015.

RUSSELL, J. J. et al. Non-model model organisms. *BMC biology*, BioMed Central, v. 15, n. 1, p. 1–31, 2017.

SANTOSA, F.; SYMES, W. W. Linear inversion of band-limited reflection seismograms. *SIAM Journal on Scientific and Statistical Computing*, v. 7, n. 4, p. 1307–1330, 1986.

SCHELLENBERGER, J. et al. Quantitative prediction of cellular metabolism with constraint-based models: the cobra toolbox v2. 0. *Nature protocols*, v. 6, n. 9, p. 1290–1307, 2011.

SCHUSTER, S.; HILGETAG, C. on Elementary Flux Modes in Biochemical Reaction Systems At Steady State. *Journal of Biological Systems*, v. 02, n. 02, p. 165–182, 1994.

SCHUSTER, S. et al. Reaction routes in biochemical reaction systems: Algebraic properties, validated calculation procedure and example from nucleotide metabolism. *Journal of Mathematical Biology*, v. 45, n. 2, p. 153–181, 2002.

SCHWARTZ, J. M.; KANEHISA, M. A quadratic programming approach for decomposing steady-state metabolic flux distributions onto elementary modes. *Bioinformatics*, v. 21, n. SUPPL. 2, p. 204–205, 2005.

SECCHI, A. R. et al. An algorithm for automatic selection and estimation of model parameters. *IFAC Proceedings Volumes*, Elsevier, v. 39, n. 2, p. 789–794, 2006.

SRIDHAR, J.; EITEMAN, M. A. Metabolic flux analysis of *Clostridium thermosuccinogenes*: effects of pH and culture redox potential. *Applied biochemistry and biotechnology*, v. 94, n. 1, p. 51–69, 2001.

STEPHANOPOULOS, G. Metabolic fluxes and metabolic engineering. *Metabolic engineering*, v. 1, n. 1, p. 1–11, 1999.

STEPHANOPOULOS, G.; ARISTIDOU, A. A.; NIELSEN, J. *Metabolic engineering: principles and methodologies*. [S.l.]: Academic press, 1998.

STFC, S. *HSL. A collection of Fortran codes for large scale scientific computation*. 2020. Disponível em: <http://www.hsl.rl.ac.uk/>.

STRUTZ, J. et al. Metabolic kinetic modeling provides insight into complex biological questions, but hurdles remain. *Current opinion in biotechnology*, Elsevier, v. 59, p. 24–30, 2019.

SURISETTY, K. et al. Model re-parameterization and output prediction for a bioreactor system. *Chemical Engineering Science*, Elsevier, v. 65, n. 16, p. 4535–4547, 2010.

TERZER, M.; STELLING, J. Accelerating the computation of elementary modes using pattern trees. *Wabi*, v. 2006, n. 1, p. 333–343, 2006.

TERZER, M.; STELLING, J. Large-scale computation of elementary flux modes with bit pattern trees. *Bioinformatics*, v. 24, n. 19, p. 2229–2235, 2008.

THIELE, I.; GUDMUNDSSON, S. Computationally efficient flux variability analysis. *BMC Bioninformatics*, v. 11, n. 489, p. 1–3, 2010.

THRAMPOULIDIS, C.; OYMAK, S.; HASSIBI, B. Regularized linear regression: A precise analysis of the estimation error. *Proceedings of Machine Learning Research*, PMLR, v. 40, p. 1683–1709, 2015.

TIBSHIRANI, R. Regression shrinkage and selection via the lasso. *Journal of the Royal Statistical Society: Series B (Methodological)*, Wiley Online Library, v. 58, n. 1, p. 267–288, 1996.

TRAN, L. M.; RIZK, M. L.; LIAO, J. C. Ensemble Modeling of Metabolic Networks. *Biophysical Journal*, v. 95, n. 12, p. 5606–5617, 2008.

TRANSTRUM, M. K. et al. Geometrically motivated reparameterization for identifiability analysis in power systems models. In: IEEE. *2018 North American Power Symposium (NAPS)*. [S.l.], 2018. p. 1–6.

TRINH, C. T. et al. Redesigning escherichia coli metabolism for anaerobic production of isobutanol. *Applied and environmental microbiology*, v. 77, n. 14, p. 4894–4904, 2011.

TRINH, C. T.; SRIENC, F. Metabolic engineering of Escherichia coli for efficient conversion of glycerol to ethanol. *Applied and Environmental Microbiology*, v. 75, n. 21, p. 6696–6705, 2009. ISSN 00992240.

TURANYI, T.; BERCES, T.; VAJDA, S. Reaction rate analysis of complex kinetic systems. *International Journal of Chemical Kinetics*, Wiley Online Library, v. 21, n. 2, p. 83–99, 1989.

UNREAN, P.; TRINH, C. T.; SRIENC, F. Rational design and construction of an efficient e. coli for production of diapolycopendioic acid. *Metabolic engineering*, v. 12, n. 2, p. 112–122, 2010.

URBANCZIK, R. Enumerating constrained elementary flux vectors of metabolic networks. *IET systems biology*, IET, v. 1, n. 5, p. 274–279, 2007.

VAJDA, S.; VALKO, P.; TURANYI, T. Principal component analysis of kinetic models. *International Journal of Chemical Kinetics*, Wiley Online Library, v. 17, n. 1, p. 55–81, 1985.

VAN KLINKEN, J. B.; VAN DIJK, K. W. FluxModeCalculator: An efficient tool for large-scale flux mode computation. *Bioinformatics*, v. 32, n. 8, p. 1265–1266, 2016.

VANDERBEI, R. J. Loqo: An interior point code for quadratic programming. *Optimization methods and software*, Taylor & Francis, v. 11, n. 1-4, p. 451–484, 1999.

VARÓN, R. et al. Kinetic analysis of the general modifier mechanism of botts and morales involving a suicide substrate. *Journal of theoretical biology*, Elsevier, v. 218, n. 3, p. 355–374, 2002.

VON KAMP, A.; SCHUSTER, S. Metatool 5.0: Fast and flexible elementary modes analysis. *Bioinformatics*, v. 22, n. 15, p. 1930–1931, 2006.

VON STOSCH, M. et al. A principal components method constrained by elementary flux modes: analysis of flux data sets. *BMC Bioinformatics*, BMC Bioinformatics, v. 17, n. 1, p. 200–218, 2016.

WÄCHTER, A.; BIEGLER, L. T. On the implementation of an interior-point filter line-search algorithm for large-scale nonlinear programming. *Mathematical programming*, Springer, v. 106, n. 1, p. 25–57, 2006.

WAGNER, C. Nullspace Approach to Determine the Elementary Modes of Chemical Reaction Systems. *The Journal of Physical Chemistry B*, v. 108, n. 7, p. 2425–2431, 2004.

WALTZ, R. A. et al. An interior algorithm for nonlinear optimization that combines line search and trust region steps. *Mathematical programming*, Springer, v. 107, n. 3, p. 391–408, 2006.

WAN, W.; BIEGLER, L. T. Structured regularization for barrier nlp solvers. *Computational Optimization and Applications*, Springer, v. 66, n. 3, p. 401–424, 2017.

WANG, K. et al. Barrier nlp methods with structured regularization for optimization of degenerate optimization problems. *Computers & chemical engineering*, Elsevier, v. 57, p. 24–29, 2013.

WEIJERS, S. R.; VANROLLEGHEM, P. A. A procedure for selecting best identifiable parameters in calibrating activated sludge model no. 1 to full-scale plant data. *Water science and technology*, Elsevier, v. 36, n. 5, p. 69–79, 1997.

WIBACK, S. J.; MAHADEVAN, R.; PALSSON, B. Reconstructing metabolic flux vectors from extreme pathways: Defining the α-spectrum. *Journal of Theoretical Biology*, v. 224, n. 3, p. 313–324, 2003.

WIECHERT, W. Modeling and simulation: Tools for metabolic engineering. *Journal of Biotechnology*, v. 94, n. 1, p. 37–63, 2002.

WIERINGEN, W. N. van. Lecture notes on ridge regression. *arXiv preprint arXiv:1509.09169*, 2015.

WLASCHIN, A. P. et al. The fractional contributions of elementary modes to the metabolism of Escherichia coli and their estimation from reaction entropies. *Metabolic Engineering*, v. 8, n. 4, p. 338–352, 2006.

YOSHIKAWA, K.; TOYA, Y.; SHIMIZU, H. Metabolic engineering of Synechocystis sp. PCC 6803 for enhanced ethanol production based on flux balance analysis. *Bioprocess and Biosystems Engineering*, v. 40, n. 5, p. 791–796, 2017.

YUAN, M.; LIN, Y. Model selection and estimation in regression with grouped variables. *Journal of the Royal Statistical Society: Series B (Statistical Methodology)*, Wiley Online Library, v. 68, n. 1, p. 49–67, 2006.

YUAN, Y. A review of trust region algorithms for optimization. In: CITESEER. *Iciam*. [S.l.], 2000. v. 99, n. 1, p. 271–282.

YUAN, Y. A new stepsize for the steepest descent method. *Journal of Computational Mathematics*, JSTOR, p. 149–156, 2006.

ZANGHELLINI, J. et al. Elementary flux modes in a nutshell: properties, calculation and applications. *Biotechnology journal*, Wiley Online Library, v. 8, n. 9, p. 1009–1016, 2013.

ZAVALA, V. M. *Computational Strategies for the Optimal Operation of Large-Scale Chemical Processes*. Tese (Doutorado) — Carnegie Mellon University, 2008.

ZHANG, K. et al. Learning multiple linear mappings for efficient single image super-resolution. *IEEE Transactions on Image Processing*, IEEE, v. 24, n. 3, p. 846–861, 2015.

ZHAO, Q.; KURATA, H. Maximum entropy decomposition of flux distribution at steady state to elementary modes. *Journal of Bioscience and Bioengineering*, v. 107, n. 1, p. 84–89, 2009.

ZOU, H. The adaptive lasso and its oracle properties. *Journal of the American statistical association*, Taylor & Francis, v. 101, n. 476, p. 1418–1429, 2006.

ZOU, H.; HASTIE, T. Regularization and variable selection via the elastic net. *Journal of the royal statistical society: series B (statistical methodology)*, Wiley Online Library, v. 67, n. 2, p. 301–320, 2005.

ZOU, H.; HASTIE, T.; TIBSHIRANI, R. Sparse principal component analysis. *Journal of computational and graphical statistics*, Taylor & Francis, v. 15, n. 2, p. 265–286, 2006.

Appendix A – Case Study: *Burkholderia sacchari*

A.1 Input file and list of reactions

The software reads and processes metabolic networks written in the same format the input files used by Metatool with some modifications to include the number of carbon atoms in each metabolite, external metabolites atomic composition, and flux rate values for boundary reactions. The first two are used for carbon and redox balances, and data reconciliation of the flux rates. The input file used for the case study of the *Burkholderia sacchari* is presented here, and it includes a list of the reactions considered for the metabolic network used to represent the core metabolism.

Biossíntese de P3HB-co-3HHx a partir de glicose e ácido hexanóico considerando também a biossíntese de biomassa
considera vias ED, PPP, CK, Glioxilato, anapleróticas e respiração aeróbia de coenzimas Considerando phaJ como única saída b-oxidação para PHA.
#
#
-ENZREV
EMP2 EMP4 EMP5 EMP6 EMP7 EMP8 EMP9 VP6 VP7 VP8 VP9 VP10

-ENZIRREV
ED1 ED2 EMP10 CPD VP1 VP5 CK1 CK2 CK3 CK4 CK5 CK6 CK7 CK8 CGLX1 CGLX2 GLN3 AD1 AD2 P3HB OXFAD OXNAD BOXI2 BOXI3 BOXI4 BOXI5 BOXI6 BOXI7 BOXI8 BOXI9 PHAJ1 PHAJ2 CR01 CR02 SDH PNTAB COx

-ENZMEAS
EMP1 BOXI1 R3HB R3HHx RCO2
1.54 0.18 1.4 0.1125 3.29

-METINT [C]
G6P [6] KDPG2 [6] NADP [0] NADPH [0] PG6 [6] PIR [3] G3P [3] BPG13 [3] PG3 [3] PG2 [3] PEP [3] AcCoA [2] Rbl5P [5] Rb5P [5] X5P [5] S7P [7] E4P [4] F6P [6] DHP [3] F16P [6] OAA [4] Cit [6] KG2 [5] IsoCit [6] SucCoA [4] Suc [4] Fum [4] Mal [4] GLX [2] FAD [0] FADH2 [0] NAD [0] NADH [0] CoASH [0] HexCoA [6] HexenCoA [6] HHexCOA [6] CHexCoA [6] ButCoA [4] ButenCoA [4] HButCoA [4] CButCoA [4] CO2 [1] O [0] 3HB [4] 3HHx [6]

-METEXT [C]
ADP [0] ATP [0] Gliex [6] Hexext [6] Oext [0] CO2ext [1] 3HBext [4] 3HHxext [6]

0 0 1 1 1 1 1 1

-CAT
EMP1 : Gliex + ATP = G6P + ADP .
EMP2 : G6P = F6P .
VP1 : G6P + NADP = PG6 + NADPH .
ED1 : PG6 = KDPG2 .
ED2 : KDPG2 = PIR + G3P .
EMP4 : F16P = G3P + DHP .
EMP5 : DHP = G3P .
EMP6 : G3P + NAD = BPG13 + NADH .
EMP7 : BPG13 + ADP = PG3 + ATP .
EMP8 : PG3 = PG2 .
EMP9 : PG2 = PEP .
EMP10 : PEP + ADP = PIR + ATP .
CPD : PIR + NAD + CoASH = AcCoA + NADH + CO2 .
VP5 : PG6 + NADP = NADPH + Rbl5P + CO2 .
VP6 : Rbl5P = Rb5P .
VP7 : Rbl5P = X5P .
VP8 : Rb5P + X5P = S7P + G3P .
VP9 : G3P + S7P = E4P + F6P .
VP10 : X5P + E4P = F6P + G3P .
CK1 : OAA + AcCoA = Cit + CoASH .
CK2 : Cit = IsoCit .
CK3 : IsoCit + NADP = KG2 + NADPH + CO2 .
CK4 : KG2 + NAD + CoASH = SucCoA + NADH + CO2 .
CK5 : SucCoA + ADP = Suc + ATP + CoASH .
CK6 : Suc + FAD = Fum + FADH2 .
CK7 : Fum = Mal .
CK8 : Mal + NAD = OAA + NADH .
CGLX1 : IsoCit = GLX + Suc .
CGLX2 : GLX + AcCoA = Mal + CoASH .
GLN3 : F16P = F6P .
AD1 : PIR + CO2 + ATP = OAA + ADP .
AD2 : OAA + ATP = PEP + ADP + CO2 .
P3HB : 2 AcCoA + 1 NADPH = 3HB + 2 CoASH + 1 NADP .
OXFAD : FADH2 + 2 ADP + O = FAD + 2 ATP .
OXNAD : NADH + 3 ADP + O = NAD + 3 ATP .
BOXI1 : Hexext + 2 ATP + CoASH = HexCoA + 2 ADP .

BOXI2 : HexCoA + NAD = HexenCoA + NADH .
BOXI3 : HexenCoA = HHexCOA .
BOXI4 : HHexCOA + NAD = CHexCoA + NADH .
BOXI5 : CHexCoA + CoASH = ButCoA + AcCoA .
BOXI6 : ButCoA + NAD = ButenCoA + NADH .
BOXI7 : ButenCoA = HButCoA .
BOXI8 : HButCoA + NAD = CButCoA + NADH .
BOXI9 : CButCoA + CoASH = 2 AcCoA .
CR01 : CHexCoA + NADPH = 3HHx + NADP + CoASH .
CR02 : CButCoA + NADPH = 3HB + NADP + CoASH .
PHAJ1 : ButenCoA = 3HB + CoASH .
PHAJ2 : HexenCoA = 3HHx + CoASH .
SDH : NADPH + NAD = NADP + NADH .
PNTAB : NADH + ATP + NADP = NAD + ADP + NADPH .
R3HB : 3HB = 3HBext .
R3HHx : 3HHx = 3HHxext .
RCO2 : CO2 = CO2ext .
COx : Oext = O .

-COMP
Gliex : 6 C + 12 H + 6 O .
Hexext : 6 C + 12 H + 2 O .
Oext : O .
CO2ext : C + 2 O .
3HBext : 4 C + 8 H + 3 O .
3HHxext : 6 C + 12 H + 3 O .

A.2 Elementary flux modes and elementary flux vectors

Table 24 shows the complete set of EFM obtained for the metabolic network used to represent the core metabolism of *Burkholderia sacchari* after removing 3 infeasible EFM without substrate uptake. Table 25 shows the complete set of EFV obtained for the second part of the case study that use experimental data with 3HHx synthesis.

Table 24 – Complete set of EFM obtained for the metabolic network used to represent the core metabolism of Burkholderia sacchari.

EFM	**1**	**2**	**3**	**4**	**5**	**6**	**7**	**8**	**9**	**10**	**11**	**12**	**13**	**14**	**15**	**16**	**17**	**18**	**19**
Group	1	1	1	1	1	1	1	1	2	2	2	2	3	3	4	5	5	5	6
EMP2	-	-1	-3	-5	-2	-2	-	-1	-	-4.5	-	-3	-	-0.75	-0.45	-	-	-1	-
EMP4	-	-1	-3	-1	-	-	-	-1	-	-1.5	-	-3	-	-0.75	-0.15	-	-	-1	-
EMP5	-	-1	-3	-1	-	-	-	-1	-	-1.5	-	-3	-	-0.75	-0.15	-	-	-1	-
EMP6	1	-	-2	-	1	1	1	-	-	-1.5	-	-3	-	-0.75	-0.15	-	-	-1	1
EMP7	1	-	-2	-	1	1	1	-	-	-1.5	-	-3	-	-0.75	-0.15	-	-	-1	1
EMP8	1	-	-2	-	1	1	1	-	-	-1.5	-	-3	-	-0.75	-0.15	-	-	-1	1
EMP9	1	-	-2	-	1	1	1	-	-	-1.5	-	-3	-	-0.75	-0.15	-	-	-1	1
VP6	-	-	-	2	1	1	-	-	-	1.5	-	-	-	-	0.15	-	-	-	-
VP7	-	-	-	4	2	2	-	-	-	3	-	-	-	-	0.3	-	-	-	-
VP8	-	-	-	2	1	1	-	-	-	1.5	-	-	-	-	0.15	-	-	-	-
VP9	-	-	-	2	1	1	-	-	-	1.5	-	-	-	-	0.15	-	-	-	-
VP10	-	-	-	2	1	1	-	-	-	1.5	-	-	-	-	0.15	-	-	-	-
ED1	1	2	4	-	-	-	1	2	-	-	-	3	-	0.75	-	-	-	1	1
ED2	1	2	4	-	-	-	1	2	-	-	-	3	-	0.75	-	-	-	1	1
EMP10	3	2	-	-	2	1	1	-	-	-	3	-	-	-	-	-	-	-	3
CPD	4	4	4	-	2	1	2	2	-	-	3	3	-	0.75	-	-	-	-	4
VP1	1	2	4	6	3	3	1	2	-	4.5	-	3	-	0.75	0.45	-	-	1	1
VP5	-	-	-	6	3	3	-	-	-	4.5	-	-	-	-	0.45	-	-	-	-
CK1	2	2	2	-	1	1	2	2	3	1.5	3	3	0.75	0.75	0.15	-	-	-	2
CK2	2	2	2	-	1	1	2	2	3	1.5	3	3	0.75	0.75	0.15	-	-	-	2
CK3	-	-	-	-	-	1	2	2	3	-	-	-	0.75	-	-	-	-	-	-
CK4	-	-	-	-	-	1	2	2	3	-	-	-	0.75	-	-	-	-	-	-
CK5	-	-	-	-	-	1	2	2	3	-	-	-	0.75	-	-	-	-	-	-
CK6	2	2	2	-	1	1	2	2	3	1.5	3	3	0.75	0.75	0.15	-	-	-	2
CK7	2	2	2	-	1	1	2	2	3	1.5	3	3	0.75	0.75	0.15	-	-	-	2
CK8	4	4	4	-	2	1	2	2	3	3	6	6	0.75	1.5	0.3	-	-	-	4
CGLX1	2	2	2	-	1	-	-	-	-	1.5	3	3	-	0.75	0.15	-	-	-	2
CGLX2	2	2	2	-	1	-	-	-	-	1.5	3	3	-	0.75	0.15	-	-	-	2
GLN3	-	1	3	1	-	-	-	1	-	1.5	-	3	-	0.75	0.15	-	-	1	-
AD1	-	-	-	-	-	-	-	-	-	-	-	-	-	-	-	-	-	1	-
AD2	2	2	2	-	1	-	-	-	-	1.5	3	3	-	0.75	0.15	-	-	1	2
P3HB	-	-	-	-	-	-	-	-	-	-	-	-	-	-	-	-	-	-	-
OXFAD	2	2	2	-	1	1	2	2	3	1.5	3	3	0.75	0.75	0.15	-	-	-	2
OXNAD	10	10	10	12	11	11	10	10	13	14.5	13	13	4	4	2.35	1	1	1	11
BOXI2	-	-	-	-	-	-	-	-	1	1	1	1	1	1	1	1	1	1	1
BOXI3	-	-	-	-	-	-	-	-	1	1	1	1	1	1	1	-	1	1	1
BOXI4	-	-	-	-	-	-	-	-	1	1	1	1	1	1	1	-	1	1	1
BOXI5	-	-	-	-	-	-	-	-	1	1	1	1	0.25	0.25	0.1	-	-	-	-
BOXI6	-	-	-	-	-	-	-	-	1	1	1	1	0.25	0.25	0.1	-	-	-	-
BOXI7	-	-	-	-	-	-	-	-	1	1	1	1	0.25	0.25	0.1	-	-	-	-
BOXI8	-	-	-	-	-	-	-	-	1	1	1	1	0.25	0.25	0.1	-	-	-	-
BOXI9	-	-	-	-	-	-	-	-	1	1	1	1	0.25	0.25	0.1	-	-	-	-
PHAJ1	-	-	-	-	-	-	-	-	-	-	-	-	-	-	-	-	-	-	-
PHAJ2	-	-	-	-	-	-	-	-	-	-	-	-	-	-	-	1	-	-	-
CR01	-	-	-	-	-	-	-	-	-	-	-	-	0.75	0.75	0.9	-	1	1	1
CR02	-	-	-	-	-	-	-	-	-	-	-	-	-	-	-	-	-	-	-
SDH	1	2	4	12	6	7	3	4	3	9	-	3	-	-	-	-	-	-	-
PNTAB	-	-	-	-	-	-	-	-	-	-	-	-	-	-	-	-	1	-	-
EMP1	1	1	1	1	1	1	1	1	-	-	-	-	-	-	-	-	-	-	1
BOXI1	-	-	-	-	-	-	-	-	1	1	1	1	1	1	1	1	1	1	1
COx	6	6	6	6	6	6	6	6	8	8	8	8	2.375	2.375	1.25	0.5	0.5	0.5	6.5
R3HB	-	-	-	-	-	-	-	-	-	-	-	-	-	-	-	-	-	-	-
R3HHx	-	-	-	-	-	-	-	-	-	-	-	-	0.75	0.75	0.9	1	1	1	1
RCO2	6	6	6	6	6	6	6	6	6	6	6	6	1.5	1.5	0.6	-	-	-	6

Table 24 continued – Complete set of EFM obtained for the metabolic network used to represent the core metabolism of Burkholderia sacchari.

EFM	**20**	**21**	**22**	**23**	**24**	**25**	**26**	**27**	**28**	**29**	**30**	**31**	**32**	**33**	**34**	**35**	**36**	**37**
Group	7	8	9	9	10	11	12	13	14	15	15	16	17	18	18	18	18	18
EMP2	-1	-	-3	-1	-2	-2	-5	-0.375	-0.5	-0.5	-	-2	-2	-	-1	-	-1	-
EMP4	-1	-	-3	-1	-	-	-1	-0.125	-0.167	-0.5	-	-	-	-	-1	-	-1	-
EMP5	-1	-	-3	-1	-	-	-1	-0.125	-0.167	-0.5	-	-	-	-	-1	-	-1	-
EMP6	-	1	-2	-	1	1	-	-0.125	-0.167	-0.5	-	1	1	-	-1	-	-1	-
EMP7	-	1	-2	-	1	1	-	-0.125	-0.167	-0.5	-	1	1	-	-1	-	-1	-
EMP8	-	1	-2	-	1	1	-	-0.125	-0.167	-0.5	-	1	1	-	-1	-	-1	-
EMP9	-	1	-2	-	1	1	-	-0.125	-0.167	-0.5	-	1	1	-	-1	-	-1	-
VP6	-	-	-	-	1	1	2	0.125	0.167	-	-	1	1	-	-	-	-	-
VP7	-	-	-	-	2	2	4	0.25	0.333	-	-	2	2	-	-	-	-	-
VP8	-	-	-	-	1	1	2	0.125	0.167	-	-	1	1	-	-	-	-	-
VP9	-	-	-	-	1	1	2	0.125	0.167	-	-	1	1	-	-	-	-	-
VP10	-	-	-	-	1	1	2	0.125	0.167	-	-	1	1	-	-	-	-	-
ED1	2	1	4	2	-	-	-	-	-	0.5	-	-	-	-	1	-	1	-
ED2	2	1	4	2	-	-	-	-	-	0.5	-	-	-	-	1	-	1	-
EMP10	2	1	-	-	2	1	-	-	-	-	-	1	1	-	-	1	-	1
CPD	4	2	4	2	2	1	-	-	-	0.5	-	1	1	-	1	1	1	1
VP1	2	1	4	2	3	3	6	0.375	0.5	0.5	-	3	3	-	1	-	1	-
VP5	-	-	-	-	3	3	6	0.375	0.5	-	-	3	3	-	-	-	-	-
CK1	2	2	2	2	1	1	-	0.125	0.167	0.5	0.5	-	-	1	1	1	1	1
CK2	2	2	2	2	1	1	-	0.125	0.167	0.5	0.5	-	-	1	1	1	1	1
CK3	-	2	-	2	-	1	-	-	-	-	0.5	-	-	1	-	-	-	-
CK4	-	2	-	2	-	1	-	-	-	-	0.5	-	-	1	-	-	-	-
CK5	-	2	-	2	-	1	-	-	-	-	0.5	-	-	1	-	-	-	-
CK6	2	2	2	2	1	1	-	0.125	0.167	0.5	0.5	-	-	1	1	1	1	1
CK7	2	2	2	2	1	1	-	0.125	0.167	0.5	0.5	-	-	1	1	1	1	1
CK8	4	2	4	2	2	1	-	0.25	0.333	1	0.5	-	-	1	2	2	2	2
CGLX1	2	-	2	-	1	-	-	0.125	0.167	0.5	-	-	-	-	1	1	1	1
CGLX2	2	-	2	-	1	-	-	0.125	0.167	0.5	-	-	-	-	1	1	1	1
GLN3	1	-	3	1	-	-	1	0.125	0.167	0.5	-	-	-	-	1	-	1	-
AD1	-	-	-	-	-	-	-	-	-	-	-	-	-	-	-	-	-	-
AD2	2	-	2	-	1	-	-	0.125	0.167	0.5	-	-	-	-	1	1	1	1
P3HB	-	-	-	-	-	-	-	-	-	-	-	0.5	0.5	-	-	-	-	-
OXFAD	2	2	2	2	1	1	-	0.125	0.167	0.5	0.5	-	-	1	1	1	1	1
OXNAD	12	13	14	14	17	18	24	2.375	2.833	3.5	3.5	7.5	13	6	6	6	6	6
BOXI2	2	3	4	4	6	7	12	1	1	1	1	-	5.5	1	1	1	1	1
BOXI3	2	3	4	4	6	7	12	1	1	1	1	-	5.5	1	1	1	1	1
BOXI4	2	3	4	4	6	7	12	1	1	1	1	-	5.5	1	1	1	1	1
BOXI5	-	-	-	-	-	-	-	0.25	0.333	0.5	0.5	-	-	1	1	1	1	1
BOXI6	-	-	-	-	-	-	-	0.25	0.333	0.5	0.5	-	-	1	1	1	1	1
BOXI7	-	-	-	-	-	-	-	-	0.333	-	-	-	-	1	-	-	1	1
BOXI8	-	-	-	-	-	-	-	-	0.333	-	-	-	-	1	-	-	1	1
BOXI9	-	-	-	-	-	-	-	-	-	-	-	-	-	-	-	-	-	-
PHAJ1	-	-	-	-	-	-	-	0.25	-	0.5	0.5	-	-	-	1	1	-	-
PHAJ2	-	-	-	-	-	-	-	-	-	-	-	-	-	-	-	-	-	-
CR01	2	3	4	4	6	7	12	0.75	0.667	0.5	0.5	-	5.5	-	-	-	-	-
CR02	-	-	-	-	-	-	-	-	0.333	-	-	-	-	1	-	-	1	1
SDH	-	-	-	-	-	-	-	-	-	-	-	5.5	-	-	1	-	-	-
PNTAB	-	-	-	-	-	-	-	-	-	-	-	-	-	-	-	-	-	1
EMP1	1	1	1	1	1	1	1	-	-	-	-	1	1	-	-	-	-	-
BOXI1	2	3	4	4	6	7	12	1	1	1	1	-	5.5	1	1	1	1	1
COx	7	7.5	8	8	9	9.5	12	1.25	1.5	2	2	3.75	6.5	3.5	3.5	3.5	3.5	3.5
R3HB	-	-	-	-	-	-	-	0.25	0.333	0.5	0.5	0.5	0.5	1	1	1	1	1
R3HHx	2	3	4	4	6	7	12	0.75	0.667	0.5	0.5	-	5.5	-	-	-	-	-
RCO2	6	6	6	6	6	6	6	0.5	0.667	1	1	4	4	2	2	2	2	2

Table 24 continued – Complete set of EFM obtained for the metabolic network used to represent the core metabolism of Burkholderia sacchari.

EFM	**38**	**39**	**40**	**41**	**42**	**43**	**44**	**45**	**46**	**47**	**48**	**49**	**50**	**51**	**52**	**53**
Group	18	18	18	19	18	20	20	21	18	18	22	22	23	23	24	25
EMP2	-1.5	-1.5	-	-	-0.5	-1	-	-1	-	-1	-0.643	-0.643	-	-0.333	-0.214	-0.5
EMP4	-0.5	-0.5	-	-	-0.167	-1	-	-1	-	-1	-0.214	-0.214	-	-0.333	-0.071	-0.5
EMP5	-0.5	-0.5	-	-	-0.167	-1	-	-1	-	-1	-0.214	-0.214	-	-0.333	-0.071	-0.5
EMP6	-0.5	-0.5	-	1	-0.167	-	1	-	-	-1	-0.214	-0.214	-	-0.333	-0.071	-0.5
EMP7	-0.5	-0.5	-	1	-0.167	-	1	-	-	-1	-0.214	-0.214	-	-0.333	-0.071	-0.5
EMP8	-0.5	-0.5	-	1	-0.167	-	1	-	-	-1	-0.214	-0.214	-	-0.333	-0.071	-0.5
EMP9	-0.5	-0.5	-	1	-0.167	-	1	-	-	-1	-0.214	-0.214	-	-0.333	-0.071	-0.5
VP6	0.5	0.5	-	-	0.167	-	-	-	-	-	0.214	0.214	-	-	0.071	-
VP7	1	1	-	-	0.333	-	-	-	-	-	0.429	0.429	-	-	0.143	-
VP8	0.5	0.5	-	-	0.167	-	-	-	-	-	0.214	0.214	-	-	0.071	-
VP9	0.5	0.5	-	-	0.167	-	-	-	-	-	0.214	0.214	-	-	0.071	-
VP10	0.5	0.5	-	-	0.167	-	-	-	-	-	0.214	0.214	-	-	0.071	-
ED1	-	-	-	1	-	2	1	2	-	1	-	-	-	0.333	-	0.5
ED2	-	-	-	1	-	2	1	2	-	1	-	-	-	0.333	-	0.5
EMP10	-	-	-	4	0.667	-	1	-	-	-	-	-	-	-	-	-
CPD	-	-	-	5	0.667	2	2	2	-	1	-	-	-	0.333	-	-
VP1	1.5	1.5	-	1	0.5	2	1	2	-	1	0.643	0.643	-	0.333	0.214	0.5
VP5	1.5	1.5	-	-	0.5	-	-	-	-	-	0.643	0.643	-	-	0.214	-
CK1	0.5	0.5	1	3	0.833	-	-	-	1	1	0.214	0.214	0.333	0.333	0.071	-
CK2	0.5	0.5	1	3	0.833	-	-	-	1	1	0.214	0.214	0.333	0.333	0.071	-
CK3	-	-	1	-	-	-	-	-	1	-	-	-	0.333	-	-	-
CK4	-	-	1	-	-	-	-	-	1	-	-	-	0.333	-	-	-
CK5	-	-	1	-	-	-	-	-	1	-	-	-	0.333	-	-	-
CK6	0.5	0.5	1	3	0.833	-	-	-	1	1	0.214	0.214	0.333	0.333	0.071	-
CK7	0.5	0.5	1	3	0.833	-	-	-	1	1	0.214	0.214	0.333	0.333	0.071	-
CK8	1	1	1	6	1.667	-	-	-	1	2	0.429	0.429	0.333	0.667	0.143	-
CGLX1	0.5	0.5	-	3	0.833	-	-	-	-	1	0.214	0.214	-	0.333	0.071	-
CGLX2	0.5	0.5	-	3	0.833	-	-	-	-	1	0.214	0.214	-	0.333	0.071	-
GLN3	0.5	0.5	-	-	0.167	1	-	1	-	1	0.214	0.214	-	0.333	0.071	0.5
AD1	-	-	-	-	-	-	-	-	-	-	-	-	-	-	-	0.5
AD2	0.5	0.5	-	3	0.833	-	-	-	-	1	0.214	0.214	-	0.333	0.071	0.5
P3HB	-	-	-	-	-	1	1	1	1	1	1.286	0.286	0.333	0.333	0.429	0.5
OXFAD	0.5	0.5	1	3	0.833	-	-	-	1	1	0.214	0.214	0.333	0.333	0.071	-
OXNAD	6.5	6.5	6	16	6.167	3	3	4	6	6	4.214	4.214	3.667	3.667	3.071	2.5
BOXI2	1	1	1	1	1	-	-	1	1	1	1	1	1	1	1	1
BOXI3	1	1	1	1	1	-	-	1	1	1	1	1	1	1	1	1
BOXI4	1	1	1	1	1	-	-	1	1	1	1	1	1	1	1	1
BOXI5	1	1	1	1	1	-	-	-	1	1	1	1	1	1	1	1
BOXI6	1	1	1	1	1	-	-	-	1	1	1	1	1	1	1	1
BOXI7	-	1	-	1	1	-	-	-	1	1	1	1	-	-	-	-
BOXI8	-	1	-	1	1	-	-	-	1	1	1	1	-	-	-	-
BOXI9	-	-	-	-	-	-	-	-	1	1	1	-	-	-	-	-
PHAJ1	1	-	1	-	-	-	-	-	-	-	-	-	1	1	1	1
PHAJ2	-	-	-	-	-	-	-	-	-	-	-	-	-	-	-	-
CR01	-	-	-	-	-	-	-	1	-	-	-	-	-	-	-	-
CR02	-	1	-	1	1	-	-	-	-	-	-	1	-	-	-	-
SDH	3	2	1	-	-	1	-	-	-	-	-	-	-	-	-	-
PNTAB	-	-	-	-	-	-	-	-	-	-	-	-	-	-	-	-
EMP1	-	-	-	1	-	1	1	1	-	-	-	-	-	-	-	-
BOXI1	1	1	1	1	1	-	-	1	1	1	1	1	1	1	1	1
COx	3.5	3.5	3.5	9.5	3.5	1.5	1.5	2	3.5	3.5	2.214	2.214	2	2	1.571	1.25
R3HB	1	1	1	1	1	1	1	1	1	1	1.286	1.286	1.333	1.333	1.429	1.5
R3HHx	-	-	-	-	-	-	-	1	-	-	-	-	-	-	-	-
RCO2	2	2	2	8	2	2	2	2	2	2	0.857	0.857	0.667	0.667	0.286	-

Table 24 continued – Complete set of EFM obtained for the metabolic network used to represent the core metabolism of Burkholderia sacchari.

EFM	**54**	**55**	**56**	**57**	**58**	**59**	**60**	**61**	**62**	**63**	**64**	**65**	**66**	**67**	**68**	**69**	**70**
Group	25	25	25	25	25	26	26	27	28	29	29	30	31	32	32	33	34
EMP2	-	-	-	-1.5	-1.5	-1	-1	-1	-1	-2	-2	-2	-5	-5	-5	-2	-5
EMP4	-	-	-	-1.5	-1.5	-1	-1	-1	-1	-	-	-	-1	-1	-1	-	-1
EMP5	-	-	-	-1.5	-1.5	-1	-1	-1	-1	-	-	-	-1	-1	-1	-	-1
EMP6	-	-	-	-1.5	-1.5	-	-	-	-	1	1	1	-	-	-	1	-
EMP7	-	-	-	-1.5	-1.5	-	-	-	-	1	1	1	-	-	-	1	-
EMP8	-	-	-	-1.5	-1.5	-	-	-	-	1	1	1	-	-	-	1	-
EMP9	-	-	-	-1.5	-1.5	-	-	-	-	1	1	1	-	-	-	1	-
VP6	-	-	-	-	-	-	-	-	-	1	1	1	2	2	2	1	2
VP7	-	-	-	-	-	-	-	-	-	2	2	2	4	4	4	2	4
VP8	-	-	-	-	-	-	-	-	-	1	1	1	2	2	2	1	2
VP9	-	-	-	-	-	-	-	-	-	1	1	1	2	2	2	1	2
VP10	-	-	-	-	-	-	-	-	-	1	1	1	2	2	2	1	2
ED1	-	-	-	1.5	1.5	2	2	2	2	-	-	-	-	-	-	-	-
ED2	-	-	-	1.5	1.5	2	2	2	2	-	-	-	-	-	-	-	-
EMP10	-	-	-	-	-	-	-	4	-	1	1	8	12	-	-	1	-
CPD	-	-	-	-	-	2	2	6	2	1	1	8	12	-	-	1	-
VP1	-	-	-	1.5	1.5	2	2	2	2	3	3	3	6	6	6	3	6
VP5	-	-	-	-	-	-	-	-	-	3	3	3	6	6	6	3	6
CK1	-	-	-	-	-	-	-	4	-	-	-	7	12	-	-	-	-
CK2	-	-	-	-	-	-	-	4	-	-	-	7	12	-	-	-	-
CK3	-	-	-	-	-	-	-	-	-	-	-	-	-	-	-	-	-
CK4	-	-	-	-	-	-	-	-	-	-	-	-	-	-	-	-	-
CK5	-	-	-	-	-	-	-	-	-	-	-	-	-	-	-	-	-
CK6	-	-	-	-	-	-	-	4	-	-	-	7	12	-	-	-	-
CK7	-	-	-	-	-	-	-	4	-	-	-	7	12	-	-	-	-
CK8	-	-	-	-	-	-	-	8	-	-	-	14	24	-	-	-	-
CGLX1	-	-	-	-	-	-	-	4	-	-	-	7	12	-	-	-	-
CGLX2	-	-	-	-	-	-	-	4	-	-	-	7	12	-	-	-	-
GLN3	-	-	-	1.5	1.5	1	1	1	1	-	-	-	1	1	1	-	1
AD1	-	-	-	1.5	1.5	-	-	-	-	-	-	-	-	-	-	-	-
AD2	-	-	-	1.5	1.5	-	-	4	-	-	-	7	12	-	-	-	-
P3HB	0.5	0.5	1.5	0.5	1.5	1.333	2	-	2	2.333	6	-	-	12	4	6	12
OXFAD	-	-	-	-	-	-	-	4	-	-	-	7	12	-	-	-	-
OXNAD	2.5	2.5	2.5	2.5	2.5	4.667	4.667	22	8	16.67	16.67	47	84	32	32	35	72
BOXI2	1	1	1	1	1	0.667	0.667	2	2	3.667	3.667	6	12	8	8	11	24
BOXI3	1	1	1	1	1	0.667	0.667	2	2	3.667	3.667	6	12	8	8	11	24
BOXI4	1	1	1	1	1	0.667	0.667	2	2	3.667	3.667	6	12	8	8	11	24
BOXI5	1	1	1	1	1	0.667	0.667	2	2	3.667	3.667	6	12	8	8	11	24
BOXI6	1	1	1	1	1	0.667	0.667	2	2	3.667	3.667	6	12	8	8	11	24
BOXI7	-	1	1	1	1	0.667	0.667	2	-	3.667	3.667	6	12	8	8	-	-
BOXI8	-	1	1	1	1	0.667	0.667	2	-	3.667	3.667	6	12	8	8	-	-
BOXI9	-	-	1	-	1	-	0.667	-	-	-	3.667	-	-	8	-	-	-
PHAJ1	1	-	-	-	-	-	-	-	2	-	-	-	-	-	-	11	24
PHAJ2	-	-	-	-	-	-	-	-	-	-	-	-	-	-	-	-	-
CR01	-	-	-	-	-	-	-	-	-	-	-	-	-	-	-	-	-
CR02	-	1	-	1	-	0.667	-	2	-	3.667	-	6	12	-	8	-	-
SDH	-	-	-	-	-	-	-	-	-	-	-	-	-	-	-	-	-
PNTAB	0.5	1.5	1.5	-	-	-	-	-	-	-	-	-	-	-	-	-	-
EMP1	-	-	-	-	-	1	1	1	1	1	1	1	1	1	1	1	1
BOXI1	1	1	1	1	1	0.667	0.667	2	2	3.667	3.667	6	12	8	8	11	24
COx	1.25	1.25	1.25	1.25	1.25	2.333	2.333	13	4	8.333	8.333	27	48	16	16	17.5	36
R3HB	1.5	1.5	1.5	1.5	1.5	2	2	2	4	6	6	6	12	12	12	17	36
R3HHx	-	-	-	-	-	-	-	-	-	-	-	-	-	-	-	-	-
RCO2	-	-	-	-	-	2	2	10	2	4	4	18	30	6	6	4	6

Table 25 – Complete set of EFV obtained for the metabolic network used to represent the core metabolism of Burkholderia sacchari using experimental flux data.

EFV	1	2	3	4	5	6	7	8	9	10	11	12	13
EMP2	-	-	-1.464	-1.464	-	-1.464	-1.464	-	-	-	-0.040	-0.100	-1.659
EMP4	-	-	-1.464	-1.464	-	-1.464	-1.464	-	-	-	-	-0.100	-1.659
EMP5	-	-	-1.464	-1.464	-	-1.464	-1.464	-	-	-	-	-0.100	-1.659
EMP6	1.464	1.464	-	-	1.464	-	-	1.464	1.464	1.464	1.464	1.364	-0.195
EMP7	1.464	1.464	-	-	1.464	-	-	1.464	1.464	1.464	1.464	1.364	-0.195
EMP8	1.464	1.464	-	-	1.464	-	-	1.464	1.464	1.464	1.464	1.364	-0.195
EMP9	1.464	1.464	-	-	1.464	-	-	1.464	1.464	1.464	1.464	1.364	-0.195
VP6	-	-	-	-	-	-	-	-	-	-	0.020	-	-
VP7	-	-	-	-	-	-	-	-	-	-	0.040	-	-
VP8	-	-	-	-	-	-	-	-	-	-	0.020	-	-
VP9	-	-	-	-	-	-	-	-	-	-	0.020	-	-
VP10	-	-	-	-	-	-	-	-	-	-	0.020	-	-
ED1	1.464	1.464	2.928	2.928	1.464	2.928	2.928	1.464	1.464	1.464	1.444	1.564	3.122
ED2	1.464	1.464	2.928	2.928	1.464	2.928	2.928	1.464	1.464	1.464	1.444	1.564	3.122
EMP10	1.464	1.464	-	-	1.659	0.195	0.195	1.558	1.659	1.659	1.638	1.558	-
CPD	2.928	2.928	2.928	2.928	3.122	3.122	3.122	3.022	3.122	3.122	3.082	3.122	3.122
VP1	1.464	1.464	2.928	2.928	1.464	2.928	2.928	1.464	1.464	1.464	1.504	1.564	3.122
VP5	-	-	-	-	-	-	-	-	-	-	0.060	-	-
CK1	0.195	0.195	0.195	0.195	0.195	0.195	0.195	0.195	0.195	0.195	0.175	0.195	0.195
CK2	0.195	0.195	0.195	0.195	0.195	0.195	0.195	0.195	0.195	0.195	0.175	0.195	0.195
CK3	0.195	0.195	0.195	0.195	-	-	-	0.100	-	-	-	-	-
CK4	0.195	0.195	0.195	0.195	-	-	-	0.100	-	-	-	-	-
CK5	0.195	0.195	0.195	0.195	-	-	-	0.100	-	-	-	-	-
CK6	0.195	0.195	0.195	0.195	0.195	0.195	0.195	0.195	0.195	0.195	0.175	0.195	0.195
CK7	0.195	0.195	0.195	0.195	0.195	0.195	0.195	0.195	0.195	0.195	0.175	0.195	0.195
CK8	0.195	0.195	0.195	0.195	0.389	0.389	0.389	0.289	0.389	0.389	0.349	0.389	0.389
CGLX1	-	-	-	-	0.195	0.195	0.195	0.094	0.195	0.195	0.175	0.195	0.195
CGLX2	-	-	-	-	0.195	0.195	0.195	0.094	0.195	0.195	0.175	0.195	0.195
GLN3	-	-	1.464	1.464	-	1.464	1.464	-	-	-	-	0.100	1.659
AD1	-	-	-	-	-	-	-	-	-	-	-	-	-
AD2	-	-	-	-	0.195	0.195	0.195	0.094	0.195	0.195	0.175	0.195	0.195
P3HB	1.446	1.446	1.446	1.446	1.446	1.446	1.446	1.446	1.446	1.446	1.446	1.446	1.446
OXFAD	0.195	0.195	0.195	0.195	0.195	0.195	0.195	0.195	0.195	0.195	0.175	0.195	0.195
OXNAD	5.324	5.324	5.324	5.324	5.324	5.324	5.324	5.324	5.324	5.324	5.344	5.324	5.324
BOXI2	0.171	0.171	0.171	0.171	0.171	0.171	0.171	0.171	0.171	0.171	0.171	0.171	0.171
BOXI3	0.171	0.053	0.053	0.171	0.053	0.053	0.171	0.171	0.071	0.171	0.171	0.171	0.053
BOXI4	0.171	0.053	0.053	0.171	0.053	0.053	0.171	0.171	0.071	0.171	0.171	0.171	0.053
BOXI5	0.053	0.053	0.053	0.053	0.053	0.053	0.053	0.053	0.053	0.053	0.053	0.053	0.053
BOXI6	0.053	0.053	0.053	0.053	0.053	0.053	0.053	0.053	0.053	0.053	0.053	0.053	0.053
BOXI7	0.053	0.053	0.053	0.053	0.053	0.053	0.053	0.053	0.053	0.053	0.053	0.053	0.053
BOXI8	0.053	0.053	0.053	0.053	0.053	0.053	0.053	0.053	0.053	0.053	0.053	0.053	0.053
BOXI9	0.053	0.053	0.053	0.053	0.053	0.053	0.053	0.053	0.053	0.053	0.053	0.053	0.053
PHAJ1	-	-	-	-	-	-	-	-	-	-	-	-	-
PHAJ2	-	0.118	0.118	-	0.118	0.118	-	-	0.100	-	-	-	0.118
CR01	0.118	-	-	0.118	-	-	0.118	0.118	0.018	0.118	0.118	0.118	-
CR02	-	-	-	-	-	-	-	-	-	-	-	-	-
SDH	0.094	0.212	1.676	1.558	0.018	1.482	1.364	-	-	-	-	-	1.676
PNTAB	-	-	-	-	-	-	-	-	-	0.100	-	-	-
Cox	2.759	2.759	2.759	2.759	2.759	2.759	2.759	2.759	2.759	2.759	2.759	2.759	2.759
EMP1	1.464	1.464	1.464	1.464	1.464	1.464	1.464	1.464	1.464	1.464	1.464	1.464	1.464
BOXI1	0.171	0.171	0.171	0.171	0.171	0.171	0.171	0.171	0.171	0.171	0.171	0.171	0.171
R3HB	1.446	1.446	1.446	1.446	1.446	1.446	1.446	1.446	1.446	1.446	1.446	1.446	1.446
R3HHx	0.118	0.118	0.118	0.118	0.118	0.118	0.118	0.118	0.118	0.118	0.118	0.118	0.118
RCO2	3.317	3.317	3.317	3.317	3.317	3.317	3.317	3.317	3.317	3.317	3.317	3.317	3.317

Table 25 continued – Complete set of EFV obtained for the metabolic network used to represent the core metabolism of Burkholderia sacchari using experimental flux data.

EFV	14	15	16	17	18	19	20	21	22	23	24	25	26	27
EMP2	-1.659	-	-	-	-	-	-0.047	-1.659	-	-	-0.019	-	-	-
EMP4	-1.659	-	-	-	-	-	-0.047	-1.659	-	-	-	-	-	-
EMP5	-1.659	-	-	-	-	-	-0.047	-1.659	-	-	-	-	-	-
EMP6	-0.195	1.464	1.464	1.464	1.464	1.464	1.417	-0.195	1.464	1.464	1.464	1.464	1.464	1.464
EMP7	-0.195	1.464	1.464	1.464	1.464	1.464	1.417	-0.195	1.464	1.464	1.464	1.464	1.464	1.464
EMP8	-0.195	1.464	1.464	1.464	1.464	1.464	1.417	-0.195	1.464	1.464	1.464	1.464	1.464	1.464
EMP9	-0.195	1.464	1.464	1.464	1.464	1.464	1.417	-0.195	1.464	1.464	1.464	1.464	1.464	1.464
VP6	-	-	-	-	-	-	-	-	-	-	0.009	-	-	-
VP7	-	-	-	-	-	-	-	-	-	-	0.019	-	-	-
VP8	-	-	-	-	-	-	-	-	-	-	0.009	-	-	-
VP9	-	-	-	-	-	-	-	-	-	-	0.009	-	-	-
VP10	-	-	-	-	-	-	-	-	-	-	0.009	-	-	-
ED1	3.122	1.464	1.464	1.464	1.464	1.464	1.511	3.122	1.464	1.464	1.454	1.464	1.464	1.464
ED2	3.122	1.464	1.464	1.464	1.464	1.464	1.511	3.122	1.464	1.464	1.454	1.464	1.464	1.464
EMP10	-	1.659	1.659	1.464	1.464	1.611	1.611	-	1.659	1.659	1.649	1.464	1.464	1.558
CPD	3.122	3.122	3.122	2.928	2.928	3.075	3.122	3.122	3.122	3.122	3.104	2.928	2.928	3.022
VP1	3.122	1.464	1.464	1.464	1.464	1.464	1.511	3.122	1.464	1.464	1.483	1.464	1.464	1.464
VP5	-	-	-	-	-	-	-	-	-	-	0.028	-	-	-
CK1	0.195	0.195	0.195	0.195	0.195	0.195	0.195	0.195	0.195	0.195	0.185	0.195	0.195	0.195
CK2	0.195	0.195	0.195	0.195	0.195	0.195	0.195	0.195	0.195	0.195	0.185	0.195	0.195	0.195
CK3	-	-	-	0.195	0.195	0.047	-	-	-	-	-	0.195	0.195	0.100
CK4	-	-	-	0.195	0.195	0.047	-	-	-	-	-	0.195	0.195	0.100
CK5	-	-	-	0.195	0.195	0.047	-	-	-	-	-	0.195	0.195	0.100
CK6	0.195	0.195	0.195	0.195	0.195	0.195	0.195	0.195	0.195	0.195	0.185	0.195	0.195	0.195
CK7	0.195	0.195	0.195	0.195	0.195	0.195	0.195	0.195	0.195	0.195	0.185	0.195	0.195	0.195
CK8	0.389	0.389	0.389	0.195	0.195	0.342	0.389	0.389	0.389	0.389	0.370	0.195	0.195	0.289
CGLX1	0.195	0.195	0.195	-	-	0.147	0.195	0.195	0.195	0.195	0.185	-	-	0.094
CGLX2	0.195	0.195	0.195	-	-	0.147	0.195	0.195	0.195	0.195	0.185	-	-	0.094
GLN3	1.659	-	-	-	-	-	0.047	1.659	-	-	-	-	-	-
AD1	-	-	-	-	-	-	-	-	-	-	-	-	-	-
AD2	0.195	0.195	0.195	-	-	0.147	0.195	0.195	0.195	0.195	0.185	-	-	0.094
P3HB	1.446	1.393	1.393	1.393	1.393	1.393	1.393	1.393	1.393	1.393	1.393	1.393	1.393	1.393
OXFAD	0.195	0.195	0.195	0.195	0.195	0.195	0.195	0.195	0.195	0.195	0.185	0.195	0.195	0.195
OXNAD	5.324	5.324	5.324	5.324	5.324	5.324	5.324	5.324	5.324	5.324	5.333	5.324	5.324	5.324
BOXI2	0.171	0.171	0.171	0.171	0.171	0.171	0.171	0.171	0.171	0.171	0.171	0.171	0.171	0.171
BOXI3	0.171	0.171	0.171	0.171	0.053	0.171	0.171	0.171	0.053	0.124	0.171	0.171	0.053	0.171
BOXI4	0.171	0.171	0.171	0.171	0.053	0.171	0.171	0.171	0.053	0.124	0.171	0.171	0.053	0.171
BOXI5	0.053	0.053	0.053	0.053	0.053	0.053	0.053	0.053	0.053	0.053	0.053	0.053	0.053	0.053
BOXI6	0.053	0.053	0.053	0.053	0.053	0.053	0.053	0.053	0.053	0.053	0.053	0.053	0.053	0.053
BOXI7	0.053	-	0.053	-	-	-	-	-	-	-	-	0.053	0.053	0.053
BOXI8	0.053	-	0.053	-	-	-	-	-	-	-	-	0.053	0.053	0.053
BOXI9	0.053	-	-	-	-	-	-	-	-	-	-	-	-	-
PHAJ1	-	0.053	-	0.053	0.053	0.053	0.053	0.053	0.053	0.053	0.053	-	-	-
PHAJ2	-	-	-	-	0.118	-	-	-	0.118	0.047	-	-	0.118	-
CR01	0.118	0.118	0.118	0.118	-	0.118	0.118	0.118	-	0.071	0.118	0.118	-	0.118
CR02	-	-	0.053	-	-	-	-	-	-	-	-	0.053	0.053	0.053
SDH	1.558	-	-	0.147	0.265	-	-	1.611	0.071	-	-	0.094	0.212	-
PNTAB	-	0.047	0.100	-	-	-	-	-	-	-	-	-	-	-
Cox	2.759	2.759	2.759	2.759	2.759	2.759	2.759	2.759	2.759	2.759	2.759	2.759	2.759	2.759
EMP1	1.464	1.464	1.464	1.464	1.464	1.464	1.464	1.464	1.464	1.464	1.464	1.464	1.464	1.464
BOXI1	0.171	0.171	0.171	0.171	0.171	0.171	0.171	0.171	0.171	0.171	0.171	0.171	0.171	0.171
R3HB	1.446	1.446	1.446	1.446	1.446	1.446	1.446	1.446	1.446	1.446	1.446	1.446	1.446	1.446
R3HHx	0.118	0.118	0.118	0.118	0.118	0.118	0.118	0.118	0.118	0.118	0.118	0.118	0.118	0.118
RCO2	3.317	3.317	3.317	3.317	3.317	3.317	3.317	3.317	3.317	3.317	3.317	3.317	3.317	3.317

Table 25 continued – Complete set of EFV obtained for the metabolic network used to represent the core metabolism of Burkholderia sacchari using experimental flux data.

EFV	**28**	**29**	**30**	**31**	**32**	**33**	**34**	**35**	**36**	**37**	**38**	**39**	**40**
EMP2	-0.100	-0.389	-0.389	-0.389	-	-1.853	-1.853	-1.853	-1.464	-0.389	-0.389	-0.040	-0.389
EMP4	-0.100	-	-	-	-	-1.464	-1.464	-1.464	-1.464	-	-	-	-
EMP5	-0.100	-	-	-	-	-1.464	-1.464	-1.464	-1.464	-	-	-	-
EMP6	1.364	1.464	1.464	1.464	1.464	-	-	-	-	1.464	1.464	1.464	1.464
EMP7	1.364	1.464	1.464	1.464	1.464	-	-	-	-	1.464	1.464	1.464	1.464
EMP8	1.364	1.464	1.464	1.464	1.464	-	-	-	-	1.464	1.464	1.464	1.464
EMP9	1.364	1.464	1.464	1.464	1.464	-	-	-	-	1.464	1.464	1.464	1.464
VP6	-	0.195	0.195	0.195	-	0.195	0.195	0.195	-	0.195	0.195	0.020	0.195
VP7	-	0.389	0.389	0.389	-	0.389	0.389	0.389	-	0.389	0.389	0.040	0.389
VP8	-	0.195	0.195	0.195	-	0.195	0.195	0.195	-	0.195	0.195	0.020	0.195
VP9	-	0.195	0.195	0.195	-	0.195	0.195	0.195	-	0.195	0.195	0.020	0.195
VP10	-	0.195	0.195	0.195	-	0.195	0.195	0.195	-	0.195	0.195	0.020	0.195
ED1	1.564	1.269	1.269	1.269	1.464	2.733	2.733	2.733	2.928	1.269	1.269	1.444	1.269
ED2	1.564	1.269	1.269	1.269	1.464	2.733	2.733	2.733	2.928	1.269	1.269	1.444	1.269
EMP10	1.558	1.464	1.464	1.464	1.659	-	-	-	0.195	1.464	1.464	1.638	1.464
CPD	3.122	2.733	2.733	2.733	3.122	2.733	2.733	2.733	3.122	2.733	2.733	3.082	2.733
VP1	1.564	1.853	1.853	1.853	1.464	3.317	3.317	3.317	2.928	1.853	1.853	1.504	1.853
VP5	-	0.584	0.584	0.584	-	0.584	0.584	0.584	-	0.584	0.584	0.060	0.584
CK1	0.195	-	-	-	0.195	-	-	-	0.195	-	-	0.175	-
CK2	0.195	-	-	-	0.195	-	-	-	0.195	-	-	0.175	-
CK3	-	-	-	-	-	-	-	-	-	-	-	-	-
CK4	-	-	-	-	-	-	-	-	-	-	-	-	-
CK5	-	-	-	-	-	-	-	-	-	-	-	-	-
CK6	0.195	-	-	-	0.195	-	-	-	0.195	-	-	0.175	-
CK7	0.195	-	-	-	0.195	-	-	-	0.195	-	-	0.175	-
CK8	0.389	-	-	-	0.389	-	-	-	0.389	-	-	0.349	-
CGLX1	0.195	-	-	-	0.195	-	-	-	0.195	-	-	0.175	-
CGLX2	0.195	-	-	-	0.195	-	-	-	0.195	-	-	0.175	-
GLN3	0.100	-	-	-	-	1.464	1.464	1.464	1.464	-	-	-	-
AD1	-	-	-	-	-	-	-	-	-	-	-	-	-
AD2	0.195	-	-	-	0.195	-	-	-	0.195	-	-	0.175	-
P3HB	1.393	1.393	1.446	1.393	1.393	1.393	1.393	1.446	1.393	1.393	1.446	1.393	1.393
OXFAD	0.195	-	-	-	0.195	-	-	-	0.195	-	-	0.175	-
OXNAD	5.324	5.518	5.518	5.518	5.324	5.518	5.518	5.518	5.324	5.518	5.518	5.344	5.518
BOXI2	0.171	0.171	0.171	0.171	0.171	0.171	0.171	0.171	0.171	0.171	0.171	0.171	0.171
BOXI3	0.171	0.053	0.053	0.053	0.071	0.171	0.171	0.171	0.171	0.171	0.171	0.171	0.171
BOXI4	0.171	0.053	0.053	0.053	0.071	0.171	0.171	0.171	0.171	0.171	0.171	0.171	0.171
BOXI5	0.053	0.053	0.053	0.053	0.053	0.053	0.053	0.053	0.053	0.053	0.053	0.053	0.053
BOXI6	0.053	0.053	0.053	0.053	0.053	0.053	0.053	0.053	0.053	0.053	0.053	0.053	0.053
BOXI7	0.053	-	0.053	0.053	0.053	-	0.053	0.053	0.053	-	0.053	0.053	0.053
BOXI8	0.053	-	0.053	0.053	0.053	-	0.053	0.053	0.053	-	0.053	0.053	0.053
BOXI9	-	-	0.053	-	-	-	-	0.053	-	-	0.053	-	-
PHAJ1	-	0.053	-	-	-	0.053	-	-	-	0.053	-	-	-
PHAJ2	-	0.118	0.118	0.118	0.100	-	-	-	-	-	-	-	-
CR01	0.118	-	-	their	0.018	0.118	0.118	0.118	0.118	0.118	0.118	0.118	0.118
CR02	0.053	-	-	0.053	0.053	-	0.053	-	0.053	-	-	0.053	0.053
SDH	-	1.044	0.991	0.991	-	2.390	2.337	2.337	1.364	0.926	0.873	-	0.873
PNTAB	-	-	-	-	-	-	-	-	-	-	-	-	-
COx	2.759	2.759	2.759	2.759	2.759	2.759	2.759	2.759	2.759	2.759	2.759	2.759	2.759
EMP1	1.464	1.464	1.464	1.464	1.464	1.464	1.464	1.464	1.464	1.464	1.464	1.464	1.464
BOXI1	0.171	0.171	0.171	0.171	0.171	0.171	0.171	0.171	0.171	0.171	0.171	0.171	0.171
R3HB	1.446	1.446	1.446	1.446	1.446	1.446	1.446	1.446	1.446	1.446	1.446	1.446	1.446
R3HHx	0.118	0.118	0.118	0.118	0.118	0.118	0.118	0.118	0.118	0.118	0.118	0.118	0.118
RCO2	3.317	3.317	3.317	3.317	3.317	3.317	3.317	3.317	3.317	3.317	3.317	3.317	3.317